CASE STUDY OF ESTIMATING WAX APPEARANCE TEMPERATURE AND APPLICATION TO WAX DEPOSITION MODELLING

A Thesis Submitted to The Faculty at African University of Science and Technology
in Partial Fulfillment of The Requirements for The Degree of Master of Science
in The Department of Petroleum Engineering

By

EZEAGU Ijeoma Vera

2021

Supervised by

Professor David Ogbe

African University of Science and Technology

www.aust.edu.ng

P.M.B 681, Garki, Abuja F.C.T, Nigeria

Abuja, Nigeria

June, 2021

CERTIFICATION

This is to certify that the thesis titled “CASE STUDY OF ESTIMATING WAX APPEARANCE TEMPERATURE AND APPLICATION TO WAX DEPOSITION MODELLING” submitted to the school of postgraduate studies, African University of Science and Technology (AUST), Abuja, Nigeria for the award of the Master's degree is a record of original research carried out by EZEAGU IJEOMA VERA in the Department of Petroleum Engineering.

CASE STUDY OF ESTIMATING WAX APPEARANCE TEMPERATURE AND APPLICATION TO WAX DEPOSITION MODELLING

By

Ezeagu Ijeoma Vera

A THESIS APPROVED BY THE PETROLEUM ENGINEERING DEPARTMENT

RECOMMENDED: ……....

Supervisor, Prof. David Ogbe

……

Committee Member, Dr. Haruna Onuh

……

Committee Member, Dr. Akeem Arinkoola

…….....

Head, Department of Petroleum Engineering

APPROVED: …….....

Chief Academic Officer

…….....

Date

COPYRIGHT

ABSTRACT

EZEAGU Ijeoma Vera: Case Study of Estimating Wax Appearance Temperature and Application to Wax Modelling
Under the direction of Prof. David Ogbe

The need for cheap energy to run the world economy has propelled a lot of petroleum companies to produce oils that have high paraffin content. The paraffin, also referred to as wax, poses a problem when it forms and deposits in wellbores or pipelines carrying this oil. This flow assurance problem is observed when the wax appearance temperature (WAT) exceeds the ambient temperature, the oil cools, and wax will form resulting in a deposition.

This research focuses on the sensitivity analysis of the impact of the number of pseudo components used to characterize the crude oil on the accuracy of models for estimating the wax appearance temperature and the application of WAT to model wax deposition. The WAT is the temperature at which the first wax crystal appears and is often used to measure the probability of crude oil to deposit wax relative to the reduction in pressure and temperature. In this study, the WAT of three crude oil samples is calculated using correlations. These correlations require the lumping or pseudoization of components to characterize the fluid compositions. The Whitson and Pedersen lumping schemes are utilized to calculate the coefficients of the correlations for estimating the WAT. A sensitivity analysis is carried out to evaluate the impact of pseudoization on the WAT. A tornado chart was plotted to show how sensitive the WAT is to each independent variable as they change over their allowed ranges.

In a case study with data collected from the Niger Delta, the Matzain (1999), Singh et al wax deposition models and the heat-mass transfer numerical model of Stubsjoen (2013) are used to estimate the wax deposition thickness as a function of time and distance from the inlet along the

pipeline. The wax deposition process is modeled using a code developed in MATLAB/Octave. The wax deposit thickness was found to increase with time. The work can be applied to estimate WAT and model wax depositional thickness to mitigate wax precipitation in crude oil pipelines.

Keywords: component lumping scheme; fluid characterization; sensitivity analysis, pseudoization; wax appearance temperature, wax precipitation, wax depositional thickness, flow assurance.

DEDICATION

I dedicate this thesis to God Almighty who has been the source of my strength throughout this program and my beloved father, Mr. William Ezeagu, for his guidance. God bless you.

ACKNOWLEDGEMENTS

Thanks be to God Almighty the one who has made it possible for me to begin and complete my research work. I would like to thank my esteemed supervisor, Prof. David Ogbe, for his invaluable supervision, support, and tutelage during my MSc degree. Also, the constructive criticism and reviews of the thesis by the committee members, Dr. Akeem Arinkoola and Dr. Haruna Onuh, are well acknowledged. My gratitude extends to AUST for the funding opportunity to undertake my studies at the Department of Petroleum Engineering. Additionally, I would like to express gratitude to Miss Amaka Udigwe, your constant support is deeply appreciated.

Thanks to my colleagues for your friendship and encouragement. Sincere gratitude to every faculty I passed through and members of staff at AUST.

Lastly, I acknowledge and appreciate my father, Mr. William Ezeagu, mother, Mrs. Chibuzo Ezeagu, amazing siblings, Chinelo, Susan, Chioma and Chidubem Ezeagu, and my best friend, Nosa Arase for your understanding, support, helping hand and prayers. May God bless you for always being there for me.

Table of Contents

List of Figures

List of Tables

Chapter One

Introduction

1.0 Background

Hydrocarbon fluids are some of the most important raw materials we have because they are the predominant sources used to meet the world's energy needs. Oil and gas provide over 50% of the world's energy (Echendu, 2011). Crude oil is a base component of transport fuel, plastics, chemicals, and petroleum products. Between 50% and 97% of the oil is composed of hydrocarbons. Other minor components of oil are nitrogen, oxygen, and sulfur. Less than 1% of oil is composed of metals such as copper, nickel, vanadium, and iron.

According to Petrowiki (2018), the petroleum constituents could be broadly classified as those belonging to the C6- or the C6+ fraction. The heavy end may be further classified with SARA (Saturates, Aromatics, Resins, and Asphaltenes) analysis. Detailed PNA [paraffinic (P), naphthenic (N), and aromatic (A) fraction] analyses also can be performed on the crude oil. The aromatic fraction may or may not include the resins and asphaltenes depending on the details of the analysis. It is also possible to determine the amounts of individual n-alkanes. Although expensive, these types of analyses are especially valuable for wax precipitation modeling because they accurately define the components of a fluid that will precipitate as wax (Petrowiki, 2018).

Wax precipitation is a major problem in oil production and transportation facilities (Jandyson, 2018). This phenomenon can result in many flow assurance problems such as decreased production rates, increased power requirements, and failure of oil and gas facilities. Wax is the

high molecular weight paraffin fraction of crude oil that can be separated with the reduction in oil temperature below the pour point of crude oil. Paraffin is a mixture of hydrocarbons constituted of linear/normal chains, comprising mainly from 20 to 40 carbon. atoms, in addition to alkanes with branched and cyclic chains. The solubility of waxes with high molecular weight decreases with decreasing temperature (Sousa, 2019). Hence, as the temperature decreases, the wax fraction precipitate and phase separation occur by wax crystallization (Jafari, 2015). In severe cases, solid deposition can ultimately lead to the shutdown of an oil field. In 2003, Gluyas and Underhill reported that the Lasmo Oil field in the United Kingdom was abandoned due to recurring paraffin plugging problems that cost the industry over US$100 million (Gluyas & Underhill, 2003).

In the transportation of waxy crude oil in a cold environment (at temperatures below the oil pour point), the temperature gradient in the oil creates a concentration gradient in the dissolved waxes due to their difference in solubility. The driving force, which is created by the concentration gradient, transfers the waxes from the oil toward the pipe wall where they precipitate and then form a solid phase. The solid phase reduces the available area for the oil flow, which in turn causes a drop in the pipe flow capacity (Jafari, 2015). According to Oyedepo (2012) there is the need to understand the composition and paraffinic nature of the hydrocarbons produced to predict wax precipitation and environment leading to deposition to reduce operating cost and proffer remediation measures (Oyedepo, 2012).

1.1 Problem Statement

Wax in crude oil is composed primarily of paraffin, a white odorless, tasteless, a chemically inert compound composed of mainly normal alkanes, varying amounts of condensed cycloalkanes, iso-alkanes, and occasionally a very low percentage of aromatic material (Huang, 2015). The flow assurance in the hydrocarbon pipelines is very important due to the precipitation of the solid phase of wax on the pipe wall creating pressure abnormalities and causing an artificial blockage, leading to a reduction or interruption in the production. Wax can precipitate as a solid phase on the pipe wall when its temperature (inlet coolant temperature) drops below the wax appearance temperature (WAT). To design the oil and gas production process efficiently, it is of great importance to predict wax appearance temperatures (WAT) and the amount of precipitated wax.

The problem of organic solids precipitation is prevalent in many places around the world such as the North Sea, West Africa (Nigeria), Middle East, North Africa, Alaska, Indonesia, China etc. (Pedersen, 1993), (Taiwo et al, 2012), (Elsharkawy et al, 2000). The Nigerian crude due to its high paraffin content can be classified as paraffin-based (Koker, 2013). This means that all the problems from organic deposition are common in Nigeria. The deposition of wax in pipeline over time reduces the area available to flow fluid and can eventually cause shut down or total well loss. This wax problem leads to increased cost of production and revenue decline. Production strings in the Niger Delta have been known to wax up leading to frequent expensive interventions (Taiwo et al, 2012). This and many other reasons had led to the development of wax precipitation solutions through complete knowledge of WAT.

Wax deposition in crude oil production systems can be reduced or prevented by one or a combination of chemical, mechanical, and thermal remediation methods. However, with the advent of extremely deep production, offshore drilling and ocean floor completions, the use of mechanical and thermal remediation methods has become prohibitive economically; as a result, the use of chemical additives as wax deposition inhibitors is becoming more prevalent (Theyab et al, 2017).

1.2 Research Objectives

The primary objective of this research is to estimate the wax appearance temperature (WAT) and its application to wax deposition modelling. This data will support the design of oil and gas facilities to mitigate wax formation problems before production. The goal is to increase hydrocarbon production, reduce cost, and enhance the development of marginal oil fields.

The specific objectives of this research are:

i. To review existing thermodynamic wax precipitation models.
ii. To compare the results obtained from the thermodynamic wax precipitation models to determine their applicability to Niger Delta crude oil.
iii. To estimate the wax appearance temperature and its impact on wax deposition modelling.
iv. To evaluate the impact of pseudoization or component lumping on the accuracy of the correlations used to estimate the wax appearance temperature.

1.3 Scope of Study

The scope of the study includes:

i. Review of the methods of estimating wax appearance temperature (WAT) including both experimental and theoretical methods.
ii. Application of the Whitson and Pedersen lumping schemes of hydrocarbon components to determine the coefficients required for WAT correlations.
iii. Sensitivity analysis of the lumping of hydrocarbon components on the estimates of the wax appearance temperature.
iv. Application of WAT in the wax deposition models to derive the wax deposition thickness.

1.4 Significance of Study

The solution provided in this study would ensure an uninterrupted flow of oil and gas during and while transporting hydrocarbons. Thus, minimizing the financial expenditures associated with wax deposition problems. In addition, the methods could be applied in other industrial settings working on the related activities for oil or gas pipelines. These methods might be commercialized thereby helping operations personnel to maintain the pipeline wall from wax deposition during crude oil production over a long time.

1.5 Organization of Study

This research work is presented in five Chapters. Chapter One is an introduction to describe the background, study objectives, and scope of work. The major publications related to this study are reviewed in Chapter Two to improve our understanding of the methods for estimating wax

appearance temperature and its use in wax deposition modelling. Chapter Three is the research methodology, and it describes the characterization of reservoir fluid, the sensitivity of lumped fractions on the accuracy of WAT estimates, and the estimation of wax deposition. Results obtained from the study are presented and discussed in Chapter Four. Explanations of major observations from this work are also discussed in this chapter. Finally, Chapter Five contains the conclusions reached in this study and a set of recommendations proposed for further studies to improve the results of this research.

Chapter Two

Literature Review

A review of the literature is presented in this Chapter. This is to foster an understanding of petroleum fluids and the characterization of petroleum fluids including the heavy fractions required for the determination of wax appearance temperature (WAT).

2.0 Petroleum fluids

Hydrocarbons occur naturally as gas, gas condensate, crude oil (from light oils to extra-heavy oils), bitumen, and coal. Crude oils are classified in terms of their physical properties (viscosity and density/API) as shown in Table 2.1 based on the UNITAR classification (Santos, 2014).

Table 2.1: UNITAR classification of oils by their physical properties at 15.6^{o}C

	Viscosity mPa.S	Density Kg/m^3	API Gravity
Convectional oil	$<10^2$	934	$>20^o$
Heavy oil	10^2 - 10^4	934 – 1000	20^o – 10^o
Bitumen	$>10^4$	>1000	$<10^o$

A reservoir fluid (Petroleum fluid) is a multi-component mixture of naturally occurring hydrocarbons (Pedersen et al, 1991). The chemical composition of reservoir fluids determines the behavior of this mixture at reservoir and surface conditions. The prevailing temperature and pressure also have significant effects on its phase behavior. A good knowledge of hydrocarbon phase behavior is critical for the development, modelling and management of reservoirs. Phase behavior is that part of thermodynamics that provides the needed tools for the detailed understanding of how hydrocarbon fluids behave with changes in the temperature and pressure.

Reservoir fluids can range from dry natural gas to viscous liquids, like heavy oil and bitumen. This depends on the prevailing temperature and pressure conditions in the reservoir. The light hydrocarbon fractions contain associated gases of low molecular weight hydrocarbons (i.e., CO2, H2S, N2, C1, C2, C3, n-C4, i-C4) while the rest of the oil can be seen as a distribution of paraffinic, naphthenic, and aromatic species of increasing complexity and molecular weight. However, within any reservoir fluid, the proportion of paraffinic hydrocarbons usually decreases with increasing molecular weight or boiling point (Santos, 2014).

2.1 Components of reservoir fluids

Crude oil is generally divided into four groups: paraffins (normal, branched), asphaltenes, naphthenes, and aromatics. Among these groups, paraffins, asphaltenes, and naphthenes are sometimes called aliphatic compounds, as different from aromatic compounds. The crystals formed from normal paraffin wax are known as macrocrystalline. Hence the crystals produced by de-oiling petrolatum, as part of the petroleum refining process are microcrystalline. Figure 2.1 shows the major components of petroleum fluids (Semir, 2020). A brief review of the components of reservoir fluids is presented in the following.

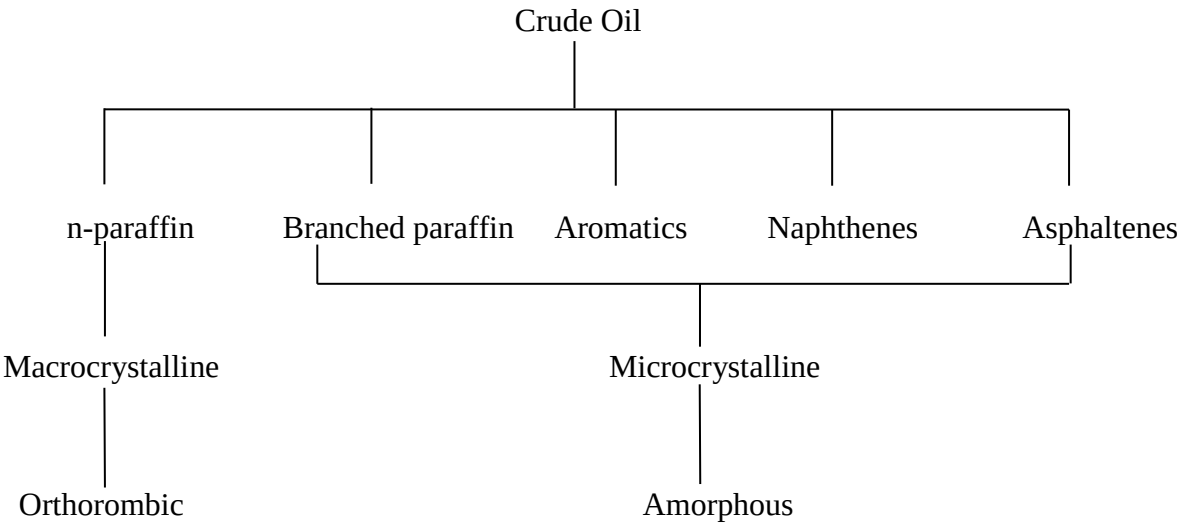

Figure 2.1: Components of reservoir fluid
Source: (Semir, 2020)

2.1.1 Paraffins

Paraffins also known as acyclic alkanes, are saturated hydrocarbons which can have straight (normal paraffin) or branched (iso-paraffin) chains but no ring structure (Akinyede O. M., 2019). The same molecular formula C_nH_{2n+2} is shared by both normal and iso-paraffins. The structure of paraffin is shown in Figure 2.2.

2.1.2 Naphthenes

Naphthenes, otherwise known as cycloalkanes, are hydrocarbons seen to be similar to paraffins in the sense that they are linked by the same types of carbon segments. They differ from paraffins in that they contain one or more cyclic structures. The carbon segments in the ring structures are linked by single bonds. There are six carbon atoms in most naphthenic ring structures, but there are also naphthenic compounds with five or seven carbon atoms linked in ring structures, which can be commonly seen in petroleum reservoir fluids (Pedersen et al, 1991).

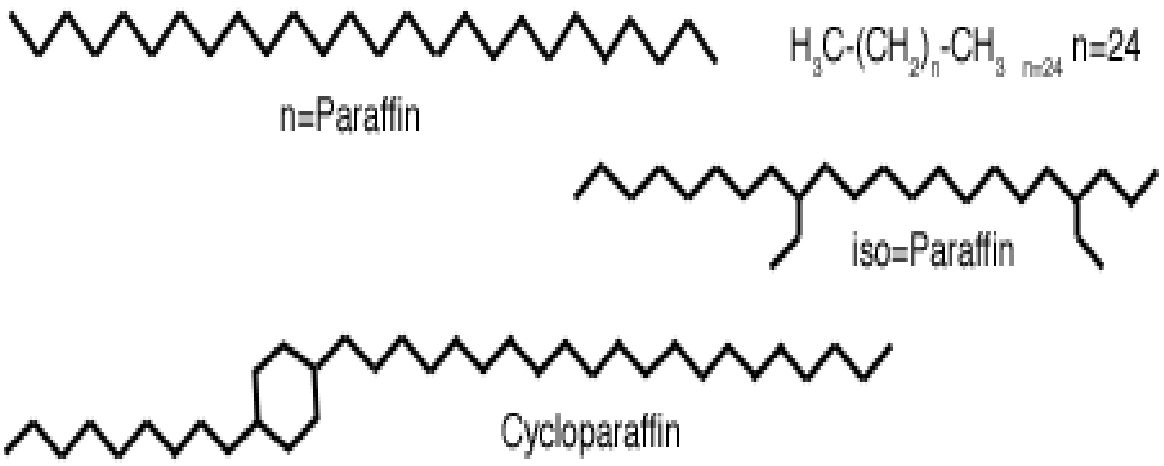

Figure 2.2: Molecular Structure of Paraffin (https://igiwax.com/wax-basics/)

2.1.3 Aromatics

These are hydrocarbons that contain at least a benzene (C_6H_6) ring. The carbon atoms in an aromatic compound are linked by double bonds. Aromatic compounds with two or more ring structures are also found in reservoir fluids which are called Polycyclic aromatics. An example of this type of component is naphthalene ($C_{10}H_8$). Numerous aromatic hydrocarbons in petroleum consist of aromatic and naphthenic rings and bear normal and/or branched alkane side chains (James G. S., 2016). Aromatics have low tendency of forming wax and are not as active as paraffins in wax formation.

Some paraffin components are depicted in fig 2.1. How these compositions vary is shown in fig 2.3.

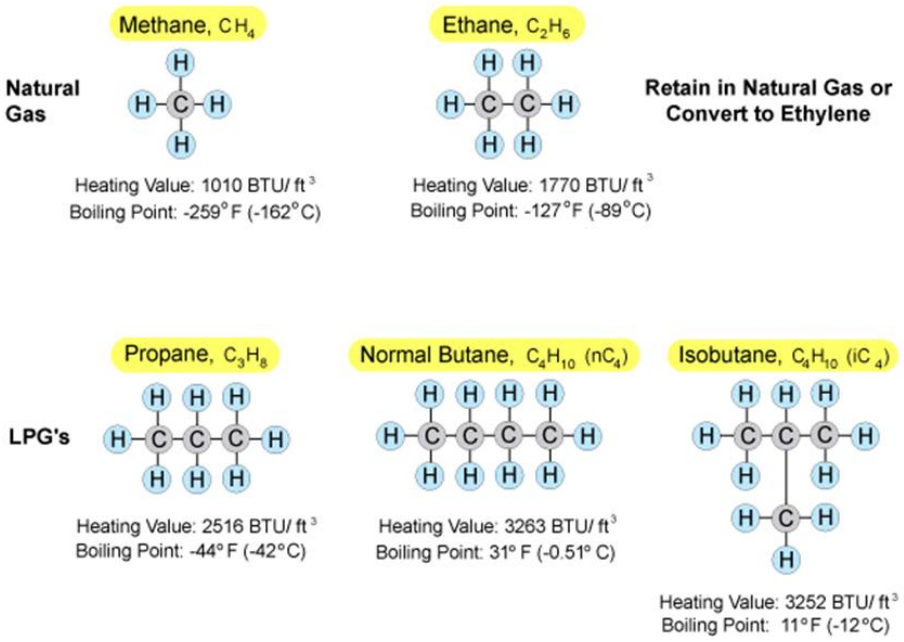

Figure 2.3: Molecular Structure of Some Petroleum Constituents
Source: (https://www.ihrdc.com/els/po-demo/module01/mod_001_02.htm))

2.2 Heavy Fractions in Petroleum Fluids

Almost all the reservoir fluids comprising the heavy fractions fluids are polydispersed. The predominant part of the heavy fractions are asphaltenes, asphaltogenic acids/compounds, diamondoids, and derivative of heavy aromatic hydrocarbons, mercaptans, organometallic, petroleum resins and wax (Mansoori, 2017). The general theory shows that heavy fractions have no significant effect on the liquid-vapor phase behavior of most of the reservoir fluids (Baker, 2015). The knowledge of most of the constituents of the reservoir fluids that form heavy fractions is important for accurate prediction of the phase behavior of the fluid.

2.3 Waxes

Many reservoir fluids have waxes as a constituent, which can precipitate and deposit under the right conditions. Waxes are precipitates of organic solids usually in the form of crystals which occur in some crudes when there are changes in thermodynamic conditions, predominately temperature. They are complex mixtures of high molecular weight alkanes of three structural types (straight-chain, branched-chain and cyclic). They vary compositionally over a wide range of molecular weights up to hydrocarbon chain lengths of approximately *C*60. Wax crystals can be separated from petroleum by cooling a mixture of the oil, ketone, and another polar or aromatic solvent (Glover, 2005). According to (Baha, 2018), paraffin wax produced from crude oil consisting long-chain saturated hydrocarbons (linear alkanes/ n-paraffins) with carbon chain lengths of C_{18} to C_{75+} is referred to as macrocrystalline wax. Naphthenic hydrocarbons (C_{18} to C_{36}) which also deposit wax are referred to as microcrystalline wax. Macrocrystalline waxes lead to paraffin problems in production and transport operations; microcrystalline waxes contribute the most to tank-bottom sludges.

2.4 Waxy Crude

Waxy crude can be a reservoir fluid that contains large amounts of long-chain paraffin wax (alkanes) components, making the reservoir fluid possess a high pour point and low API gravity. A waxy crude oil is separated by the bases that it shows non-Newtonian rheological behavior at low temperatures (i.e., about 20 F above the pour point). For such non-Newtonian-behaved crude oils, the effective viscosity is not only temperature-dependent but also a function of the effective rate of shear in the pipeline (Mysara, 2019).

At reservoir temperature and pressures, waxy crude oil would behave typically as a Newtonian fluid with low viscosity. As the reservoir fluid is produced and flows through subsea pipelines

and tubings, it would experience a low-temperature environment. As the temperature drops below the wax appearance temperature (WAT), wax deposits begin to precipitate out of the solution with a high increase in viscosity which indicates a typical Non-Newtonian fluid behavior (Mysara, 2019). The properties of waxes found in petroleum fluids are discussed in the following section.

2.5 Properties of Waxy Crude Oils

There are three important properties of waxy crude oils, namely, wax appearance temperature (WAT), pour point, and wax content.

2.5.1 Wax Appearance Temperature (WAT) or Cloud Point

Wax appearance temperature is the temperature above which a slight decrease in temperature will result in wax formation in waxy crude. When a high-temperature waxy crude loses heat to a temperature lower than the WAT, the paraffin molecules would form clusters of aligned chains. Once these nuclei reach a critical size and establish a stability, more attachment of molecules would contribute to the growth of the crystal. The formation of these nuclei causes the fluid to take on a cloudy appearance, hence the name cloud point. This also is referred to as the wax crystallization temperature or WAT (Mysara, 2019).

2.5.2 Pour point

When waxy crude is flowing through a pipeline, and as a result of the continuous cooling of the crude below the WAT caused by the transfer of heat towards the surrounding, crystals of wax form and grow in sizes to form partial to total blockage of the pipe cross-sectional area. The pour point temperature can be seen to be the lowest temperature at which the waxy crude is mobile. This can be identified as the stock tank oil gelation temperature. (Mysara, 2019).

2.5.3 Wax content

This can be defined as the quantity of wax that will precipitate in excess acetone at approximately -25℃ . The amount of material remaining after washing with the cold solvent is called wax content of the oil sample. (Kök, 2007).

2.6 Wax Precipitation

The deposited organic materials removed from the production strings usually contain asphaltene resin, and wax. Most reservoir fluids contain paraffins of high molecular weight, which may solidify into a wax phase at temperatures below the WAT. The wax formation is a result of the decrease in temperature which is different from the formation of asphaltenes. Thus, wax often accumulates at a certain spot inside the producing well (Alian, Singh, Mohammed, Ismail, & Anwar, 2013). The wax deposition process involves two distinct stages: nucleation and growth. Nucleation is the formation of a paraffin cluster in a critical size (also called nuclei), that is stable in crude oil. The insoluble wax tends to disperse in the hydrocarbon liquid. Wax deposition in the production system ("growth") generally requires a "nucleating agent," such as asphaltenes and inorganic solids. The wax deposits vary in consistency from a soft mush to hard, brittle material. Paraffin deposits will be harder, if longer-chain n-paraffins are present (Nur, 2016).

2.7 Problems of Waxy Crude

Waxy crude causes flow assurance problems during its production and transportation in the oil industry. Wax precipitation and deposition also cause a significant change in the original

rheology of the oil. While wax crystals are precipitating, the viscosity of the crude oil increases resulting to convert it to a high viscous fluid that adheres to the internal pipe wall. This phenomenon decreased the effective cross-sectional area of the pipe. The solution to this problem can be achieved by applying various methods to lower the viscosity and pour point. The methods that have been extensively implemented include the heating of the transported crude, dilution of the crude with lighter fluid, and addition of chemical additives, known as flow modifiers, to the flow stream. Each of these methods has its own advantages and disadvantages. However, in general, chemical additives are the most common solution for handling wax precipitates (Girma, 2018; Mysara, 2019). According to Zhou (1996), paraffin issues cause a loss of billions of dollars to the petroleum industry because of: cost of chemicals, reduced production, well shut-in, equipment failure, choking of the flowlines, less utilization of capacity, extra horse-power requirement, and increased man-power attention (Kempton & Golczynski, 2006).

2.8 Nigerian Waxy Crude

Nigeria has substantial reserves of paraffinic crude oils ranging from moderate to high. It contains moderate to high contents of paraffin wax with densities at 15°C ranging from 0.813-0.849 g/ml for light crude oil, 0.866-0.886 g/ml for medium oil, and 0.925-0.935 g/ml for heavy crude oil. The waxy crude oils possess undesirable high pour points and can be difficult to handle when flowing at ambient temperatures are lesser than the pour-point (Taiwo et al, 2012). Niger Delta crude oils exhibit non-Newtonian flow behavior at temperatures lower than the cloud point due to wax crystallization. Pipelines have been known to wax up beyond recovery

in Nigeria likewise production tubing which necessitates frequent expensive interventions (Taiwo et al, 2012).

2.9 WAT Estimation techniques

There are different techniques for measuring precipitated wax. The measurement can be in the form of the amount/quantity of wax precipitated (relative to oil quantity), the size of the wax crystals, and the number of wax crystals. All these affect the sensitivity of the measurement techniques. It is also known that some techniques detect wax crystals at the microscopic level (nucleation stage of wax crystal formation), while others detect wax crystals at the early stage of growth. There are various experimental and theoretical methods of estimating the WAT (Lize, et al., 2018). Some of these techniques will be described in the following section.

2.9.1 Experimental Methods of Estimating WAT

In terms of nature of signals, the different experimental techniques can be grouped as follows:

Amount of wax precipitated: Differential Scanning Calorimetry (DSC), Viscometry

Size of wax crystals: Microscopy, Viscometry, Cold filter plugging test

Number of wax crystals: Light Transmittance (LT), Light Scattering (Near-Infrared (NIR), Fourier Transform Infrared (FTIR).

A review of these experimental methods is presented below.

ASTM Standard Techniques

WAT can be determined according to ASTM (American Society of Testing and Materials) standard procedures ASTM D2500. In this method, the starting transparent sample oil is poured

into a test jar. A thermometer is used to monitor the oil temperature. The entire jar is then put into a constant temperature bath. The cooling bath temperature is reduced by 1°C step by step and the sample oil is examined visually through a microscope for crystal formation. The WAT is determined as the temperature at which the crystals first appear. This method is quite time-consuming and is not automatic, and it needs operator interaction (Hosseinipour et al, 2019).

Differential Scanning Calorimetry (DSC)

DSC measures the heat flow from or to the sample when the sample is heated or cooled. Since crystallization will give out heat, it will show up in the DSC curve as an exothermic peak during cooling. Only a small amount of sample oil is needed for DSC analysis. Since it utilizes heat to detect the onset of wax crystallization the sample doesn't need to be transparent. This method detects the latent heat of fusion released on crystallization. Although there can be some uncertainty in the interpretation of the results, differential-scanning calorimetry has been widely used for WAT determination and also can provide data on the heat capacities and heats of fusion or transition associated with liquid/solid and solid/solid phase transitions (James O. P., 2011).

Viscometry

The viscometry technique employs the linear relationship between fluid viscosity and temperature. Wax formation changes the crude oil from Newtonian to non-Newtonian fluid behavior. The viscosity (μ) of Newtonian fluids is related to the temperature by the Arrhenius equation. That is,

$$\mu = C \exp (E_a / RT) \quad (2.1)$$

Where μ = viscosity in Pa.s

C = constant dependent on entropy

E_a = activation energy of viscous flow in J/mol

R = universal constant

T = absolute temperature in K

The WAT was determined from a plot of natural log of viscosity (LN Viscosity) versus inverse of absolute temperature (1/T) to be the point at which deviation from linearity occurs as temperature was lowered. Figure 2.4 shows Ln (kinematic viscosity) versus 1/T using equation (2.1). This observation is supported with an overall R-squared value of 0.989. This suggests that the experimental data are well-fitted by the Arrhenius model. (BelgharzaI, 2014)

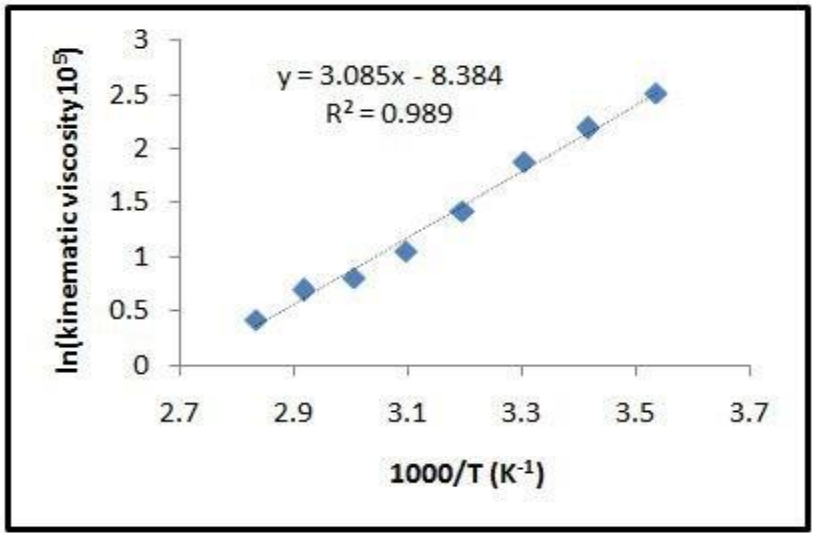

Figure 2.1: schematic plot of the Ln (μ) vs. 1/T (Arrhenius equation)

Source: (BelgharzaI, 2014)

Cross Polar Microscopy (CPM)

This measurement technique works based on the principle that all crystalline material rotates the plane of polarized light. Therefore, upon crossing two prisms on the opposite side of the oil sample, the oil appears black due to the blocking of light. As the temperature cools, wax precipitates and the crystals appears as bright spot (Kunal et al., 2000). The first bright spots

appear when the temperature reaches the wax appearance temperature. This technique has been considered by many researchers as the most accurate for the determination of WAT since it can identify the very first crystal of wax (Lee et al, 2007; Kunal et al, 2000; Alghanduri et al, 2010) (Koker, 2013).

Cool filter Plugging point

This technique is based on the continuous monitoring of the pressure drop across a filter while the oil flows through a temperature-controlled flow-loop. It has quite several interesting features since it is applicable to both live and dead oils at low or high pressures unlike most of the other techniques that are restricted to dead oils at low pressures. Filters with 0.5 mm are commonly used along with very low flow rates (inferior to 0.5 cm3 /min) to minimize the shear stress at the filter promoting the wax deposition and the pressure build-up (Tao, 2008).

Light Transmittance

The light transmittance method uses an experimental apparatus that consists of a PVT cell with a light source and a light power receiver mounted on opposite sides of the cell. When wax crystals appear in the fluid, the amount of light transmitted is reduced dramatically, and the WAT can be seen as a sharp drop in a plot of light power received vs. temperature. This method can be used at high pressure and, therefore, can be applied to live reservoir fluids as well as stock-tank oils (Uba, 2004).

2.9.2 Theoretical techniques of determining WAT

Ideally, WAT is determined from laboratory analysis of representative fluid samples. In the alternative, rigorous thermodynamic models are employed. However, both the laboratory and

rigorous thermodynamic methods are expensive and time demanding, in addition, they do not always guarantee accurate results for the full range of expected operating conditions. Several empirical correlations have been proposed for predicting WAT either as a complement or substitute to these rigorous methods. Some of these techniques include composition-based WAT models (Hosseinipour et al, 2019), the Patel-Teja EOS (Farayola, Adeboye, Adekomaya, & Olatunde, 2010), the influence of electromagnetic and ultrasonic waves (Taheri-Shakib Hamedani, Shekarifard, & Naderi, 2018), Peng-Robinson Equation of State (Chung, 1992), Multi-solid Phase Model (Vafaie-Sefti, Mousavi-Dehghani, & Bahar, 2000), and the new GOR-based model (Eyitayo, et al., 2020), etc. In this study, the composition-based models, the GOR-based model, and the T_f correlation were used in estimating the WAT.

Composition-based WAT models by Hosseinipour et al. (2019)

(Hosseinipour et al, 2019) proposed two different WAT correlations based on their description of crude oil as a simple mixture of pseudo components. The WAT correlations are defined as functions of the compositions of certain hydrocarbon components in the mixture. The following are the two (Hosseinipour et al, 2019) correlations, which we refer to as HOS-1 and HOS-2, respectively.

HOS-1 WAT Model

This is a four-pseudo component model given by

$$\text{Twax} = 6.808X1 + 0.366X2 + 3.381X3 + 3.028X4 \quad (2.2)$$

Where Twax is the Wax Appearance Temperature (K), X1, X2, X3, and X4 are the total content of hydrocarbon components (wt. %) in the range C1-C9, C10-C15, C16-C20, and C20+, respectively.

HOS-2 WAT Model

The second Hosseinipour et al. (2019) correlation is a three-pseudo component model defined as

$$\text{Twax} = 1.017\text{X1} + 0.075\text{X2} + 1.6111\text{X3} + 213.586 \quad (2.3)$$

where X1, X2, and X3 are the total content of hydrocarbon components (wt. %) of the C10-C15, C16-C20 and C20+, respectively. Note that unlike the HOS-1 correlation, the C1-C9 pseudo component is constant in the HOS-2 model.

GOR-Based WAT Model by Eyitayo et al (2020)

This semi-empirical model by (Eyitayo, et al., 2020) was developed using experimental datasets collected from some oil reservoirs in the Niger Delta region. According to Eyitayo et al. (2020), the samples were subjected to standard screening procedure in selecting the suitable data source for constructing the correlation. The data covers the gas-oil ratio (GOR) range of 1 – 1180 scf/stb, with the lower bound of GOR approximating dead-oil conditions. The wax contents measured in the laboratory for these samples were reported to be in the range 5 – 49.5% by weight (i.e. 5 – 9.3 mol%). (Eyitayo, et al., 2020)

The resulting correlation is given by the following expression.

$$\text{Twax} = 301.43\text{Rs} - 0.0060 \quad (2.4)$$

where Twax is the WAT (K) and Rs is the solution GOR (scf/stb). Note that the validity of this equation is limited to the GOR range, $1 \leq \text{Rsi} \leq 1180$ scf/stb, used in developing the correlation.

T_f Correlation by Akinyede et al, (2019)

This correlation was developed using a mixed linear stochastic model (Akinyede O. M., 2019). The model is built on the step-by-step mathematical procedure, from step 1 to step k (injection of k predictor variables stepwise). The response at step *i* depends only on the previous step (*i*-1) and

the effect of the incoming transfer function $b_i X_i$, where b_i is model constant and X_i is the incoming predictor variable for the response variable, Y_i.

Consider, $Y = f(X_1, X_2, X_3, \cdots, X_k)$ (2.5)

Where:

Y = response variable,

X_i = predictor random variable $for\ i = 1, 2, \cdots, k$

$Y_i = f(X_1, X_2, \cdots, X_k)$

The model equations are

$$\frac{X_i}{Y_i} = a + \sum_{i=1}^{k} b_i X_i \quad for\ i = 1,2, \cdots, k \tag{2.6}$$

Where a, b_i $for\ i = (1,2, \cdots, k)$ are model constants for these types of models.

This model type can be analyzed using statistical principles of multiple linear regression analysis with k predictors random variables. Akinyede (2019) used Minitab software for the regression analysis. She developed new correlations for estimating T_i^f for n-paraffins, which is a function of molecular weight of the component. Branching of the identified iso-paraffins was also considered and the composition data of C_{7+} fractions from four Niger-Delta wells were used in the Akinyede (2019) study. Experimental data from NIST (National Institute of Standards and Technology) Chemistry WebBook, SRD 69 were used to validate the correlation. The Akinyede et al, (2019) correlation is given by

$$T_i^f = \frac{Mw_i}{0.218 + 0.00243 Mw_i} \tag{2.7}$$

Where T_i^f is the temperature of melting and Mw_i is the molecular weight of components. The details of the development of the correlation can be found in (Akinyede O. M., 2019).

2.10 Wax Deposition

The wax deposition has been a big challenge for the Oil & Gas industry. Some techniques have been developed to deal with the wax formation or deposition problems; however, it is difficult to accurately predict wax deposit thickness and location. The close interrelationship between the wax deposition process and wax thermodynamics, heat & mass transfer, and fluid mechanics brings additional complexity to wax deposition analysis (Fernando, 2020).

2.11 Wax Deposition Mechanisms

Several researchers have proposed different models to describe wax deposition mechanisms such as molecular diffusion, Soret diffusion, shear stripping, shear dispersion, Brownian diffusion and gravity settling (Aiyejina, 2011; Beryl, Moorwood, Szczepanski, & Zhang, 2007; Pan, 2009).
Many studies have reported that molecular diffusion and shear dispersion are the principal mechanisms of wax deposition (Hoffmann, 2010; Oluwatosin, 2013). A quick review of each of these mechanisms is presented to underline their importance on wax behavior.

2.11.1 Molecular diffusion

The temperature of the flowing hydrocarbon would continue to decrease due to the surrounding cold seawater in an offshore pipeline. Molecular diffusion acts as soon as the temperature of the wall reaches the WAT. At that temperature, the oil is saturated with wax in solution and wax precipitates out. Wax precipitation creates a concentration gradient between dissolved wax in the turbulent core and the wax remaining in the solution at the wall side. Due to this, dissolved wax diffuses towards the wall where it is subsequently precipitated (Schou, 2007). Figure 2.4 illustrates wax deposition by molecular diffusion

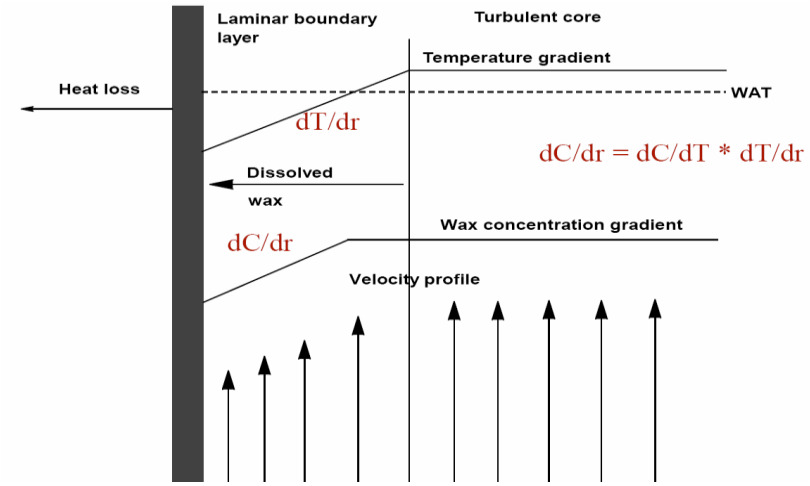

Figure 2.2: Wax deposition by molecular diffusion (Aiyejina, 2011)

Where $\frac{dM_w}{dt}$ is the rate of wax deposited (kg/s), ρ_w is the density of the solid wax (kg/m^3), D_w is the diffusion coefficient of the wax in the oil phase (m^2/s), A_w is the area of wax deposition (m^2), $\frac{dC}{dr}$ is the wax concentration gradient (1/m) of wax concentration over pipe radial coordinate r (m), $\frac{dC}{dT}$ is the solubility coefficient of the wax crystal in the oil phase (1/°C),$\frac{dT}{dR}$ is the radial temperature gradient of the wall (°C/m) (Ajayi, 2013).

2.11.2 Shear dispersion

When wax crystals are suspended in the flowing oil, the wax particles move with the mean speed in the direction of flow. The shearing of the fluid close to the pipe wall also includes a lateral movement of wax particles known as shear dispersion. This way the precipitated wax is transported from the turbulent core to the pipe wall (Ana, 2016). Wax crystals in the oil will migrate towards the wall where they deposit, because of the lower velocity near the wall compared to the center of the pipe. At the wall the wax may form a deposit on its own or link with wax which is already deposited by molecular diffusion.

According to Bern (Bern, 1981), the parameters likely to affect the shear dispersion mechanism are:

- The wall shear rate
- The shape and size of particles
- The amount of wax formed from the solution

Shear dispersion becomes important when the precipitated wax content in the turbulent core is high. This occurs when the bulk oil temperature is below the WAT. Increasing shear rate leads to more wax particles dispersing toward the pipe wall, but the corresponding increase in wall shear stress may cause the looser held deposits to be stripped from the wall (Schou, 2007).

The shear dispersion coefficient proposed by Burger (1981) is expressed as

$$Ds = \frac{\alpha^2 Cw^* \gamma}{10} \tag{2.8}$$

Where a is particle diameter, C_w is the volume fraction concentration of wax out of solution at the wall and γ is the oil shear rate at the wall.

2.11.3. Gravity Settling

Density effects on the wax crystal as compared to its surrounding oil solvent presents a potential gravity deposition mechanism in non-interacting oil-wax systems. Burger (1981) accounts for the settling effect in gravity fields due to the wax settling velocity (Leiroz., 2005). This velocity diminishes asymptotically to zero as wax-oil fluid reaches complete settling. In typically active systems as found in oil and gas pipelines, gravity settling has been reported to be negligible as suggested shear dispersion mechanism or active fluid forces create a dispersion of precipitated wax particles eliminating gravity settling (Karianne, 2008; Leiroz., 2005).

However, in low flow rates, at typical, shut-in conditions or in storage tanks, gravity effect is expected to contribute to significant wax deposition particularly observed for low viscous fluids (Brevik, 2013). The settling velocity U (m/s) is given by the modified stokes law of settling crystals in a pseudoplastic fluid.

$$U = [\frac{g\Delta P\alpha^{(1+n)}}{18K}]^{1/n} \quad (2.9)$$

Where $\Delta\rho$ is the density difference (kg/m^3) between the settling wax and the oil, α is the particle diameter (m), *n is* the power-law index, *g is* the acceleration due to gravity (m/s^2) and *K* is the power-law consistency index. The shear rate and shear stress relationship of a power law fluid implied in the correlation is given in equation 2.10 to be

$$\tau = Kp\gamma\, n \quad (2.10)$$

where τ is the shear stress (N/m^2) and γ is the shear rate of the fluid (s^{-1}).

2.11.4 Brownian diffusion

When small, solid waxy crystals are suspended in oil, they will be bombarded continually by thermally agitated oil molecules. Such collisions lead to small random Brownian movements of the suspended particles. For a particular concentration gradient, Brownian motion will lead to a net transport which is similar to diffusion (Abass, 2021). The Brownian diffusion coefficient for special, non-interacting particles can be defined as:

$$Db = \frac{RTa}{6\pi\mu aN} \quad (2.11)$$

Where R is the gas constant, T is the absolute temperature, μ is the viscosity, α is the particle diameter, and N is Avogadro's number.

Several contributing pieces of research such as from the work of (Burger, 1981), (Karianne, 2008), and (Singh P. , 2000) considers no significant influence of Brownian diffusion but Azevedo (2013) believes there are no experimental evidence to justify this conclusion (Karianne, 2008).

2.11.5. Soret diffusion

Mass transfer between the bulk fluid and the inner wall of the pipeline due to thermal diffusion is called Soret diffusion or the Soret effect. Soret diffusion is modelled by Fick's diffusion equation with a Soret coefficient. Although some authors have categorized thermal diffusion to be negligible, it is comprehensive to represents diffusion terms by all possible diffusion effects that could potentially influence wax deposition in wax deposition modelling. (Azevedo, 2003).

2.11.6. Shear stripping

Shear stripping, also known as shear sloughing, or shear removal is the mechanism of wax removal from the walls due to shear stress exerted by a flowing stream of oil on the wax solid. The inflowing velocity can slough pieces of wax from the deposition layer thereby acting as a wax removal mechanism. Shear stripping is observed if a concentration gradient develops between the wax on the walls and sloughed waxes in the bulk fluid. The negative wax transfer due to shear forces is modelled as a function of the shear stress τ, the thickness of the wax layer δ (m), and the wax layer yield stress. It is recorded by Pan (2009) that the wax yield stress is proportional to $\omega^{2.3}$ such that ω is the mass fraction of wax in the gel layer.

The wax shearing rate is derived based on the (Beryl, Moorwood, Szczepanski, & Zhang, 2007) shear rate equation of (2.12).

$$J^{sr} = C\frac{\delta\tau}{\omega^{2.3}} \quad (2.12)$$

Where *C* is the shear constant, ω is the fraction of wax in the gel layer, δ (m) is the thickness of the wax layer, τ is the shear stress (N/m^2 mass) as obtained by the equation (2.13) such that *f* is the fanning frictional factor, ρ is the density of the flowing oil (kg/m^3), and *u* is the oil velocity (m/s).

$$\tau = \frac{1}{2} f \rho u^2 \quad (2.13)$$

2.12 Thermodynamic models

Thermodynamic models are useful tools for the prediction of the solubility of wax components, their fractions in the fluid and the wax concentration (Ellison, 2000). Fugacity and the Gibbs free energy change of a pure liquid compound are used to estimate the corresponding variables for the pure solid. Essentially, the various wax models differ in the way how liquid and solid (wax) fugacities are estimated. Different thermodynamic approaches are used to analyze these non-idealities and calculate the activity coefficients. (Montero, 2020)

The condition for Thermodynamic equilibrium are provided below:

$$f_i^v\left(P, T, y_i\right) = f_i^l\left(P, T, x_i\right) = f_i^s\left(P, T, s_i\right) \quad (2.14)$$

For liquid-solid equilibrium:

$$f_i^l = f_i^s \quad (2.15)$$

Where f_i^l= fugacity of component *i* in the liquid-phase mixture, and

f_i^s = fugacity of component *i* in the solid-phase mixture.

The liquid-phase fugacity of component *i* in the mixture can be expressed as

$$f_i^l = \gamma_i^l x_i\, f_i^{ol} \quad (2.16)$$

Where γ_i^l is the activity coefficient of component *i* in the liquid phase (the activity coefficient is generally a function of composition of the phase); x_i is the mole fraction of component *i* in the liquid phase; and f_i^{ol} is the standard state fugacity of component *i* in the liquid phase. It can also be described as the liquid phase fugacity of pure component *i*.

The solid phase fugacity of component *i* in the mixture can be expressed as

$$f_i^s = \gamma_i^s s_i f_i^{os} \tag{2.17}$$

Where γ_i^s is the activity coefficient of component *i* in the solid phase, s_i is the mole fraction of component *i* in the solid phase, and f_i^{os} is the standard state fugacity of component *i* in the solid phase. It can also be described as the solid phase fugacity of pure component *i* (Pedersen et al, 1991).

From Equations (2.15), (2.16) and (2.17) we get

$$\gamma_i^l x_i f_i^{ol} = \gamma_i^s s_i f_i^{os} \tag{2.18}$$

$$K_i^{sl} = \frac{s_i}{x_i} \tag{2.19}$$

$$K_i^{sl} = \frac{s_i}{x_i} = \left(\frac{\gamma_i^l}{\gamma_i^s}\right)\left(\frac{f_i^{ol}}{f_i^{os}}\right) exp\left[\int_0^P \frac{\Delta V_i}{RT} dp\right] \tag{2.20}$$

Where,

γ_i^l = activity coefficient of component *i* in the liquid phase,

x_i = mole fraction of component *i* in the liquid phase,

f_i^{ol} = standard state fugacity of component *i* in the liquid phase,

γ_i^s = activity coefficient of component *i* in the solid phase,

s_i = mole fraction of component *i* in the solid phase,

f_i^{os} = standard state fugacity of component *i* in the solid phase,

v_i = Molar volume change of component *i*,

R = gas rate constant,

T = temperature,

P=Pressure.

These terms represent factors that determine K-value

$\left(\frac{f_i^{ol}}{f_i^{os}}\right)$ = Effect of Temperature,

$\left(\frac{\gamma_i^l}{\gamma_i^s}\right)$ = Effect of intermolecular interactions between components,

$\left[\int_0^P \frac{\Delta V_i}{RT} dp\right]$ = Effect of Pressure.

For solid-liquid equilibrium modelling, the change in molar volume, ΔV_i is usually small therefore negligible when pressure is not significantly changing. The relationship between the standard state fugacity of components i in the liquid phase, f_i^{ol} and in the solid phase (Lira-Galeana, 1996),

f_i^{os} , is obtained as follows:

$$\ln\left(\frac{f_i^{ol}}{f_i^{os}}\right) = \frac{\Delta H_i^f}{RT}\left(1 - \frac{T}{T_i^f}\right) \quad (2.21)$$

Such that, substituting equation 2.21 into 2.20, the solid-liquid equilibrium parameter, K_i^{sl} then becomes:

$$\boldsymbol{K_i^{sl} = \frac{s_i}{x_i} = \left(\frac{\gamma_i^l}{\gamma_i^s}\right) exp\left[\frac{\Delta H_i^f}{RT}\left(1 - \frac{T}{T_i^f}\right)\right]} \quad (2.22)$$

2.13 Wax Deposition Models

In the following, we review some of the common wax depositional models used in the petroleum industry.

2.13.1 The RRR model

The RRR (Rygg, Rydahl and Rønningsen, 1998) model is a multi-phase flow wax deposition model which predicts wax deposition in wells and pipelines. The RRR model is not applicable for laminar flow (Josh, 2017). A standard steady-state multi-phase point model is used to predict pressure drop and liquid hold-up along the pipeline. The effect of deposition on the pressure drop and temperature is calculated by integration in time. The multi-component wax model continuously estimates the wax precipitation along the pipeline and the viscosity of the composition. The wax deposition is then estimated from the diffusion of wax from the bulk fluid towards the surface of the pipeline, due to temperature gradients and shear dispersion effect. The inner pipe wall friction is varied due to wax deposition (Rygg, 1998).

The wax deposition model is divided into separate sub-models, where each sub-model concentrates on specific technical aspect and the components are treated individually. (Rygg, 1998)

The sub-models in the RRR wax depositional model are:

- Flow model to calculate the pressure drop and flow regime
- Thermodynamic Wax Model (TWM) to determine the number and properties of the different phases for each section
- Viscosity model to calculate the viscosity as function of time and location

- Wax deposition model is used to predict the amount of wax that deposits in a section of the pipeline.

The wax porosity is an important wax property and it represents the amount of oil trapped within the wax pore spaces (Karianne, 2008).

The total volume rate of deposited wax (*lwax)* is calculated as a sum of two contributing mechanism namely the molecular diffusion and the shear dispersion according to equation (2.23). Where φ is the wax porosity with values in the range of 0.6-0.9.

$$lwax = \frac{VOL_{wax}^{diff} + VOL_{wax}^{shear}}{(1-\emptyset)2\pi rL} \quad (2.23)$$

The volume rate of wax deposited by molecular diffusion imputed into the RRR model for each wax forming component *i* is obtained. According to (Hayduk, 1982), the Hayduk and Minhas correlation can be used to calculate the wax diffusion coefficient, *Di,* for component *i* in the wax phase. The molecular diffusion component is given by the equation (2.24).

$$VOL_{wax}^{diff} = \sum_{i=1}^{Nw} \frac{Di(\Delta Ci)S_f M_i}{\delta \rho_w} 2\pi rL \quad (2.24)$$

Where *Nw* is the number of wax component, *Di* is the diffusion coefficient (m^2/s), ΔCi is the concentration difference between the bulk phase and the wax phase for component *i*, S_f is the fraction of wetted perimeter by wax, M_i is the molecular weight (g/mol), *L* is the length of the pipe (m), *r* is the effective inner pipeline radius to account for wax deposition (m), ρ_w is the density of wax component *i* (kg/m^3), and δ is the thickness of the laminar sub-layer (m).

The thickness of the laminar sub-layer in the pipeline is obtained by the Bendiksen (1991) correlation in equation (2.25) where α is a correction factor used for tuning the thickness of the wax layer to conform to the experimental data.

$$\delta = \alpha \times 11.6\sqrt{2}\frac{D}{Re}\frac{1}{\sqrt{f}} \tag{2.25}$$

In equation (2.19), we define, *D* as the pipe diameter (m), Re is the Reynolds number and *f* is the friction factor. The Blasius equation is used to calculate the thickness of the sub-layer in turbulent flows (Karianne, 2008). The shear dispersion contribution in the volume of wax deposited is derived by the modified Burger et al. (1981) given in equation (2.26).

$$VOL_{wax}^{shear} = \frac{K\gamma A\emptyset_w}{\rho_w} \tag{2.26}$$

where *K* is the shear deposition constant, φ_w is the volume fraction of the deposited wax in the bulk fluid, γ is the shear rate in the oil (s^{-1}),ρ_w is the average density of wax precipitated in the bulk fluid (kg/m^3) and *A* is the surface area available for deposition (m^2) (GROUP, 2012).

The dissolved wax concentration found at the cloud point for each pressure section is calculated as follows

$$C_{w,wall} = C_{w,TWS} + \frac{dC_{wax}}{dT}_{WAT}(TWS - WDT) \tag{2.27}$$

Where $C_{W,wall}$ is the concentration of the wax at the wall obtained from the normal diffusion equation, $C_{W,TWS}$ is the concentration of wax adjusted to account for the increase in wall temperature, TWS is the wall surface temperature, WDT is the wax dissolution temperature,

WAT is the wax appearance temperature, and $\frac{dC_{wax}}{dT}_{WAT}$ is the concentration derivative with respect to temperature at the cloud point. The wax dissolution temperature is obtained as the sum of the wax appearance temperature and the dissolution difference $\Delta T_{dissolution}$ given in equation (2.28).

$$WDT = WAT + \Delta T_{dissolution} \quad (2.28)$$

The RRR model is implemented in a dissolution model of wax from the wall. It is calculated as a function of the concentration derivative of the wax for temperature change between the bulk fluid and the wall. For a wax melting process, the concentration difference condition must be present such that the concentration of wax at the wall is greater than the precipitated wax in the bulk fluid: $C_{W,wall} > C_{W,bulk}$ (GROUP, 2012). The dissolution model in the RRR provides an advantage over other wax deposition model when wax removal or wax loosening modelling is to be considered in active deposition systems. Additional discussion on this model can be found in Chapter Three.

2.13.2 Singh et al wax deposition model

Singh (2000), developed another wax deposition model using the thin-film concept. Underlining modelling principle in the thin film concept rests on the University of Michigan deposition experiments where particulate deposition was studied in the wax layer. Singh (2000), opined that a non-uniform diffusion occurs in wax deposits due to a concentration gradient existing in the sub layer of the wax deposits. It considered an internal diffusion mechanism for the waxy gel layers inducing physical gelation on the wall (Singh P. e., 2001). The initial formation of wax at the wall serves as the beginning of the deposition process while trapped oil between successive

wax layers provide opportunity for further internal diffusion for continued wax deposition. An incipient wax, gels in the 3-D network structure of the wax such that strong physical affinity between wax layer and incipient wax is produced.

The thin film wax, therefore, gels with cooling. Gelation rate depends on thecooling rate between waxy oil and pipe walls. The wax molecules diffuse to form wax deposits due to *n*-existing concentration gradient between diffusing wax molecules and the wax deposition surface, which creates a non-uniform hardening in the pipe radial direction. This confirms the porous characteristics of wax layers. The increase in the wax fraction in the wax deposit with time is called the aging of wax (Singh P. e., 2001). The Singh et al model further considers a counter diffusion process of oil molecules out of wax deposit in the wax layers. Wax deposition prediction is implemented through the coupling of the thin film approach with heat and mass balances to calculate the thickness and radial composition in pipelines. The heat mass balance is obtained from a combination of the coupled partial differential and algebraic equations found in the work of Singh (2001).

$$\frac{d\delta}{dt} = \frac{D_{ow}\frac{dC}{dr}_i(1-\emptyset(x))}{\rho x} \tag{2.29}$$

$$\frac{dx}{dt} = \frac{D_{ow}\frac{dC}{dr}_i\emptyset x2(R-\delta)}{\rho\delta(2R-\delta)} \tag{2.30}$$

Where δ is the deposit thickness, x the wax content of the deposit, R is the radius of the clean pipe and D_{ow} is the diffusion coefficient for wax in oil. $\emptyset(x)$ is a coefficient describing diffusion in a porous network and can be found by Cussler as

$$\emptyset(x) = \frac{1}{1+\alpha^2\left[\frac{x^2}{1-x}\right]} \tag{2.31}$$

Where a is the average aspect ratio of the wax crystals, t is time in secs.

$$\frac{dC}{dr} = \frac{dC}{dT} \times \frac{dT}{dr} \quad (2.32)$$

Where $\frac{dC}{dr}$ is the wax concentration gradient (1/m) of wax concentration over pipe radial coordinate *r* (m), *Dow* is the diffusion coefficient of the wax in the oil phase (m2/s), $\frac{dC}{dT}$ is the solubility coefficient of the wax crystal in the oil phase (1/°C), $\frac{dT}{dr}$ is the radial temperature gradient of the wall (°C/m). $\frac{dC}{dr_i}$ is the wax concentration gradient for component i.

The Michigan model is the only model that include the aging of the deposit. Most models stated that the wax-oil deposit has constant wax content, and the wax porosity is used as an adjustable parameter. However, experiments by (Singh P. e., 2001) proved the assumption that the composition of the deposit is time-invariant to be invalid (Karianne, 2008); (Labes-Carrier, 2002).

2.13.3 The MATZAIN model

The Matzain model is a semi-empirical kinetic model used for the prediction the wax thickness. The model is accurate and results acceptable, especially at high flow rates. The Matzain model, like the RRR model, is based on mechanisms such as molecular diffusion and shear dispersion, but shear dispersion is found to be of minor importance. Matzain (2001), proposed that the rate may be influenced by other mechanisms as well. Shear stripping will result to a reduced deposition rate, and rate enhancement may occur due to the entrapment of oil and other mechanisms.

The total wax deposition rate is expressed as follows:

$$\frac{d\delta}{dT} = -\frac{\prod_1}{1+\prod_2} D_{ow} \left[\frac{dW_w}{dT}\frac{dT}{dr}\right] \quad (2.33)$$

Where δ is the thickness of the wax layer deposited on the wall (m), D_{ow} is the diffusion coefficient(m^2/s), W_w is the concentration of wax in solution (weight %), r is the radial distance (m), and T is the temperature (°C). The term $\prod_1$ is the empirical relation for the rate enhancement due to oil being trapped in the deposited wax layer, and $\prod_2$ is the empirical relation for the rate reduction due to shear stripping.

The two empirical relations are defined as follow:

$$\prod_1 = \frac{C_1}{1-C_{oil}/100} \quad (2.34)$$

$$\prod_2 = C_2 N_{SR}^{C_3} \quad (2.35)$$

The diffusion constant is given by the Wilke and Chang correlation (C.R. Wilke, 1955), but this diffusion correlation is not sufficient to represent the proportionality constant that drives the diffusion process. C_1, C_2 *and* C_3 are three empirical constants which are correlated from the single phase and two-phase flow data. Their values were found to be: C_1 = 15.0, C_2 = 0.055 and C_3 =1.4. Also, C_{oil} is the percentage of oil trapped in wax deposit (%) and is expressed as

$$C_{oil} = 100\left(\frac{1-N_{RE,f}^{0.15}}{8}\right) \quad (2.36)$$

$$N_{RE,f} = \frac{\rho_o\left(\frac{v_{sl}}{E}\right)d_w}{\mu_{o,f}} \quad (2.37)$$

Where ρ_o is the oil density (kg/m^3), v_{sl} is the liquid superficial velocity (m/s), E is the liquid hold up, d_w is the inside diameter as a result of wax build-up (m) and $\mu_{o,f}$ is the oil viscosity (kg/(m s).

The empirical constant C_1 attempts to correct the offset in wax deposition prediction considering that flow turbulence enhances the diffusion process via turbulent eddies effect. The empirical constants C_2 and C_3 affect the wax removal due to shear stripping; however, considering that the age of the deposit increases its hardness, making the wax removal more difficult, the constants C_2 and C_3 should be changed through time.

N_{SR} is a dimensionless variable expressed in the form of a flow regime dependent Reynolds number. The variable was derived for each flow pattern.

Single phase:

$$N_{SR} = \frac{\rho_o v_o \delta}{\mu_{o,f}} \tag{2.38}$$

Intermittent/bubbly:

$$N_{SR} = \frac{\rho_m \left(\frac{v_{sl}}{E}\right) \delta}{\mu_{o,f}} \tag{2.39}$$

Annular:

$$N_{SR} = \frac{\sqrt{\rho_m} \rho_o \left(\frac{v_{sl}}{E}\right) \delta}{\mu_{o,f}} \tag{2.40}$$

Stratified smooth/wavy:

$$N_{SR} = \frac{\rho_o \left(\frac{v_{sl}}{E}\right) \delta}{\mu_{o,f}} \tag{2.41}$$

Where v_o is the oil velocity (m/s), d is the thickness of the wax layer (m) and ρ_m is the average density of the gas-oil mixture (kg/m3). (Karianne, 2008)

2.14 General Algorithm for Wax Deposition Modeling

According to Anand (2017), the algorithm for wax depositional modeling can be described using the following major steps (Figure 3.3):

- Input data—contains oil properties, pipeline dimensions, and operating conditions used to execute all the hydrodynamic and heat transfer calculations.
- Temperature profile calculation—calculate the temperature profile as function of location and time.
- Mass transfer and wax deposition mechanism—use some wax precipitation curves as input to determine the mass transfer and other processes governing the wax deposition on the wall.
- Calculate the amount of wax growth over time along the pipe wall.

In summary, wax deposition is a public problem, a critical operational challenge and one of the main flow assurance problems in the oil industry around the world including the offshore and onshore oil fields. Wax precipitates and deposits on the cold pipeline wall when the inner wall temperature falls below the wax appearance temperature, and it occurs with the paraffin components in crude oil. A lot of researchers in previous works estimate this temperature experimentally. This present study expands on the theoretical aspect of estimating WAT and the sensitivity of hydrocarbon component lumping schemes to the estimates of the wax appearance temperature.

Chapter Three

Methodology

In this chapter, the methodology is presented as the sequence of steps utilized to achieve the research objectives. The workflow describing the study methodology is presented below in Figure 3.1. The major steps of the workflow are data collection, characterization of reservoir fluid, estimation of wax appearance temperature, lumping of heavy fractions, sensitivity analysis and modelling of wax deposition.

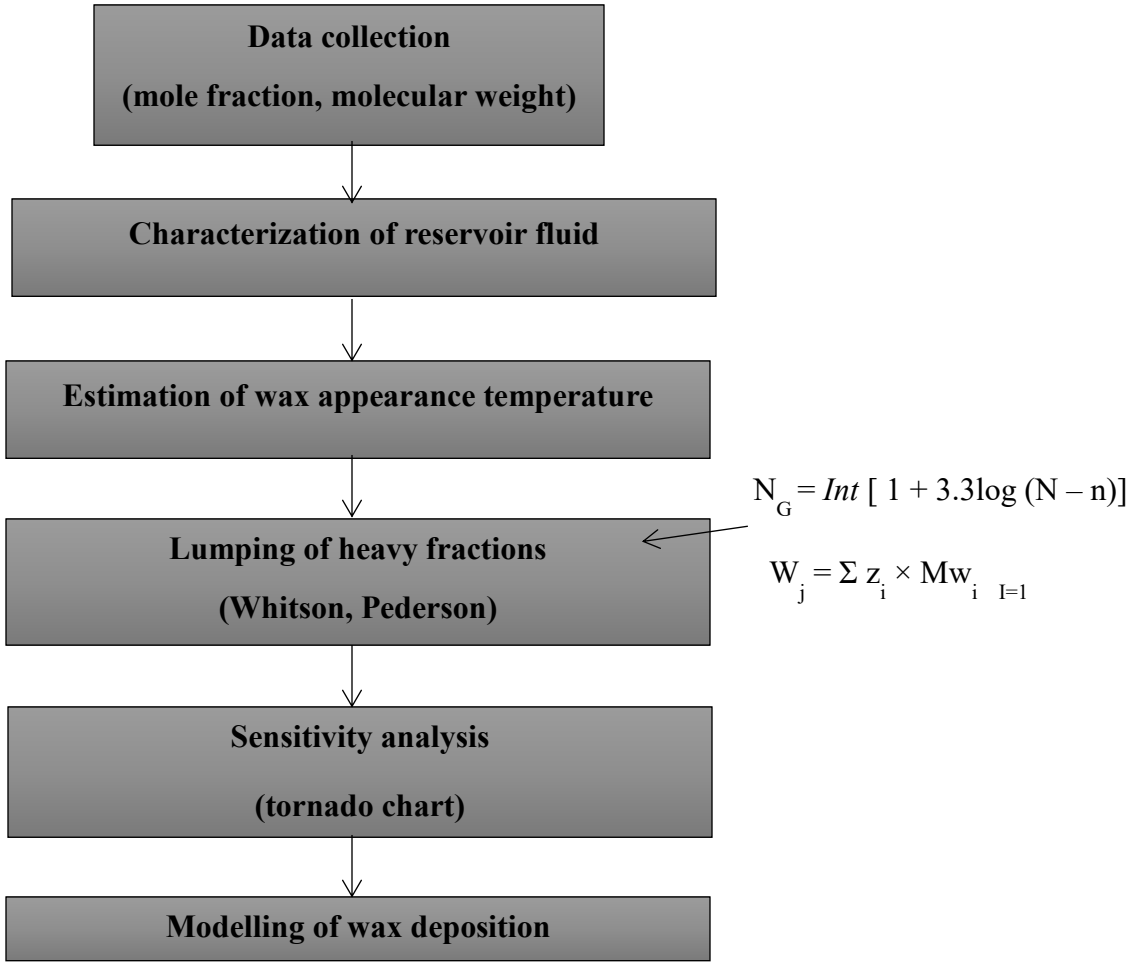

Figure 3.1: Schematic of Study Methodology

3.0 Data Collection

Three oil samples are used in this study. The compositions of the three oil samples are the primary data collected from the various publications. Data listed in Tables 3.1, 3.2 and 3.3 are used for the fluid characterization and analysis presented in this work. Note the data shown in Tables 3.2 and 3.3 are found in many journals ((Otung, 2012); (Hamidreza, 2013)). Data for Sample A (Table 3.1) is from the Niger Delta. It has 37(C2-C36+) hydrocarbon components. Oil Sample B listed in Table 3.2 is from the North Sea and it contains 32(CN1-CN30+) components. Table 3.3 shows the data for Sample C taken from one of the gas condensate oil fields, and it has 22(C1-C20+) components. The experimental WAT values used in this present study were estimated using the cross polar microscopy (CPM) method. The tables present both the mole fraction and molecular weight of each component.

Table 3.1: Oil Composition of Sample A, Niger-Delta Crude Mixture

Component	**mole %**	**Mw (g/mol)**
C2	0.36	30.07
C3	0.86	44.1
i-C4	0.32	58.12
n-C4	0.52	58.12
i-C5	0.51	72.15
n-C5	0.55	72.15
C6	1.82	84
C7	4.92	96
C8	8.75	107
C9	7.42	121

C10	6.57	134
C11	5.53	147
C12	5.85	161
C13	6.18	175
C14	5.49	190
C15	5.96	206
C16	4.58	222
C17	3.64	237
C18	3.64	251
C19	3.07	263
C20	2.83	275
C21	2.56	291
C22	2.31	300
C23	2.08	312
C24	1.96	324
C25	1.71	337
C26	1.5	349
C27	1.44	360
C28	1.29	372
C29	1.13	382
C30	1.04	394
C31	0.92	404
C32	0.71	415
C33	0.61	426
C34	0.47	437
C35	0.3	445

C36+	0.6	608

Table 3.2: Oil Composition Data of Sample B from the North Sea
Source: (Otung, 2012)

Composition	**mol %**	**MW (g/mol)**
CN1	0.2457	16
CN2	0.3433	30.1
CN3	1.2781	44.1
i-CN4	2.3328	58.1
n-CN4	0.8048	58.1
i-CN5	2.2744	72.2
n-CN5	1.8304	72.2
CN6	4.3526	86.2
CN7	7.0409	97.5
CN8	8.5073	111.1
CN9	6.2413	124.7
CN10	5.9502	138.7
CN11	4.7261	153
CN12	4.1475	167.2
CN13	4.276	179.3
CN14	3.6538	193.6
CN15	4.0267	207.9
CN16	3.0915	222.1
CN17	2.7944	236.2
CN18	2.895	250.3
CN19	2.6891	264.5

CN20	2.2191	278.6
CN21	2.0459	292.7
CN22	1.9448	306.8
CN23	1.7398	320.8
CN24	1.6283	334.9
CN25	1.466	348.9
CN26	1.2924	362.9
CN27	1.1907	376.9
CN28	1.1033	390.9
CN29	0.9935	404.9
CN30+	10.9902	442.8

Table 3.3: Oil Composition Data of Sample C
Source: (Hamidreza, 2013)

Component	**mol%**	**Mw(g/mol)**
C1	0.413506	16
C2	0.0403	30.07
C3	0.2153	44.1
i-C4	0.0539	58.12
n-C4	0.0543	58.12
i-C5	0.0515	72.15
n-C5	0.0519	72.15
C6	0.1039	84
C7	0.00347	96
C8	0.00268	107

C9	0.00207	121
C10	0.00159	134
C11	0.00123	147
C12	0.00095	161
C13	0.00073	175
C14	0.000566	190
C15	0.000437	206
C16	0.001671	259
C17	0.0307	263
C18	0.0283	275
C19	0.0256	291
C20+	0.0231	300

3.1 Characterization of Reservoir Fluid

To perform phase equilibrium calculations during reservoir fluid characterization, the critical pressure, Pc, critical temperature, Tc, and acentric factor, ω (the measure of non-sphericity (centricity) of a molecule) are required for each component contained in the mixture**.** Oil or gas condensate mixtures are made up of many components. Pedersen et al., (2015) gave the classes of the components as follows:

1) Defined components to $C_{6.}$ These are components lower than C_7. That is N_2, CO_2, H_2S, C_1, C_2, C_3, iC_4, nC_4, iC_5, nC_5, and C_6.
2) True boiling point fractions (TBP, fractions). These cover the fractions of C_7 up to $C_{30,}$ where each fraction contains different components, and information may only be available for density and the average molecular weight of each fraction.

3) Plus fraction. These are components that are too heavy to be separated into different carbon fractions and left as a lump sum. Measured quantities typically available are density, the average molecular weight and mole fractions.

A proper description of the PVT relationship for real hydrocarbon fluids is necessary for determining the volumetric and phase behavior of petroleum reservoir fluids and predicting the performance of surface separation facilities. (Akinyede O. M., 2019).

3.1.1 Characterization of a Niger-Delta Crude Mixture

The approach used to characterize the Niger-Delta crude mixture is taken from the work of Akinyede (2019). The following exponential distribution functions were used to represent the TBP fraction:

$$z_i = \exp(A + BMw_i) \tag{3.1}$$

Where A and B are adjustable parameters, and z_i and Mw_i are the mole fraction and molecular weight of ith component, respectively. For pseudo components, the molecular weight is related to the carbon number as:

$$Mw_i = 14CN_i - 4 \tag{3.2}$$

Where, CN_i is the carbon number of component i. To ensure that the distribution of pseudo components reflects the actual condition of the plus fraction, two constraints were imposed. The first constraint requires that the total mole fraction of pseudo-components be the same as the mole fraction of plus fraction expressed as:

$$\sum_{i=1}^{n} \exp(A + BMw_i) = z_{plus\ fraction} \tag{3.3}$$

Note, the summation in equation (3.3) begins from the first pseudo-component, not the first component in the mixture. The second constraint states that the average molecular weight of the pseudo-components should be the same as the molecular weight of the plus fraction, or:

$$\frac{\sum_{i=1}^{n} z_i Mw_i}{\sum_{i=1}^{n} z_i} = Mw_{plus\ fraction} \tag{3.4}$$

The molecular weight of each pseudo component was estimated using the equation (3.2). Constraints given in Equations 3.3 and 3.4 can be written as:

$$f(A,B) = \sum_{i=1}^{n} \exp(A + BMw_i) - z_{plus\ fraction} \tag{3.5}$$

$$g(A,B) = \frac{\sum_{i=1}^{n} Mw_i \exp(A+BMw_i)}{\sum_{i=1}^{n} \exp(A+BMw_i)} - Mw_{plus\ fraction} \tag{3.6}$$

Equations (3.5) and (3.6) were solved simultaneously to determine the parameters, A and, B that matches the mole fraction and molecular weight of the plus fraction.

Critical Properties and Acentric Factor Estimate

Accurate estimation of the critical properties and acentric factor is important in determining solid precipitation. Several researchers use correlations proposed by Cavet (1964) and Kesler (1976) for these estimates. (Sofyan, 2003), gave a correlation for estimating these properties (Tc, Pc, **ω**) for heavy hydrocarbon ends.

Using the method described above to characterize the Niger-Delta (ND) crude mixture gives,

$Mw_{plus\ fraction}$ = 608 g/mol

$z_{plus\ fraction} = 0.6$

The following is the procedure used to determine the other properties of Sample A.

1. The average molecular weight of pseudo-components is 608g/mol; therefore, pseudo-components ranges from CN= 36 – 51.
2. Use equation 3.2 to estimate Mw.
3. Deduce the parameters A and B from the following equations,

$$A = ln\left[\frac{z_{plus\ fraction}}{\sum_{i=1}^{n}\exp(BMw_i)}\right] \tag{3.7}$$

$$\frac{\sum_{i=1}^{n} Mw_i \exp(BMw_i)}{\sum_{i=1}^{n}\exp(BMw_i)} = Mw_{plus\ fraction} \tag{3.8}$$

Equations 3.7 and 3.8 were solved numerically using a MATLAB function to find the parameters A and B. The parameter B was solved first by plotting Molecular weight of pseudo components represented by CN =36 to 51 vs the values of B as deduced from equation 3.8. The corresponding value of B is read at the coordinate of the $Mw_{plus\ fraction}(constant\ value)$ as shown on the plot of Figure 3.2. Figure 3.2 below shows value of B at Mw= 608 g/mol from the plot of Molecular weight vs values of B.

Using this value of parameter B, A is then calculated from equation 3.7. That is,

B = 0.000689889; A = -3.694937

4. Estimate mole fractions of the pseudo components from equation 3.1.

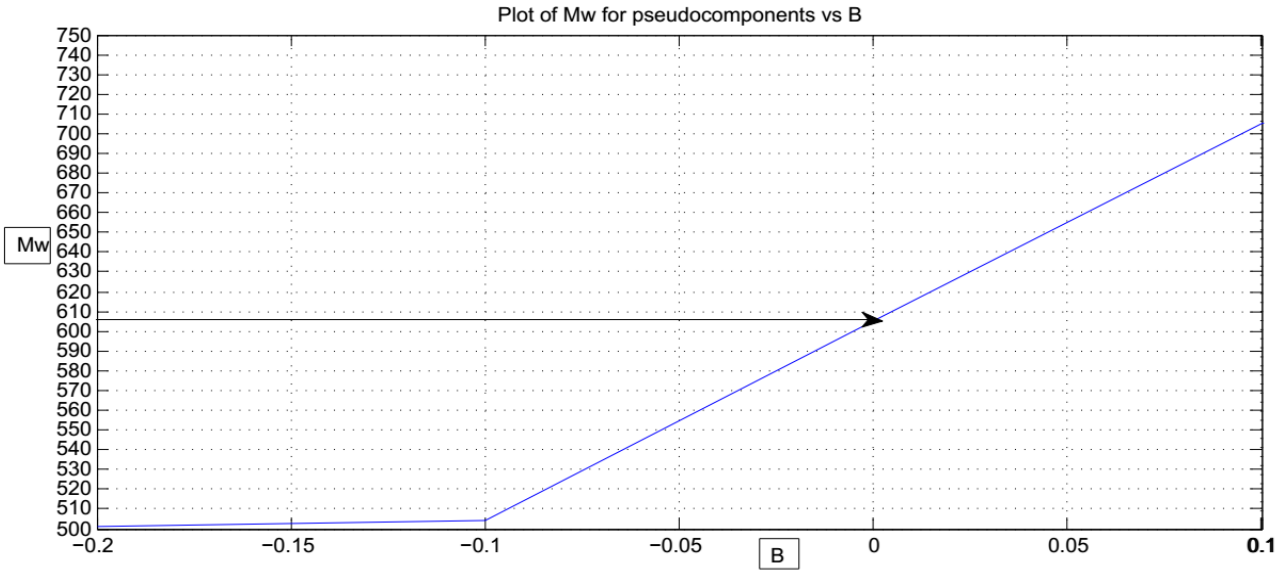

Figure 3.2: Plot of Mw(s) vs B

5. Critical properties and acentric factor were calculated from Sofyan et al., 2003.

The number of pseudo components added make up the total components in the mixture from C_2-C_{51}. Table 3.4 lists the data obtained from the characterization of the Nige-Delta Sample A.

Table 3.4: Data obtained from Characterization of Niger-Delta Sample

z	Pc (atm)	Tc (K)	ω	Mw	CN
0.0036	48.3916	300.4939	0.0994	30.07	2
0.0086	41.8850	370.1000	0.1515	44.10	3
0.0032	36.9774	424.5204	0.2023	58.12	4
0.0052	36.9774	424.5204	0.2023	58.12	4
0.0051	33.0687	469.3334	0.2518	72.15	5
0.0055	33.0687	469.3334	0.2518	72.15	5
0.0182	29.8499	507.3941	0.3001	84.00	6
0.0492	27.1377	540.3962	0.3474	96.00	7
0.0875	24.8134	569.4441	0.3936	107.00	8
0.0742	22.7954	595.3040	0.4389	121.00	9
0.0657	21.0251	618.5333	0.4833	134.00	10

0.0553	19.4588	639.5521	0.5269	147.00	11
0.0585	18.0630	658.6859	0.5696	161.00	12
0.0618	16.8115	676.1929	0.6116	175.00	13
0.0549	15.6834	692.2817	0.6529	190.00	14
0.0596	14.6620	707.1234	0.6934	206.00	15
0.0458	13.7334	720.8604	0.7333	222.00	16
0.0364	12.8860	733.6127	0.7726	237.00	17
0.0364	12.1102	745.4820	0.8112	251.00	18
0.0307	11.3979	756.5558	0.8492	263.00	19
0.0283	10.7421	766.9096	0.8866	275.00	20
0.0256	10.1368	776.6092	0.9235	291.00	21
0.0231	9.5770	785.7121	0.9599	300.00	22
0.0208	9.0581	794.2692	0.9957	312.00	23
0.0196	8.5762	802.3253	1.0310	324.00	24
0.0171	8.1278	809.9206	1.0658	337.00	25
0.0150	7.7099	817.0906	1.1002	349.00	26
0.0144	7.3199	823.8674	1.1341	360.00	27
0.0129	6.9554	830.2799	1.1675	372.00	28
0.0113	6.6142	836.3541	1.2005	382.00	29
0.0104	6.2944	842.1137	1.2331	394.00	30
0.0092	5.9943	847.5800	1.2653	404.00	31
0.0071	5.7123	852.7727	1.2970	415.00	32
0.0061	5.4472	857.7096	1.3283	426.00	33
0.0047	5.1975	862.4070	1.3593	437.00	34
0.0030	4.9623	866.8800	1.3899	445.00	35
0.00035	4.7403	871.1423	1.4200	500.00	36
0.00035	4.5308	875.2066	1.4499	514.00	37
0.00036	4.3328	879.0847	1.4794	528.00	38
0.00036	4.1455	882.7875	1.5085	542.00	39
0.00036	3.9683	886.3249	1.5373	556.00	40
0.00037	3.8004	889.7062	1.5658	570.00	41
0.00037	3.6413	892.9402	1.5939	584.00	42
0.00038	3.4904	896.0347	1.6217	598.00	43
0.00038	3.3471	898.9975	1.6492	612.00	44
0.00038	3.2110	901.8355	1.6764	626.00	45
0.00039	3.0817	904.5551	1.7033	640.00	46
0.00039	2.9588	907.1625	1.7300	654.00	47
0.00039	2.8418	909.6634	1.7562	668.00	48
0.00040	2.7304	912.0631	1.7822	682.00	49
0.00040	2.6243	914.3668	1.8080	696.00	50
0.00041	2.5234	916.5790	1.8334	710.00	51

3.1.2 Characterization of Other Crude Mixtures

Recall, we used three samples (A, B, C) in this study. Sample A was taken from the Niger Delta, and it was characterized using the procedure described earlier. The other samples (B and C) were also characterized by following the same procedure described for Sample A.

3.2 Estimation of Wax Appearance Temperature

The three methods for estimating the wax appearance temperature in this present study include the composition-based WAT models by Hosseinipour et al, (2019), the GOR-Based WAT Model by Eyitayo et al, (2020) and the Tf Correlation by Akinyede et al, (2019) discussed in Chapter Two.

Sensitivity and comparative analysis were carried out on the results estimated through these models to provide inferences as to the efficiency of each one of them.

3.3 Hydrocarbon Component Lumping Schemes

There are problems associated with hydrocarbon component lumping or pseudoization, i.e., "regrouping" the original hydrocarbon components into a smaller number without losing the predicting power of the equation of state. These problems include how to select the groups of pure components to be represented by one pseudo-component. In the following section, we describe the two lumping schemes used in the estimation of the WAT.

3.3.1 Whitson's lumping scheme

Whitson (Whitson, 1983) proposed a regrouping scheme whereby the compositional distribution of the C_{7+} fraction is reduced to only a few multiple carbon-number (MCN) groups. Whitson suggested that the number of MCN groups necessary to describe the plus fraction is given by the following empirical rule:

$$N_g = Int[\ 1 + 3.3\log\ (N - n)] \tag{3.15}$$

Where Ng is the number of MCN groups, Int is the integer, N is the number of carbon atoms of the last component in the hydrocarbon system, and n is the number of carbon atoms of the first component in the plus fraction, i.e., n = 7 for C_7. The molecular weight of each group is given by

$$M_{wi} = M_{wn}\left[\frac{M_{wN}}{M_{wn}}\right]^{1/N_g} \tag{3.16}$$

Where ;$(Mw)_{N+}$ is the molecular weight of the last reported component in the extended analysis of the hydrocarbon system, M_{C7} is the molecular weight of C_7, i = 1, 2,⋯ ,Ng.

The accuracy of the Whitson's lumping scheme can be attributed to function of the number of MCN groups, and an iterative method is used to find the molecular weight of each group.

3.3.2 Pedersen Lumping Scheme

The second lumping scheme considered in this study is developed by (Pedersen et al, 1991). Pedersen et al. (Ahmed 2010, 1989; Hong 1982; Guo and Du 1989; Lee et al. 1981; Montel and Gouel 1984; Al-Meshari 2004) suggested the process of grouping the components of

approximately the same weight fraction (equal weight fraction), which will give all hydrocarbon segments of the C_{7+} fractions equal importance. The C_{7+} fraction is divided into three or more groups that, by weight, are equal size approximately. The weight for each pseudo component, Wj, can be calculated as:

$$W_j = \frac{1}{n}\sum_{i=1} Z_i \, M_{wi} \tag{3.17}$$

Where Wj is the weight for each pseudo component, Zi is mole fraction for each i^{th} component, Mw_i is the molecular weight of the i^{th} component, and n is the desired number of pseudo-component groups.

3.3.3 Use of Pedersen Lumping Scheme for the three Samples

We now describe how the Pedersen lumping scheme was used to calculate the W_j in equation (3.17) for the three samples.

For sample A, $W_j = \frac{\sum Z_i M_{wi}}{n} = \frac{202.9087}{n}$ (3.18)

Consider the HOS-1 correlation.

The desired number of pseudo-component groups is 4. According to equation (3.18), the values of W_j groups are,

$$W_j = \frac{\sum Z_i M_{wi}}{n} = \frac{202.9087}{4} = 50.73 \tag{3.19}$$

Now, consider the HOS-2 correlation.

The desired number of pseudo-component groups is 3. Applying equation (3.18), the value of W_j is given by,

$$W_j = \frac{\sum Z_i M_{wi}}{n} = \frac{202.9087}{3} = 67.64 \quad (3.20)$$

Consider the T_f correlation by Akinyede et al (2019)

The desired number of pseudo-component groups is 6. Using equation 3.17, the value of W_j groups are

$$W_j = \frac{\sum Z_i M_{wi}}{n} = \frac{202.9087}{6} = 33.8 \quad (3.21)$$

The above stated procedure was used to find the values of the W_j groups for Sample B and Sample C. Table 3.5 summarizes the results obtained in this case.

Table 3.5: Summary of Values of Pedersen W_j for Samples A, B and C

Sample	Pedersen, W_j Equation	Correlation	Desired No of Pseudo Component Group, n	Values of W_j
Sample A	$W_j = \frac{\sum Z_i M_{wi}}{n}$ 202.0987	HOS-1	4	50.73
		HOS-2	3	67.37
		Tf	6	33.68
Sample B	$W_j = \frac{\sum Z_i M_{wi}}{n}$ 207.165	HOS-1	4	51.79
		HOS-2	3	69.06
		Tf	5	41.43
Sample C	$W_j = \frac{\sum Z_i M_{wi}}{n}$ 72.21061	HOS-1	4	18.05
		HOS-2	3	24.07
		Tf	4	18.05

3.4 Sensitivity analysis

Sensitivity Analysis is a tool used in modeling to analyze how the different independent variables affect a specific dependent variable under certain specific conditions. In general, sensitivity analysis is used in a wide range of fields, ranging from biology and geography to economics and engineering. In this study, the dependent variable is the wax appearance temperature (Twax), and the independent variables are the total content (wt %) of hydrocarbon pseudo components (X1, X2, X3, X4). The sensitivity analysis was carried out for two oil samples. The uniform distribution was used to define the input variables and the simulation was run using @Risk software (Palisade, 2020). A tornado chart was used to show how sensitive the WAT is to the different lumping schemes (Pedersen et al, 1991; Whitson, 1983) which were used to regroup the hydrocarbon components (X1, X2, X3, X4) as they are changed over the allowed ranges (minimum, maximum).

3.5 Modelling of Wax Deposition

Thermodynamic models for wax precipitation are used to calculate the amount of solid wax precipitated as a function of pressure, temperature, and fluid composition. Wax precipitation does not necessarily lead to solid deposition. Thermodynamic models for solid/liquid K values have been coupled with models for predicting the wax deposition in pipelines. According to Svendsen, there are certain conditions that must be met for wax deposition to occur in pipelines (Svendsen, 1993). These conditions include:

1. Pipeline wall temperature must be below the wax appearance temperature (WAT) for the fluid.
2. Negative radial temperature gradient must be present in the flow. That is, the wall temperature must be lower than the centerline temperature. A zero gradient implies that no deposition will occur.
3. Wall friction must be large enough so that wax crystals can stick to the wall.

3.5.1 General Algorithm for Wax Modelling

Figure 3.3 shows the major steps used in wax depositional modeling presented in this study (Anand, 2017)

.

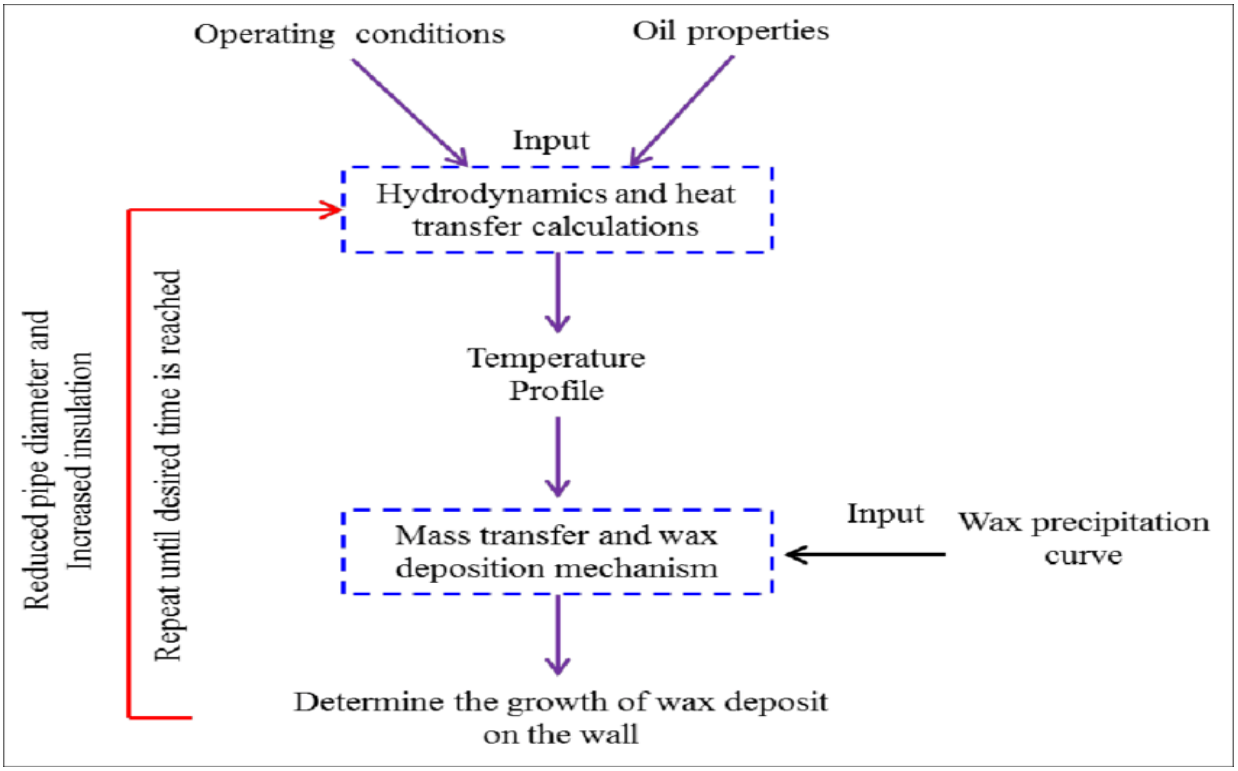

Figure 3.3: General Algorithm for wax modelling

Source: (Anand, 2017)

3.5.2 Case Study: DEEIVE Field Pipeline

The case study of wax depositional modeling is described for a Niger-Delta field. Sample A gotten from the DEEIVE FIELD in the Niger-Delta was used in this exercise. The sample has an estimated wax appearance temperature of 304K and wax content of 14%wt. The input data for the simulation are presented in Table 3.6.

Table 3.6: Physical Properties of Crude and Pipe Dimensions

Variable	Symbol	Value	Unit
Inner pipe diameter	d	0.02	m
Wall thickness	Δr_{wall}	0.015	m
Pipe length	L	1000	m
Ambient temperature	T_{sea}	4	℃
Inlet temperature	T_{inlet}	25	℃
Average Velocity of flow	u	0.0189	m/s
Density of oil	ρ_{oil}	855	kg/m^3
Density of wax	ρ_{wax}	855	kg/m^3
Dynamic viscosity of oil	μ_{oil}	0.5	mPa.s
Activation energy	E_A	30500	J/mol
Molecular volume	V_a	430	cm^3/mol
Heat capacity of oil	C_p	2300	J/kg.K
Aspect ratio of wax crystal	α	3	-
Thermal conductivity of oil	k_{oil}	0.579	W/m.K
Thermal conductivity of wax	k_{wax}	0.75	W/m.K

Thermal conductivity of pipe	k_{pipe}	0.70	W/m.K
Heat capacity of pipe material	C	502.4	J/kg.K
Overall heat transfer coefficient	U	0.25	W/m^2K
Time step	Δt	60	min
Number of steps in radial direction	n_j	100	-
Number of steps in axial direction	n_i	10000	-

The wax depositional thickness is simulated using the model proposed by MATZAIN, (1999), and Singh et al, (2001) Model discussed earlier in Chapter Two. The numerical model proposed by Stubsjoen in (Marte, 2013) was also used to calculate the deposit wax thickness along the pipeline for simulation times of 1, 2, 7, 20, and 30 days. MATLAB programs were written to model the wax deposition in the section of the pipeline as a function of time. Refer to the Appendix A for the MATLAB codes.

The major assumptions used in the Stubsjoen model (Marte, 2013) include:

- The fluid is assumed to be incompressible; it is treated as a Newtonian fluid and the density of wax is assumed equal to the density of oil.
- Above the WAT the flow is single-phase and below it is a two-phase mixture of liquid oil and solid wax. The maximum amount of wax dissolved in solution is determined by the WAT and the solubility function.
- Zero water content and zero gas rate in the pipeline is assumed, and the surrounding seawater is assumed to hold a constant temperature of 4℃. To calculate the effective thermal conductivity of the deposit, the effective medium theory (Wang, 2006; Awad,

2008) has been applied. To calculate the inner convective heat transfer coefficient, the Dittus-Boelter (Dittus and Boetler, 1930) correlation is used.

- The fluid flow is treated as one dimensional and the fluid velocity assumed constant. No shear removal is accounted for and there is no thermal insulation of the pipeline. The precipitation kinetics of wax is accounted for by a precipitation rate constant, correlating the heat and mass transfer phenomena.
- The solid wax content in the deposit is assumed to increase with time. The growth rate of the paraffin wax deposit is calculated as the difference in radial flux from the bulk to the oil/deposit interface and the flux from the interface into the deposit.

The results obtained from the execution of the proposed methodology using the input data from Sample A, Sample B, and Sample C are presented in the next chapter.

Chapter Four

Results and Discussions

The results obtained from this study are presented in this chapter. The results were discussed to gain some insights into the estimation of wax appearance temperature and its application to wax depositional modeling.

4.0 Results of Estimating WAT

Table 4.1 below shows the experimental and predicted wax appearance temperatures and their absolute deviations (AD). A comparison of the experimental versus theoretical WAT for Sample A indicated that the HOS-1 model was the least accurate with an absolute deviation (AD) of 7.9%, while the AD for HOS-2 is 4.5%, GOR-based and Tf correlations had ADs of 4.6%, and 1.7%, respectively. The results from HOS-2 and GOR-based correlations are about the same for Sample A. Table 4.1 also shows that the WAT from the PVTsim software with an AD of 1.3% is more accurate compared to the results from the HOS-1, HOS-2, GOR-based and T_f correlations. The superior performance of the Hosseinipour et al HOS-2 model over the HOS-1 model agrees with the observations made by (Hosseinipour et al, 2019) and (Eyitayo, et al., 2020) from the results of the validation tests performed on both correlations.

Table 4.1: WAT Predicted Using Theoretical Models

SAMPL	**EXPT WAT (K)**	**HOS-1 WAT (K)**	**AD** (%)	**HOS-2 WAT (K)**	**AD** (%)	**GOR-Based WAT (K)**	**AD** (%)	**T_f correlation WAT**	**AD** (%)	**PVTSim 20**	**AD (%)**

E								**(K)**			
A	304	280.9	7.9	290.9	4.5	290.6	4.6	299	1.7	300	1.3
B	322	310.8	3.9	320.7	0.4	315.3	2.3	320.80	0.4	320.14	0.5
C	312	319.5	2.6	307.9	1.4	310.3	0.6	315	1.0	315.5	1.1

For Sample B and Sample C, the results from Table 4.1 show that the HOS-2 model and the T_f correlations outperformed the HOS-1 model. For these two samples, both T_f correlation and PVTSim20 software gave about the same accuracy. The improved performance of the T_f correlations compared to the other widely WAT correlations has been demonstrated by Akinyede in 2019. (Akinyede O. M., 2019).

4.1 Results of Hydrocarbon Pseudo Component Lumping Schemes

The results presented in the previous section did not consider any explicit lumping scheme such as the (Whitson, 1983) and (Pedersen et al, 1991) lumping schemes. The results obtained for the three samples after using the two lumping schemes are presented below.

4.1.1 WHITSON Pseudo Component Lumping Scheme

Table 4.2 shows the result after lumping the original hydrocarbon components of Sample A into new pseudo components using the scheme proposed by (Whitson, 1983).

4.1.1.1 WHITSON Pseudoization for Sample A for HOS-1 and HOS-2 models

For the HOS-1 model, the first pseudo component includes all components with a molecular weight in the range of 30.07 to 58.12 with an Mwi of 63.7641. This group then includes C_2 to n-C_4. The second pseudo component contains all components with a molecular weight higher than 58.12 to a molecular weight of 134 with an Mwi of 135.2130. This group includes i-C_5 to C_{10}. The third pseudo component includes components with molecular weight higher than 134 to a molecular weight of 275 with an Mwi of 286.7220. Therefore, this group includes C_{11} to C_{20}. The fourth pseudo component includes all the remaining components with an Mwi of 608.0001, i.e., C_{21} to C_{36+}.

The hydrocarbon components defined in the HOS-2 model which is a three-pseudo component model were also regrouped using this scheme. The first pseudo component includes all hydrocarbon components with a molecular weight ranging from 30.07 to 72.15 with an Mwi of 81.9200; this group includes C_2 to n-C_5. The second pseudo component contains all components with a molecular weight higher than 72.15 to a molecular weight of 222 and Mwi of 223.1757. This group includes C_6 to C_{16}. The third pseudo component is a grouping of C_{17} to C_{36+}; it includes hydrocarbon components with a molecular weight higher than 222 to a molecular weight of 608 and the Mwi of 608.0001.

4.1.1.2 WHITSON Pseudoization for Sample A for T_f Correlation

The T_f correlation was lumped into six-pseudo components. The first pseudo component includes all C_2 and C_3 components with a molecular weight in the range of 30.07 to 44.1 with an Mwi of 49.632. The second pseudo component contains all components with a molecular weight higher than 44.1 to a molecular weight of 72.15 and Mwi of 81.920. This group includes i-C_4 to

n-C_5. The third pseudo component is grouping of C_6 to C_{10}; it includes components with molecular weight higher than 72.15 to molecular weight of 134 and the Mwi of 135.2130. The fourth pseudo component groups C_{11} to C_{16} including components with a molecular weight higher than 134 to a molecular weight of 222 and Mwi of 223.1756. The fifth group is the lumping of C_{17}-C_{27} with an Mwi of 368.3624; and the sixth group includes C_{28}-C_{36+} pseudo components with Mwi of 608.0001. Table 4.2 shows the results of the application of the Whitson lumping scheme to Sample A.

Table 4.2: Lumped fractions for Sample A using Whitson pseudoization scheme

Component	**Zi**	**Mw**	**Mwi (HOS-1 MODEL)**	**Mwi (HOS-2 MODEL)**	**Mwi (T_f correlation)**
C2	0.0036	30.07	63.7641		
C3	0.0086	44.1			49.6320
i-C4	0.0032	58.12			
n-C4	0.0052	58.12		81.9200	
i-C5	0.0051	72.15			81.9200
n-C5	0.0055	72.15			
C6	0.0182	84	135.2130		
C7	0.0492	96			
C8	0.0875	107			135.2130
C9	0.0742	121			
C10	0.0657	134			
C11	0.0553	147		223.1757	
C12	0.0585	161			
C13	0.0618	175			

C14	0.0549	190			223.1756
C15	0.0596	206	286.7220		
C16	0.0458	222			
C17	0.0364	237			
C18	0.0364	251			
C19	0.0307	263			
C20	0.0283	275			
C21	0.0256	291			
C22	0.0231	300			368.3624
C23	0.0208	312			
C24	0.0196	324			
C25	0.0171	337		608.0001	
C26	0.015	349			
C27	0.0144	360			
C28	0.0129	372	608.0001		
C29	0.0113	382			
C30	0.0104	394			
C31	0.0092	404			608.0001
C32	0.0071	415			
C33	0.0061	426			
C34	0.0047	437			
C35	0.003	445			
C36+	0.006	608			

4.1.1.3 WHITSON Pseudoization for Sample B for HOS-1 and HOS-2 models

Table 4.3 shows the result after regrouping Sample B into new pseudo components using the (Whitson, 1983) lumping scheme. For the HOS-1 model, the first pseudo component includes all components with a molecular weight in the range of 16 to 30.1 with an Mwi of 36.6980. This group then includes C_1 and C_2. The second pseudo component is the C_3 to n-C_5 grouping which contains all components with a molecular weight higher than 30.1 to a molecular weight of 72.2 with an Mwi of 84.1713. The third pseudo component includes components with a molecular weight higher than 72.2 to a molecular weight of 179.3 with an Mwi of 193.0571. Therefore, this group includes C_6 to C_{13}. The fourth pseudo component includes all the remaining components with an Mwi of 442.8000, i.e., C_{14} to C_{30+}.

The hydrocarbon components defined in the HOS-2 model which is a three-pseudo component model were also regrouped using the Whitson pseudoization scheme. The first pseudo component includes all components with a molecular weight in the range of 16 to 44.1 with an Mwi of 48.3967; this group contains C_1 to C_3. The second pseudo component contains all components with a molecular weight higher than 44.1 to a molecular weight of 138.7 with an Mwi of 146.3901. This group includes i-C_4 to C_{10}. The third pseudo component is a grouping of C_{11} to C_{30+} to include all components with a molecular weight higher than 138.7 to a molecular weight of 442.8 with an Mwi of 442.8.

4.1.1.4 WHITSON Pseudoization for Sample B for T_f Correlation

For Sample B, the hydrocarbon components were lumped into five pseudo components for the T_f correlation. The first pseudo component combines C_1 and C_2; it includes all components with a molecular weight in the range of 16 to 30.1 with an Mwi of 31.0840. For the second pseudo

component, the C_3 to n-C_4 were grouped to include all components with a molecular weight higher than 30.1 to a molecular weight of 58.1 with an Mwi of 60.3886. The third pseudo component includes components with a molecular weight higher than 58.1 to a molecular weight of 111.1 with an Mwi of 117.3201. Hence, this group includes i-C_5 to C_8. The fourth pseudo component is a grouping of C_9 to C_{16} to include components with a molecular weight higher than 111.1 to a molecular weight of 222.1 with an Mwi of 227.9240. The fifth pseudo component includes a grouping of the components with a molecular weight higher than 222.1 to a molecular weight of 442.8; this group has an Mwi of 442.8000 and it includes C_{17} to C_{30+}. The results of the application of the Whitson lumping scheme to Sample B are shown in Table 4.3.

Table 4.3: Lumped fractions for Sample B using Whitson pseudoization scheme

Component	**Zi**	**Mw**	**Mwi (HOS-1 MODEL)**	**Mwi (HOS-2 MODEL)**	**Mwi (T_f correlation)**
C1	0.002457	16	36.6980	48.3967	31.0840
C2	0.003433	30.1			
C3	0.012781	44.1	84.1713	146.3901	60.3886
i-C4	0.023328	58.1			
n-C4	0.008048	58.1			
i-C5	0.022744	72.2			117.3201
n-C5	0.018304	72.2			
C6	0.043526	86.2	193.0571		
C7	0.070409	97.5			
C8	0.085073	111.1			
C9	0.062413	124.7			
C10	0.059502	138.7			

C11	0.047261	153			
C12	0.041475	167.2			
C13	0.04276	179.3			227.9240
C14	0.036538	193.6			
C15	0.040267	207.9			
C16	0.030915	222.1			
C17	0.027944	236.2			
C18	0.02895	250.3			
C19	0.026891	264.5			
C20	0.022191	278.6		442.8000	
C21	0.020459	292.7	442.8000		
C22	0.019448	306.8			
C23	0.017398	320.8			442.8000
C24	0.016283	334.9			
C25	0.01466	348.9			
C26	0.012924	362.9			
C27	0.011907	376.9			
C28	0.011033	390.9			
C29	0.009935	404.9			
C30+	0.109902	442.8			

4.1.1.5 WHITSON Pseudoization of Sample C hydrocarbon components

Table 4.4 shows the result after lumping the hydrocarbon components of Sample C into new pseudo components using the (Whitson, 1983) pseudoization scheme. The HOS-1 and the T_f correlation were lumped into four pseudo components having the same results for the Mwi. The

first pseudo component includes all components with a molecular weight in the range of 16 to 30.07 with an Mwi of 33.2943. This group includes C_1 and C_2. The second pseudo component is the grouping of the C_3 to n-C_4 and it contains all the components with a molecular weight higher than 30.07 to a molecular weight of 58.12 with an Mwi of 69.282. The third pseudo component includes the components in the group, i-C_5 to C_{10}, with a molecular weight higher than 58.12 to a molecular weight of 134 and the Mwi of 144.1687. The fourth pseudo component includes all the remaining components with an Mwi of 300.0000, i.e., C_{11} to C_{20+}.

For Sample C, the hydrocarbon components defined in the HOS-2 model which is a three-pseudo component model were also regrouped using the (Whitson, 1983) scheme. The first pseudo component includes all components with a molecular weight in the range of 16 to 30.07 with an Mwi of 42.5063; this group includes C_1 and C_2. For the second pseudo component, the C_3 to C_7 were grouped to contain all components with a molecular weight higher than 30.07 to a molecular weight of 96 with an Mwi of 112.9243. The third pseudo component includes all the components with a molecular weight higher than 96 to a molecular weight of 300 and the Mwi of 300; this group includes C_8 to C_{20+}. The results of the application of the Whitson lumping scheme to Sample C are shown in Table 4.4.

Table 4.4: Lumped fractions for sample C using Whitson pseudoization scheme

Component	Zi	Zi	Mw	Mwi (HOS-1 MODEL)	Mwi (HOS-2 MODEL)	Mwi (T_f correlation)
C1	0.413506	0.413506	16	33.2943	42.5063	33.2943
C2	0.0403	0.0403	30.07			
C3	0.2153	0.2153	44.1			

i-C4	0.0539	0.0539	58.12	69.2820		69.2820
n-C4	0.0543	0.0543	58.12			
i-C5	0.0515	0.0515	72.15		112.9243	
n-C5	0.0519	0.0519	72.15			
C6	0.1039	0.1039	84	144.1687		144.1687
C7	0.00347	0.00347	96			
C8	0.00268	0.00268	107			
C9	0.00207	0.00207	121			
C10	0.00159	0.00159	134			
C11	0.00123	0.00123	147		300.0000	
C12	0.00095	0.00095	161			
C13	0.00073	0.00073	175	300.0000		300.0000
C14	0.000566	0.000566	190			
C15	0.000437	0.000437	206			
C16	0.001671	0.001671	259			
C17	0.0307	0.0307	263			
C18	0.0283	0.0283	275			
C19	0.0256	0.0256	291			
C20+	0.0231	0.0231	300			

4.1.2 PEDERSEN Pseudo Component Lumping Scheme

The second lumping scheme studied in this work is the Pedersen pseudoization scheme. The results from this lumping scheme for all three samples are shown in Tables 4.5 through 4.7.

4.1.2.1 PEDERSEN Pseudoization for Sample A for HOS-1 and HOS-2 models

Table 4.5 lists the results after lumping the hydrocarbon components of Sample A into new pseudo components using the (Pedersen et al, 1991) pseudoization scheme. For the Hosseinipour et al HOS-1 model, which is a four-pseudo component model, the weight for each pseudo component, W_j groups are 50.73. The first pseudo component includes all components with a molecular weight in the range of 30.07 to 147; this group includes C_2 to C_{11}. For the second pseudo component, the C_{12} to C_{16} are grouped to contains all components with a molecular weight higher than 147 to a molecular weight of 222. The third pseudo component includes components in a group of C_{17} to C_{23} with a molecular weight higher than 222 to a molecular weight of 312. The fourth pseudo component combines all the remaining components with a molecular weight higher than 312 to a molecular weight of 608 into; this group includes C_{24} to C_{36+}.

For HOS-2 model, which is a three-pseudo component model, the weight for each pseudo component, W_j groups are 67.64. The first pseudo component is a grouping of all components with a molecular weight in the range of 30.07 to 175, this group includes C_2 to C_{13}. The second pseudo component contains all components with a molecular weight higher than 175 to a molecular weight of 275, this group includes C_{14} to C_{20}. The third pseudo component includes components with a molecular weight higher than 275 to a molecular weight of 608, this group includes C_{21} to C_{36+}.

4.1.2.2 PEDERSEN Pseudoization for Sample A for T_f correlation

For the T_f correlation, the weight for each pseudo component, W_j groups are 33.80. This correlation uses six (6) groups of pseudo components for Sample A. The first pseudo component

combines all components with a molecular weight in the range of 30.07 to 134 into one group; this group includes C_2 to C_{10}. The second pseudo component is a grouping of C_{11} to C_{14} to contain all components with a molecular weight higher than 134 to a molecular weight of 190. For the third pseudo component, the C_{15} to C_{17} were lumped to include components with a molecular weight higher than 190 to a molecular weight of 237. The fourth pseudo component contains all components with a molecular weight higher than 237 to a molecular weight of 291; this group includes C_{18} to C_{21}. The fifth pseudo component is a group of C_{22} to C_{26} which includes components with a molecular weight higher than 291 to a molecular weight of 349. The sixth pseudo component contains all components with a molecular weight higher than 349 to a molecular weight of 608, and this group includes C_{27} to C_{36+}. Table 4.5 shows the results of the application of the Pedersen lumping scheme to Sample A.

Table 4.5: Lumped fractions for Sample A using Pedersen pseudoization scheme

Component	**Zi**	**Mw**	**ZiMwi**	**(HOS-1 MODEL)** W_j = 50.73	**(HOS-2 MODEL)** W_j = 67.64	**(T_f correlation)** W_j = 33.80
C2	0.0036	30.07	0.108252			
C3	0.0086	44.1	0.37926			
i-C4	0.0032	58.12	0.185984			
n-C4	0.0052	58.12	0.302224			
i-C5	0.0051	72.15	0.367965			
n-C5	0.0055	72.15	0.396825			C2-C10
C6	0.0182	84	1.5288	C2-C11	C2-C13	
C7	0.0492	96	4.7232			

C8	0.0875	107	9.3625			
C9	0.0742	121	8.9782			
C10	0.0657	134	8.8038			
C11	0.0553	147	8.1291			C11-C14
C12	0.0585	161	9.4185	C12-C16		
C13	0.0618	175	10.815			
C14	0.0549	190	10.431		C14-C20	
C15	0.0596	206	12.2776			C15-C17
C16	0.0458	222	10.1676			
C17	0.0364	237	8.6268	C17-C23		
C18	0.0364	251	9.1364			C18-C21
C19	0.0307	263	8.0741			
C20	0.0283	275	7.7825			
C21	0.0256	291	7.4496			
C22	0.0231	300	6.93			C22-C26
C23	0.0208	312	6.4896			
C24	0.0196	324	6.3504			
C25	0.0171	337	5.7627			
C26	0.015	349	5.235			
C27	0.0144	360	5.184			

C28	0.0129	372	4.7988	C24-C36+	C21-C36+	C27-C36+
C29	0.0113	382	4.3166			
C30	0.0104	394	4.0976			
C31	0.0092	404	3.7168			
C32	0.0071	415	2.9465			
C33	0.0061	426	2.5986			
C34	0.0047	437	2.0539			
C35	0.003	445	1.335			
C36+	0.006	608	3.648			
			∑ZiMwi = 202.9087			

4.1.2.3 PEDERSEN Pseudoization for Sample B for HOS-1 and HOS-2 models

Table 4.6 shows the results after lumping the hydrocarbon components of Sample B into new pseudo components using the (Pedersen et al, 1991) pseudoization scheme. For the four-pseudo component HOS-1 model, the weight for each pseudo component, W_j group is 51.79. The first pseudo component includes all components with a molecular weight in the range of 16 to 153; this group includes C_1 to C_{11}. The C_{12} to C_{18} formed second pseudo component group; it contains all components with a molecular weight higher than 153 to a molecular weight of 250.3. For the third pseudo component, C_{19} to C_{24} are lumped to include all components with a molecular weight higher than 250.3 to a molecular weight of 334.9. The fourth pseudo component includes

all the remaining components with a molecular weight higher than 334.9 to a molecular weight of 442.8, and this group includes C_{25} to C_{30+}.

For the three-pseudo component HOS-2 model, the weight for each pseudo component, W_j group is 69.06. The first pseudo component combines all components with a molecular weight in the range of 16 to 179.3 into one group; this group includes C_1 to C_{13}. The second pseudo component is a group of the C_{14} to C_{24}; it contains all components with a molecular weight higher than 179.3 to a molecular weight of 334.9. The third pseudo component includes components with a molecular weight higher than 334.9 to a molecular weight of 442.8, and this group includes C_{25} to C_{30+}.

4.1.2.4 PEDERSEN Pseudoization for Sample B for T_f correlation

The T_f correlation requires five (5) groups of pseudo components for Sample B. For T_f correlation, the weight for each pseudo component, W_j group is 41.43. The first pseudo-component includes all components with a molecular weight in the range of 16 to 111.1; this group includes C_1 to C_8. The hydrocarbon components, C_9 to C_{14}, formed the second pseudo component group. It contains all components with a molecular weight higher than 111.1 to a molecular weight of 193.6. For the third pseudo component, C_{15} to C_{20} were lumped to include all the components with a molecular weight higher than 193.6 to a molecular weight of 278.6. The fourth pseudo component contains all components with a molecular weight higher than 278.6 to a molecular weight of 404.9 and this group includes C_{21} to C_{29}. The fifth pseudo component includes all the remaining hydrocarbon components i.e., C_{30+}. Table 4.6 shows the results of the application of the Pedersen lumping scheme to Sample B.

Table 4.6: Lumped fractions for sample B using Pedersen pseudoization scheme

Component	**Zi**	**Mw**	**ZiMwi**	**(HOS-1 MODEL)** W_j = 51.79	**(HOS-2 MODEL)** W_j = 69.06	**(T_f correlation)** W_j = 41.43
C1	0.002457	16	0.039312	C1-C11	C1-C13	C1-C8
C2	0.003433	30.1	0.103333			
C3	0.012781	44.1	0.563642			
i-C4	0.023328	58.1	1.355357			
n-C4	0.008048	58.1	0.467589			
i-C5	0.022744	72.2	1.642117			
n-C5	0.018304	72.2	1.321549			
C6	0.043526	86.2	3.751941			
C7	0.070409	97.5	6.864878			
C8	0.085073	111.1	9.45161			
C9	0.062413	124.7	7.782901			C9-C14
C10	0.059502	138.7	8.252927			
C11	0.047261	153	7.230933			
C12	0.041475	167.2	6.93462	C12-C18		
C13	0.04276	179.3	7.666868			
C14	0.036538	193.6	7.073757			
C15	0.040267	207.9	8.371509			
C16	0.030915	222.1	6.866222			
C17	0.027944	236.2	6.600373			

C18	0.02895	250.3	7.246185		C14-C24	C15-C20
C19	0.026891	264.5	7.11267	C19-C24		
C20	0.022191	278.6	6.182413			
C21	0.020459	292.7	5.988349			C21-C29
C22	0.019448	306.8	5.966646			
C23	0.017398	320.8	5.581278			
C24	0.016283	334.9	5.453177			
C25	0.01466	348.9	5.114874	C25-C30+	C25-C30+	
C26	0.012924	362.9	4.69012			
C27	0.011907	376.9	4.487748			
C28	0.011033	390.9	4.3128			
C29	0.009935	404.9	4.022682			
C30+	0.109902	442.8	48.66461			C30+
			∑ZiMwi = 207.165			

4.1.2.5 PEDERSEN Pseudoization of Hydrocarbon Components of Sample C

Table 4.7 shows the results after lumping the hydrocarbon components of Sample C into new pseudo components using the (Pedersen et al, 1991) pseudoization scheme. For the three-pseudo component HOS-2 model, the weight for each pseudo component, W_j group is 24.07 The first pseudo component combines C_1 to n-C_4 to capture all components with a molecular weight in the

range of 16 to 58.12. The second pseudo component lumps i-C_5 to C_{17} into one group and it contains all components with a molecular weight higher than 58.12 to a molecular weight of 263. The C_{18} to C_{30+} are grouped as the third pseudo component. It includes all the components with a molecular weight higher than 263 to a molecular weight of 442.8.

For the HOS-1 model and T_f correlation, the hydrocarbon components of Sample C were lumped into four (4) groups. The weight for each pseudo component, W_j group is 18.05. The first pseudo component includes all components with a molecular weight in the range of 16 to 44.1, and this group includes C_1 to C_3. For the second pseudo component, i-C_4 to C_6 were lumped to contain all components with a molecular weight higher than 44.1 to a molecular weight of 84. The third pseudo component combines the C_7 to C_{18} components into one group with a molecular weight higher than 84 to a molecular weight of 275. The fourth pseudo component includes all the remaining components with a molecular weight higher than 275 to a molecular weight of 442.8, and this group includes C_{19} to C_{30+}. Table 4.7 shows the results of the application of the Pedersen lumping scheme to Sample C.

Table 4.7: Lumped fractions for sample C using Pedersen pseudoization scheme

Component	**Zi**	**Mw**	**ZiMwi**	**(HOS-1 MODEL)** W_j = 18.05	**(HOS-2 MODEL)** W_j = 24.07	**(T_f correlation)** W_j = 18.05
C1	0.413506	16	6.616096	C1-C3	C1-n-C4	C1-C3
C2	0.0403	30.07	1.211821			
C3	0.2153	44.1	9.49473			

i-C4	0.0539	58.12	3.132668	i-C4-C6		i-C4-C6
n-C4	0.0543	58.12	3.155916			
i-C5	0.0515	72.15	3.715725		i-C5-C17	
n-C5	0.0519	72.15	3.744585			
C6	0.1039	84	8.7276			
C7	0.00347	96	0.33312	C7-C18		C7-C18
C8	0.00268	107	0.28676			
C9	0.00207	121	0.25047			
C10	0.00159	134	0.21306			
C11	0.00123	147	0.18081			
C12	0.00095	161	0.15295			
C13	0.00073	175	0.12775			
C14	0.000566	190	0.10754			
C15	0.000437	206	0.090022			
C16	0.001671	259	0.432789			
C17	0.0307	263	8.0741			
C18	0.0283	275	7.7825		C18-C20+	
C19	0.0256	291	7.4496	C19-C20+		C19-C20+
C20+	0.0231	300	6.93			
			∑ZiMwi = 72.21061			

It was observed from the results that the accuracy of the lumping scheme proposed by (Pedersen et al, 1991) was not high compared to the results from the Whitson (1983) scheme. This deficiency can be explained by limitation of number of groups used in the correlations and the approximation of the weight for each pseudo component. This observation agrees with the work done by (Hamidreza, 2013).

Tables 4.8, 4.9 and 4.10 below show the experimental and predicted wax appearance temperatures and their absolute deviations after lumping the hydrocarbon components using the Whitson (Whitson, 1983) and Pedersen (Pedersen et al, 1991) pseudoization schemes for Samples A, B and C, respectively. These lumping schemes were coded as MATLAB computer programs to estimate the theoretical WAT of each sample using the various correlations.

Table 4.8 shows the results of the WAT for Sample A after regrouping the pseudo-components as listed in Table 4.5. For the Whitson's lumping scheme, the HOS-1 model produced the least accurate result with an absolute deviation (AD) between the experimental and numerical value of WAT of 9.5%. The results from the HOS-2 model and T_f correlations show improvements in accuracy of the WAT estimates with AD's of 0.5% and 0.7%, respectively.

The results from Table 4.8 indicate that the HOS-1 model also produced the least accurate result using Pedersen's lumping scheme for Sample A. The results from the HOS-1 model had an AD of 6.6% compared to the ADs of 0.6% and 2.4% obtained from the HOS-2 and T_f correlations, respectively. The superior performance of the HOS-2 model over the HOS-1 model agrees with the observations made by (Hosseinipour et al, 2019) and (Eyitayo, et al., 2020) from their validation tests performed on both correlations.

Table 4.8: WAT Predicted After Lumping Heavy Fractions for Sample A

SAMPLE A LUMPING SCHEME	EXPERIMENTAL VALUE WAT(K)	HOS-1 MODEL WAT(K)	AD (%)	HOS-2 MODEL WAT(K)	AD (%)	T_f correlation WAT(K)	AD (%)
WHITSON	304	276.30	9.5	302.54	0.5	305.95	0.7
PEDERSEN		323.20	6.6	305.76	0.6	311	2.4

Table 4.9 shows the results of the WAT for Sample B after regrouping the pseudo-components listed in Table 4.6. The results from Sample B are like those from Sample A using the Whitson's lumping scheme. In this case, the T_f correlations produced the most accurate results with an AD of 3.9% as compared to the HOS-1 model (AD=5.5%) and HOS-2 model with AD of 7.6%.

The T_f correlations also produced the most accurate result using the Pedersen's lumping scheme for Sample B. In this case, the absolute deviation (AD) between the experimental and numerical WAT is 1.0% from the T_f correlations compared to the HOS-1 and HOS-2 models with ADs of 3.7% and 6.6%, respectively. The superior performance of the T_f correlations in estimating WAT agrees with the findings of (Akinyede O. M., 2019).

Table 4.9: WAT Predicted After Lumping Heavy Fractions for Sample B

SAMPLE B LUMPING SCHEME	EXPERIMENTAL VALUE WAT(K)	HOS-1 MODEL WAT(K)	AD (%)	HOS-2 MODEL WAT(K)	AD (%)	T_f correlation WAT(K)	AD (%)
WHITSON	322	306.06	5.5	344.17	7.6	310.69	3.9
PEDERSEN		332.85	3.7	302.79	6.6	319	1.0

The results of the WAT for Sample C after lumping the pseudo-components (Table 4.7) are listed in Table 4.10. For Whitson's lumping scheme, the HOS-1 model produced the least accurate result with an AD of 6.2% as compared to the HOS-2 model and T_f correlations with AD's of 4.3% and 4.2%, respectively. The T_f correlation also produced the most accurate result of WAT using Pedersen's lumping scheme. In this case, the T_f correlation produced an AD of 0.6% as compared to the HOS-1 model with AD of 2.6%, and HOS-2 model with AD of 4.6%.

Table 4.10: WAT Predicted After Lumping Heavy Fractions for Sample C

SAMPLE C LUMPING SCHEME	EXPERIMENTAL VALUE WAT(K)	HOS-1 MODEL WAT(K)	AD (%)	HOS-2 MODEL WAT(K)	AD (%)	T_f correlation WAT(K)	AD (%)
WHITSON	312	293.93	6.2	299.54	4.3	299.87	4.2
PEDERSEN		319.44	2.6	299.03	4.6	310.25	0.6

Figure 4.1 and Table 4.11 illustrate the percentage absolute deviations in the WAT estimates using the Whitson lumping scheme for Sample A. As seen in this table, there was a 4.0% improvement in the WAT predicted using the HOS-2 model after lumping; a 1.6% deviation in the WAT predicted using the HOS-1 model after lumping, and a 1.0% improvement in the WAT predicted using the Tf correlation after lumping.

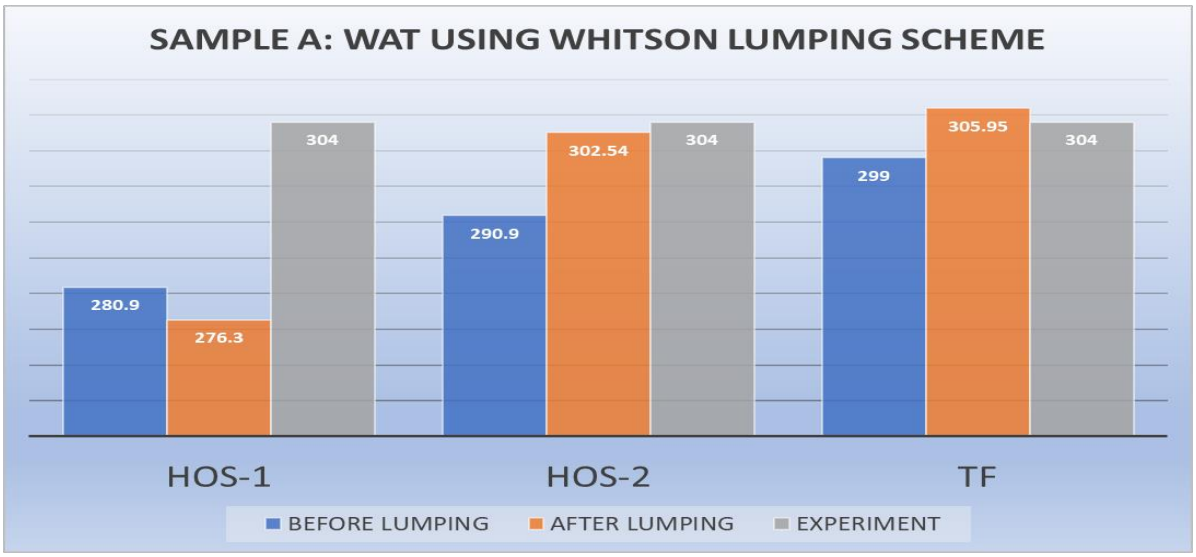

Figure 4.1: Impact of Whitson Lumping Scheme on WAT for Sample A

Table 4.11: Impact of Whitson Lumping Scheme on WAT for Sample A

	BEFORE LUMPING	**AFTER LUMPING**	**% AD**
EXPERIMENTAL	304		
HOS-1	280.9	276.3	1.6
HOS-2	290.9	302.54	4.0
Tf	299	305.95	1.0

The percentage absolute deviations in WAT Using Whitson Lumping Scheme for Sample B are shown in Figure 4.2 and Table 4.12. The results from this table show a 6.5% deviation in the WAT predicted using the HOS-2 model after lumping. Also, a 1.5% deviation in the WAT predicted using the HOS-1 model after lumping, and a 3.1% deviation in the WAT predicted using the T_f correlation after lumping for Sample B.

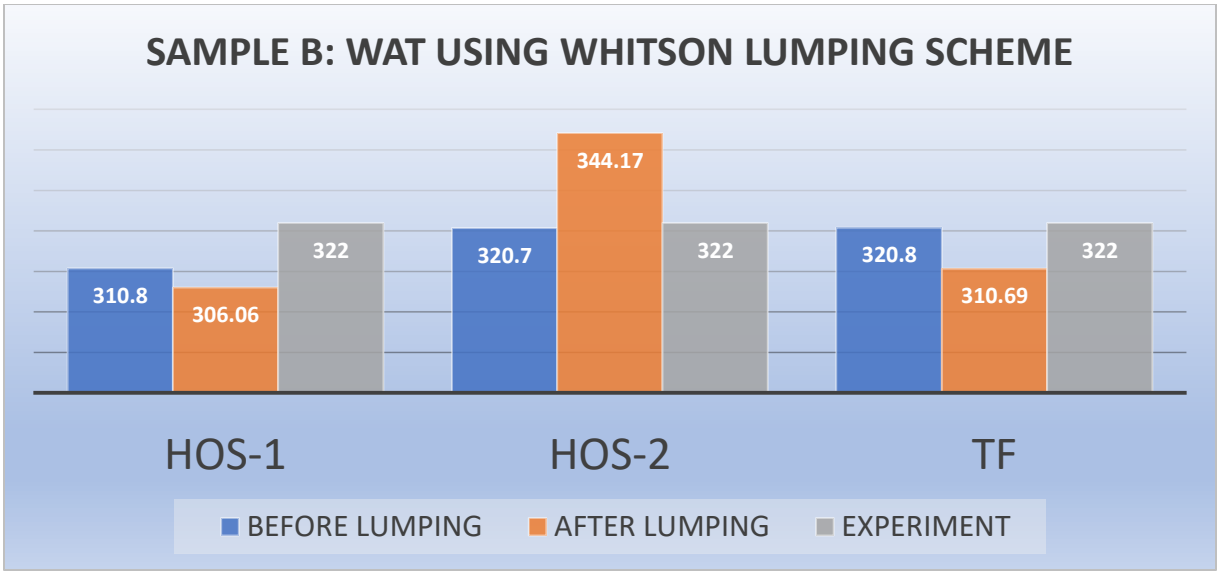

Figure 4.2: Impact of Whitson Lumping Scheme on WAT for Sample B

Table 4.12: Impact of Whitson Lumping Scheme on WAT for Sample B

	BEFORE LUMPING	**AFTER LUMPING**	**% AD**
EXPERIMENTAL	322		
HOS-1	310.8	306.06	1.5
HOS-2	320.7	344.17	6.5
Tf	320.8	310.69	3.1

Figure 4.3 illustrates the percentage absolute deviations in WAT calculated using the Whitson lumping scheme to regroup hydrocarbon components of Sample C. As seen in Table 4.13, there was a 2.7% deviation in the WAT predicted using the HOS-2 model after lumping, a 3.4% deviation in the WAT predicted using the HOS-1 model after lumping, and a 2.9% deviation in the WAT predicted using the T_f correlation after lumping.

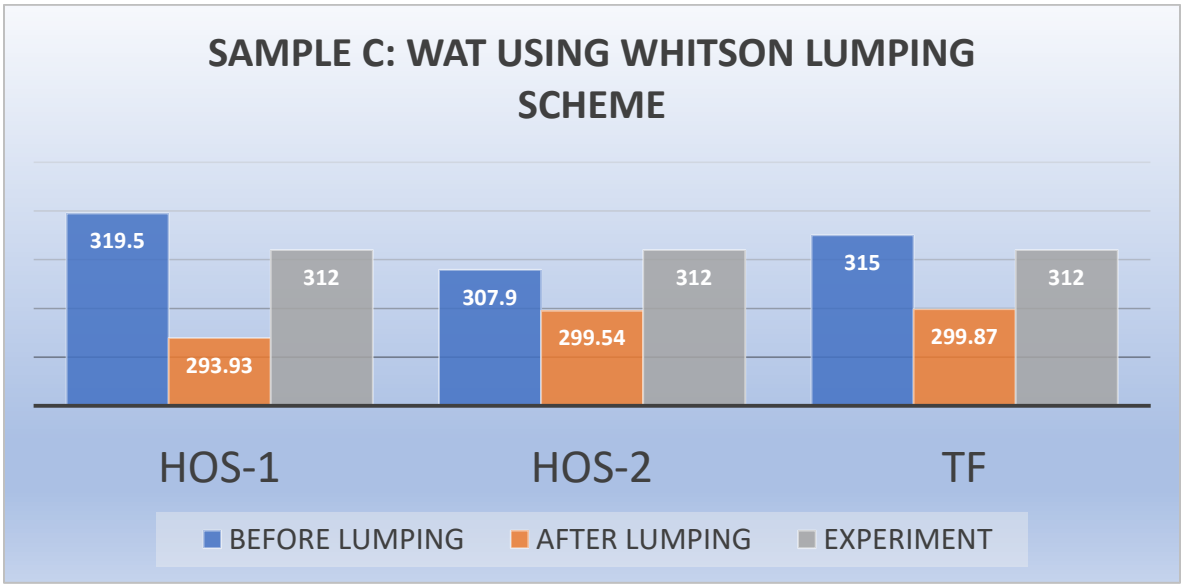

Figure 4.3: Impact of Whitson Lumping Scheme on WAT for Sample C

Table 4.13: Impact of Whitson Lumping Scheme on WAT for Sample C

	BEFORE LUMPING	**AFTER LUMPING**	**% AD**
EXPERIMENTAL	312		
HOS-1	319.5	293.93	3.4
HOS-2	307.9	299.54	2.7
Tf	315	299.87	2.9

The percentage absolute deviations in WAT predicted after using the Pedersen et al lumping schemes for Samples A, B and C, are presented in Figures 4.4 through 4.6. The results are also summarized in Tables 4.14, 4.15 and 4.16.

Figure 4.4 and Table 4.14 illustrate the improvement in WAT predicted after using Pedersen lumping scheme for regrouping the hydrocarbon components in Sample A. The results listed in Table 4.14 indicate a 1.3% improvement in the WAT predicted using the HOS-1 model after

lumping. Furthermore, for Sample A, it is observed that a 3.7% improvement in the WAT predicted using the HOS-2 model after lumping, and a 0.7% deviation in the WAT predicted using the T_f correlation after lumping with the Pedersen et al scheme.

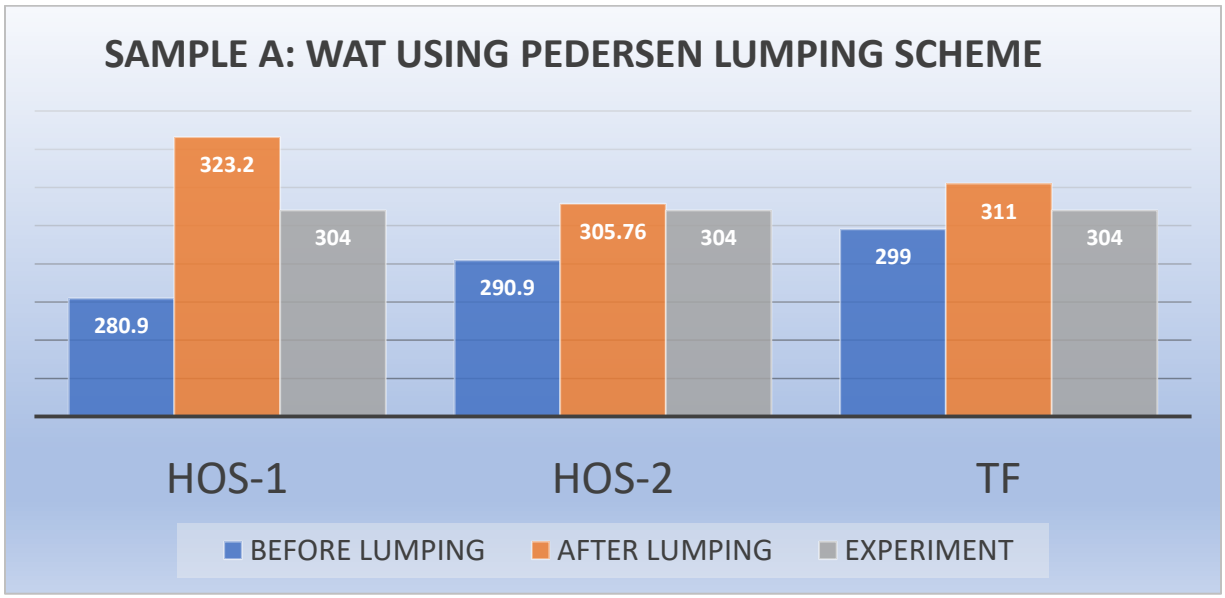

Figure 4.4: Impact of Pedersen Lumping Scheme on WAT for Sample A

Table 4.14: Impact of Pedersen Lumping Scheme on WAT for Sample A

	BEFORE LUMPING	**AFTER LUMPING**	**% AD**
EXPERIMENTAL	304		
HOS-1	280.9	323.20	1.3
HOS-2	290.9	305.76	3.7
Tf	299	311	0.7

Using Pedersen Lumping Scheme for Sample B, we observe the percentage absolute deviations in WAT predictions as illustrated in Figure 4.5 and Table 4.15. The results presented in Table 4.15 show a 0.1% improvement in the WAT predicted using the HOS-1 model after lumping; a 5.6% deviation in the WAT predicted using the HOS-2 model after lumping, and a 0.6% deviation in the WAT predicted using the T_f correlation after lumping.

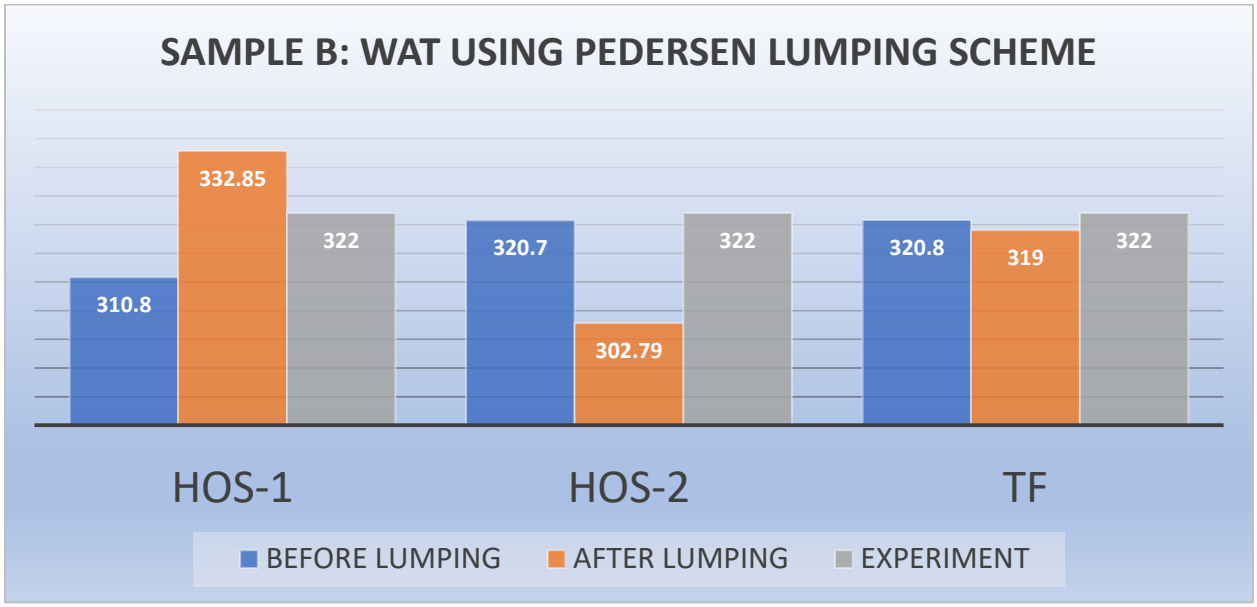

Figure 4.5: Impact of Pedersen Lumping Scheme on WAT for Sample B

Table 4.15: Impact of Pedersen Lumping Scheme on WAT for Sample B

	BEFORE LUMPING	**AFTER LUMPING**	**% AD**
EXPERIMENTAL	322		
HOS-1	310.8	332.85	0.1
HOS-2	320.7	302.79	5.6
Tf	320.8	319	0.6

Figure 4.6 and Table 4.16 show the percentage absolute deviations in WAT calculated using Pedersen lumping scheme to regroup the hydrocarbon components of Sample C. Table 4.16 indicates a 0.02% improvement in the WAT predicted using the HOS-1 model after lumping; a 2.8% deviation in the WAT predicted using the HOS-2 model after lumping, and a 0.4% improvement in the WAT predicted using the Tf correlation after lumping.

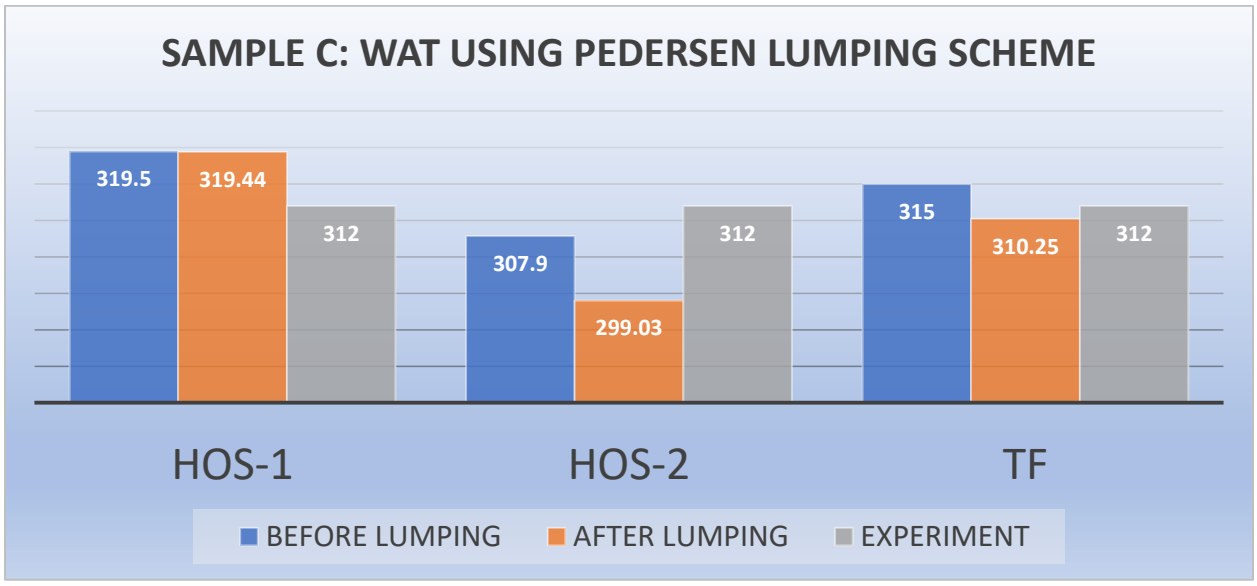

Figure 4.6: Impact of Pedersen Lumping Scheme on WAT for Sample C

Table 4.16: Impact of Pedersen Lumping Scheme on WAT for Sample C

	BEFORE LUMPING	**AFTER LUMPING**	**% AD**
EXPERIMENTAL	312		
HOS-1	319.5	319.44	0.02
HOS-2	307.9	299.03	2.8
Tf	315	310.25	0.4

The WAT estimates after lumping using both the Whitson and Pedersen pseudoization schemes indicate some improvements in the WAT compared to the values before applying the lumping schemes. The values of WAT predicted from the HOS-1 and HOS-2 models showed more remarkable improvements after applying the lumping schemes compared to the experimentally determined WAT for all three samples used in this work. A comparison of the results before and after application of Whitson and Pedersen lumping schemes showed little or no improvement in the WAT predicted using the T_f correlations. This observation further validates the superiority of the T_f correlations in WAT estimation.

4.2 Results of the Sensitivity Analysis

The sensitivity analysis was carried out for the two Samples A and B using @Risk. (Palisade, 2020). Tornado charts are used to show how sensitive the WAT is to the two lumping schemes (Pedersen et al, 1991; Whitson, 1983) used to regroup the hydrocarbon components into pseudo components (i.e., X1, X2, X3, X4) required in the (Hosseinipour et al, 2019) models. As discussed in Chapter Three, the weights of the pseudo components (i.e., X1, X2, X3, X4) are changed over the allowed ranges (minimum, maximum) using the uniform distribution. The inputs used were the total weight (wt %) of hydrocarbon components before and after lumping of each group. The results of the sensitivity analysis using the HOS-1 and HOS-2 WAT models and Whitson and Pedersen lumping schemes are presented in the following section.

4.2.1 Results of Sensitivity Analysis using HOS-1 Model for Samples A and B

Recall, the Hosseinipour et al (2019) HOS-1 model for estimating WAT is given by:

$$T_{wax} = 6.808X_1 + 0.366X_2 + 3.381X_3 + 3.028X_4$$

The results show the impacts of the pseudo components (i.e., X1, X2, X3, X4) on the accuracy of WAT as they are changed over the allowed ranges (minimum, maximum). Figures 4.7 and 4.8 illustrate the sensitivity of the wax appearance temperature (WAT) to the lumping (Whitson, Pedersen) of the hydrocarbon components in the composition-based HOS-1 model by (Hosseinipour et al, 2019) for Samples A. Figure 4.7 shows the results of the sensitivity analysis for HOS-1 model using input data from the initial and Whitson lumped groups for Sample A. The results indicate that WAT is more sensitive to the lumping of X4 using Whitson lumping scheme and is least sensitive to lumping of X2.

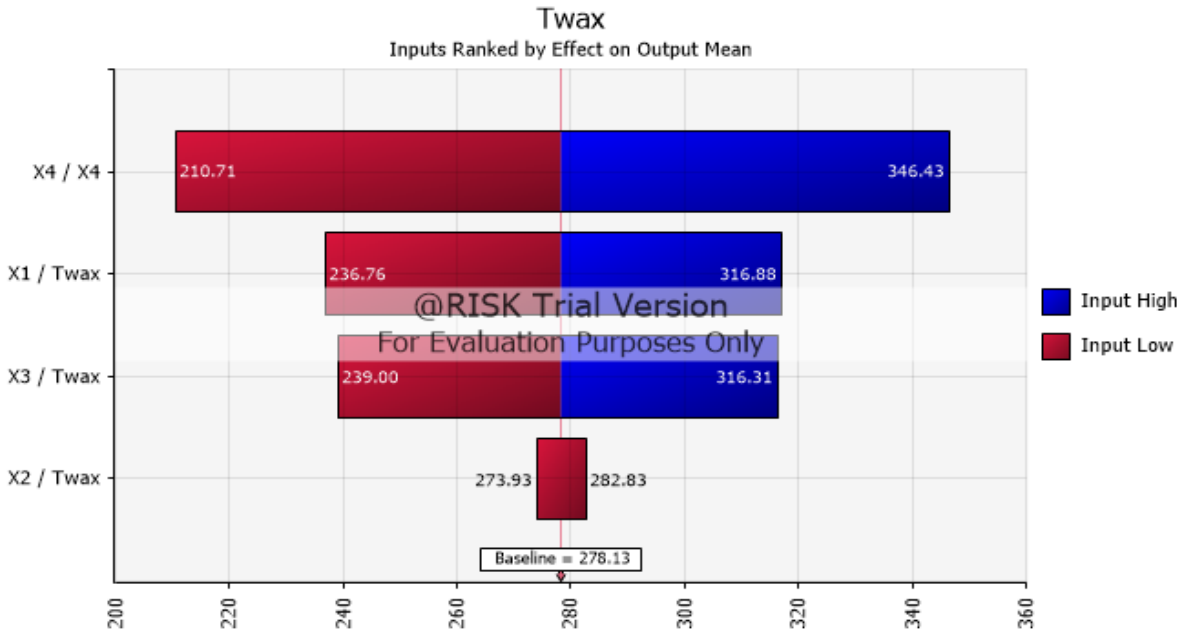

Figure 4.7: Sensitivity analysis of WAT Using HOS-1 Model for Sample A before and after applying Whitson lumping Scheme

Figure 4.8 shows the results of the sensitivity analysis for HOS-1 model using input data from the initial and Pedersen lumped groups for Sample A. In this case, it is observed that the WAT is more sensitive to the lumping of X1 using the Pedersen lumping scheme and is least sensitive to lumping of X2.

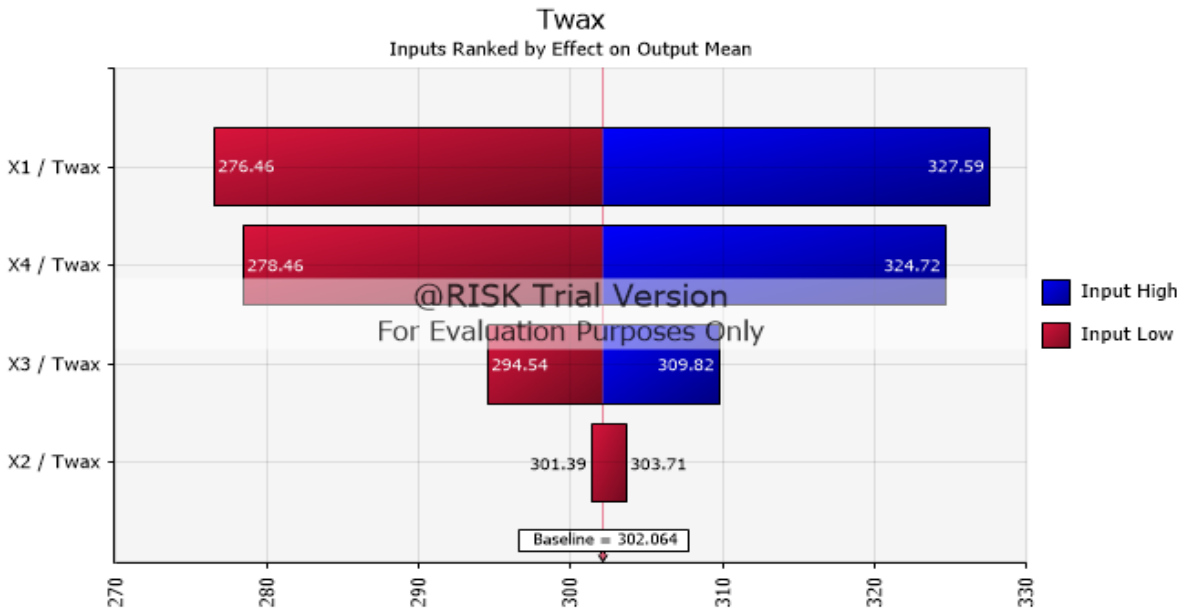

Figure 4.8: Sensitivity analysis of WAT Using HOS-1 Model for Sample A before and after applying Pedersen lumping Scheme

Figures 4.9 and 4.10 illustrate the sensitivity of the wax appearance temperature (WAT) to the lumping (Whitson, Pedersen) of the hydrocarbon components of Samples B using the composition-based HOS-1 model by (Hosseinipour et al, 2019). Figure 4.9 shows the results of the sensitivity analysis for Sample B using input data before and after application of the Whitson lumping scheme. The WAT of Sample B is more sensitive to the lumping of X4 using Whitson lumping scheme and is least sensitive to lumping of X2.

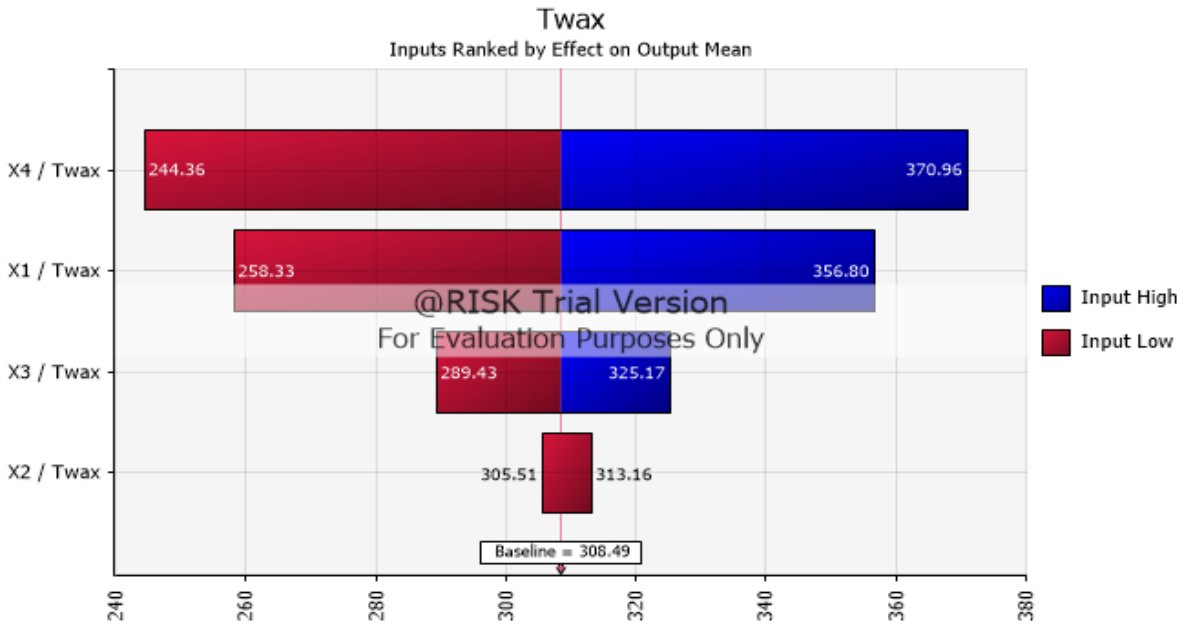

Figure 4.9: Sensitivity analysis of WAT Using HOS-1 Model for Sample B before and after applying Whitson lumping Scheme

Figure 4.10 shows the results of the sensitivity analysis for Sample B using the HOS-1 model and input data (X1, X2, X3, X4) before and after applying the Pedersen lumping scheme. The results for Sample B indicate that the WAT is more sensitive to the lumping of X1 using the Pedersen lumping scheme; and it is least sensitive to lumping of X2.

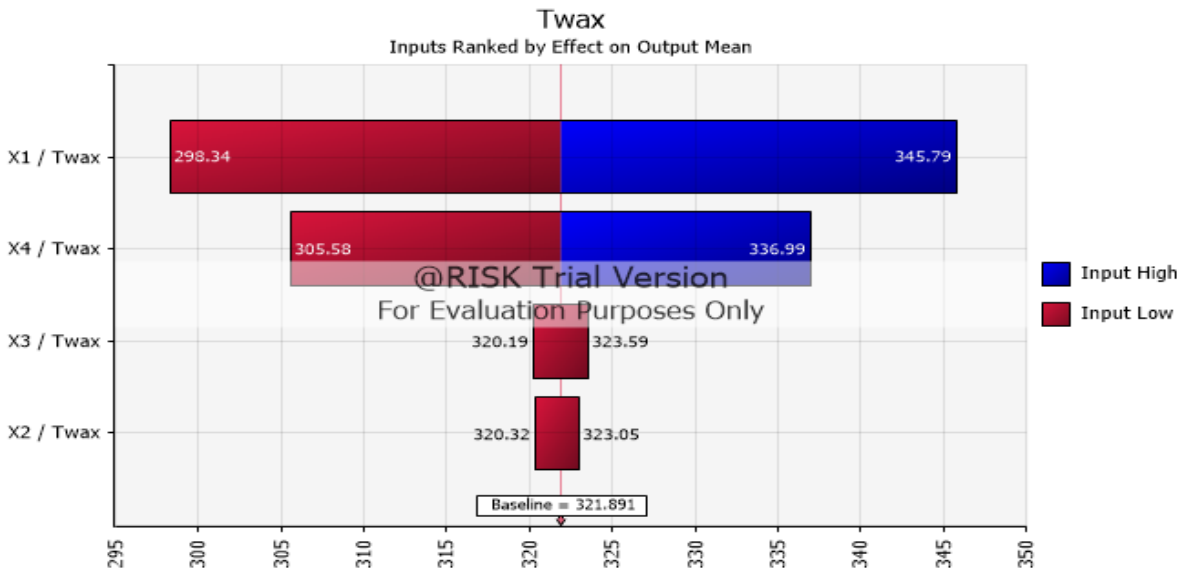

Figure 4.10: Sensitivity analysis of WAT Using HOS-1 Model for Sample B before and after applying Pedersen lumping Scheme

4.2.2 Results of Sensitivity Analysis using HOS-2 Model for Samples A and B

The equation for estimating WAT using the HOS-2 model by Hosseinipour et al (2019) is:

$$T_{wax} = 1.017X_1 + 0.075X_2 + 1.6111X_3 + 213.586$$

The results of the sensitivity analysis for Sample A are shown in Figures 4.11 and 4.12 using the HOS-2 model and the Whitson and Pedersen lumping schemes, respectively. Figure 4.11 shows the results of the sensitivity analysis for X1, X2 and X3 of Sample A using the HOS-2 model and input data before and after applying the Whitson lumping scheme. It is observed that the WAT is more sensitive to the lumping of X3 and is least sensitive to lumping of X2 based on the Whitson lumping scheme.

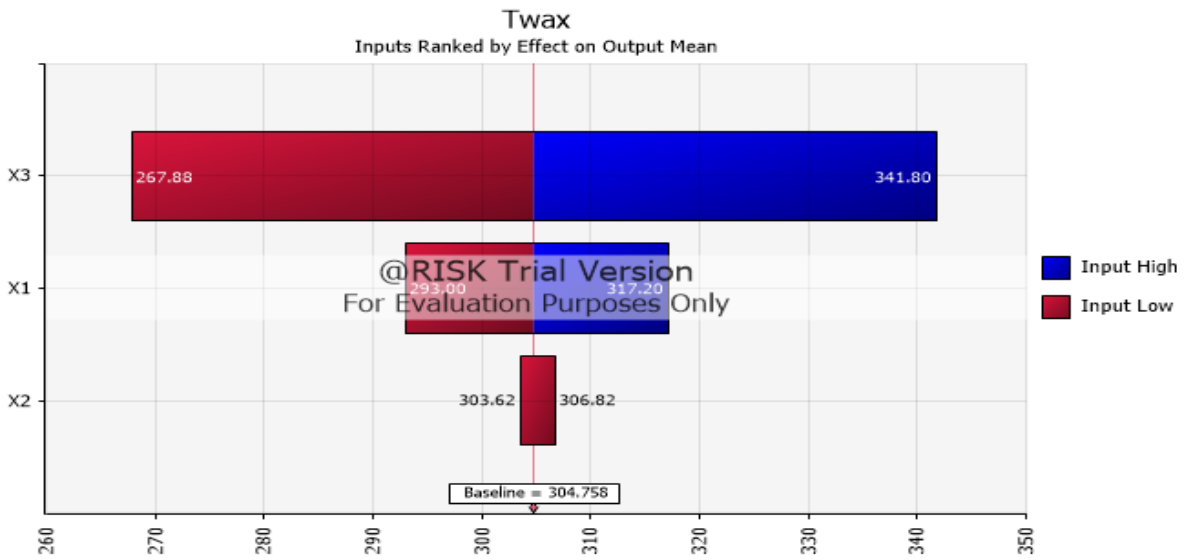

Figure 4.11: Sensitivity analysis WAT Using HOS-2 Model for Sample A before and after applying Whitson lumping Scheme

Figure 4.12 shows the results of the sensitivity analysis for X1, X2 and X3 of Sample A using the HOS-2 model and input data before and after applying the Pedersen lumping scheme. .The results in this case show that the WAT is more sensitive to the lumping of X3 based on the Pedersen lumping scheme and is least sensitive to lumping of X2.

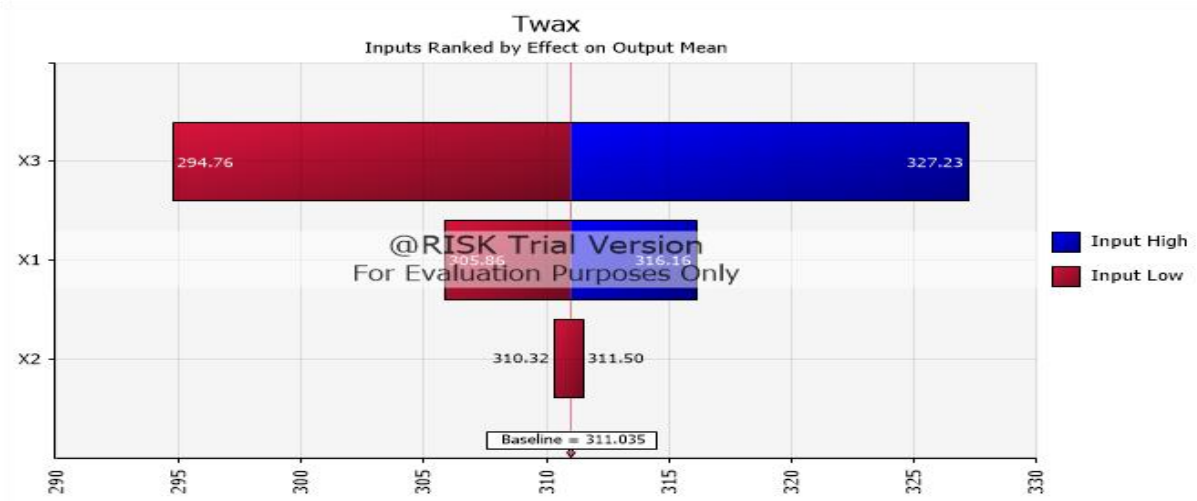

Figure 4.12: Sensitivity analysis of WAT Using HOS-2 Model for Sample A before and after applying Pedersen lumping Scheme

Figures 4.13 and 4.14 show the results of the sensitivity of the wax appearance temperature (WAT) of Sample B to the lumping of the hydrocarbon components into X1, X2 and X3 groups used in the composition-based HOS-2 model by (Hosseinipour et al, 2019). The results for Sample B using the Whitson lumping scheme are shown in Figure 4.13 and they indicate that the WAT is more sensitive to the lumping of X3 and is least sensitive to lumping of X2. Figure 4.14 shows the results of the sensitivity of the WAT of Sample B to X1, X2 and X3 grouping based on the Pedersen lumping scheme. It is observed that the WAT is more sensitive to the lumping of X3 using Pedersen lumping scheme and is least sensitive to lumping of X2.

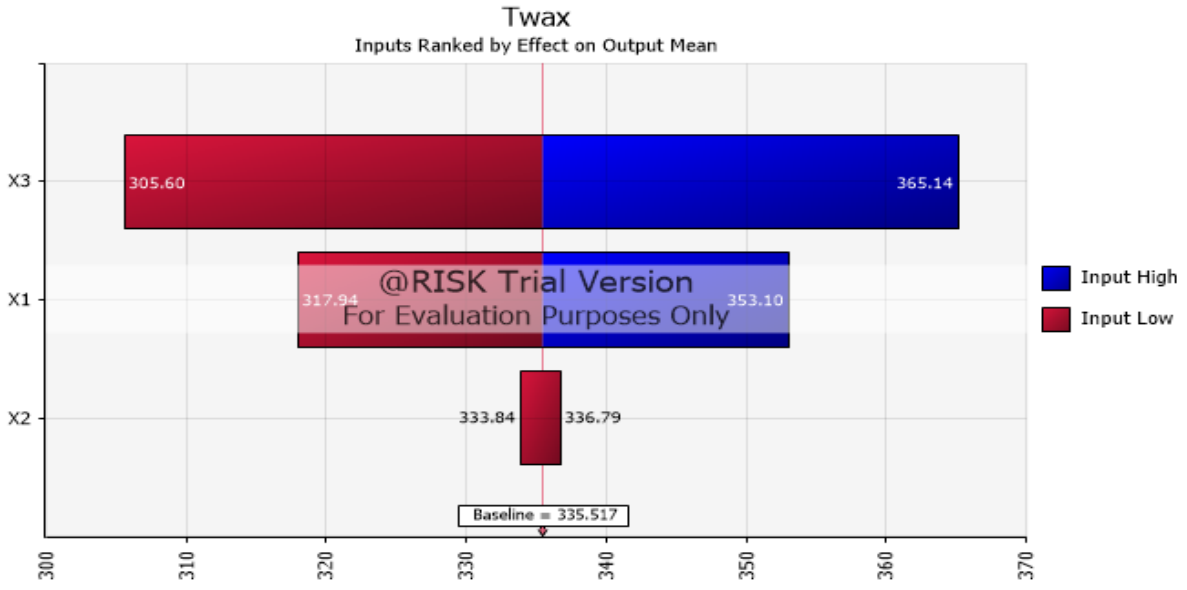

Figure 4.13: Sensitivity analysis of WAT Using HOS-2 Model for Sample B before and after applying Whitson lumping Scheme

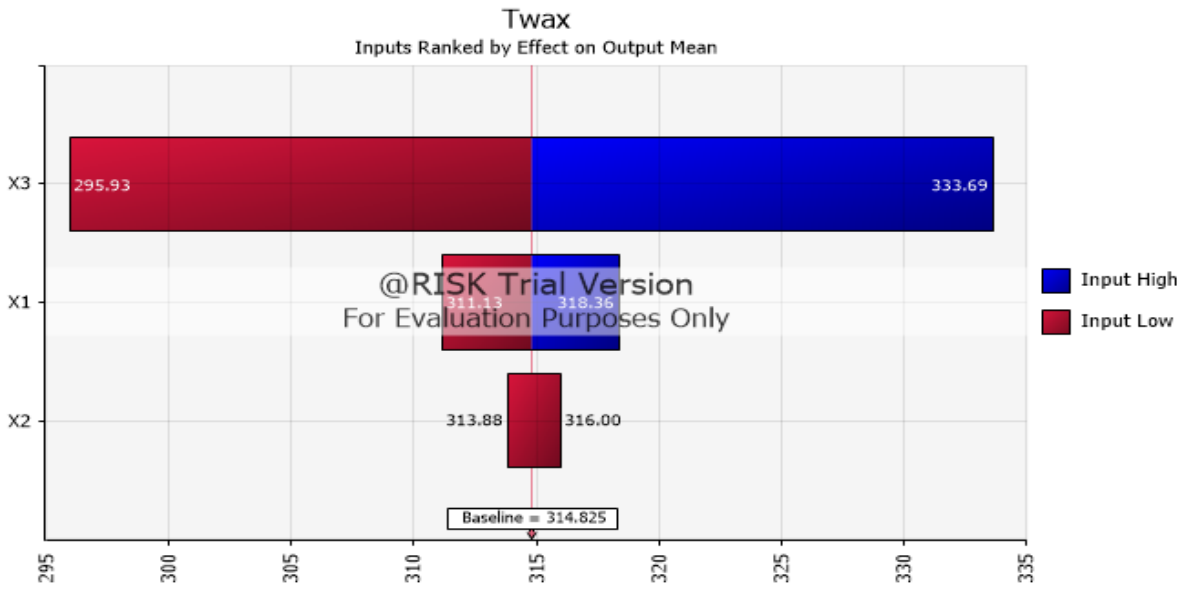

Figure 4.14: Sensitivity analysis of WAT Using HOS-2 Model for Sample B before and after applying Pedersen lumping Scheme

4.3 Results of Applying Wax Appearance Temperature to Depositional Modeling

MATLAB programs are written to model the wax deposition in the section of the pipeline as a function of time. Sample A obtained from a Niger Delta field was used for this experiment. The MATZAIN (1999) and Singh et al models discussed earlier in Chapter 3 were used to estimate the wax deposition thickness at the inlet of the pipeline as a function of time varying from 1, 2, 7, 20, to 30 days. The numerical model proposed by Stubsjoen (Marte, 2013) was also used to simulate wax deposition thickness along the length of the pipeline as a function of time.

Figure 4.15 illustrates the wax deposit thickness profiles after 1 day, 2 days, 7 days, 20 days and 30 days obtained from the numerical model proposed by Marte Stubsjoen (Marte, 2013). The maximum deposit thickness is found at 51 meters from the pipeline inlet, where the WAT is reached in the near-wall region. The shape of the deposit profiles observed can be attributed to

the temperature difference in the near-wall region which is at its maximum when the WAT is reached, and then decreasing along the pipeline. The deposit thicknesses from the model at 51 meters from the pipeline inlet for the wax deposition models are reported in Table 4.17. The results show a gradual growth of the deposit thickness with time and the decreased thickness with axial distance. The growth rate of the wax deposit layer decreasing with time has been reported by Stubsjoen and others (Marte, 2013).

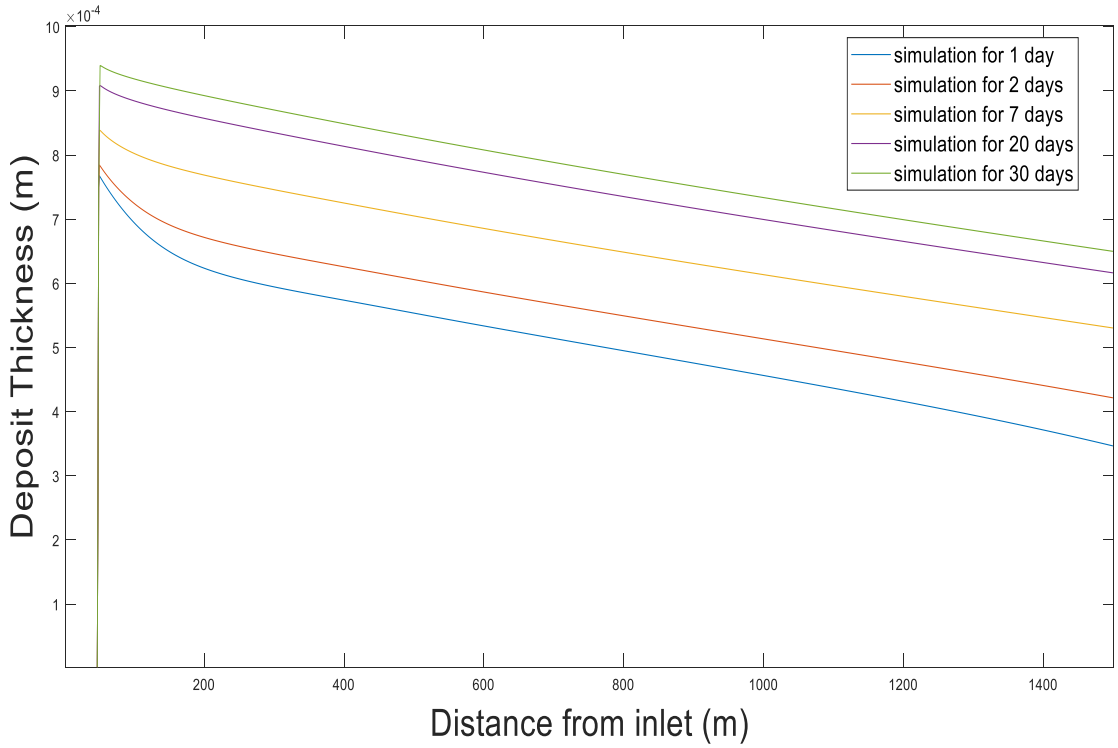

Figure 4.15: Deposit thickness profiles after 1 day, 2 days, 7 days, 20 days and 30 days along the pipeline wall using the numerical model by Marte Stubsjoen (2013).

Figure 4.16 illustrates the wax deposit thickness profiles after 1 day obtained from the MATZAIN (Matzain, 2001) and the Singh et al (Singh P. e., 2001) models. The total wax deposited at the inlet of the pipeline after the first day of crude oil transportation is 1.0007mm using the MATZAIN model and 0.9998mm from the Singh et al model.

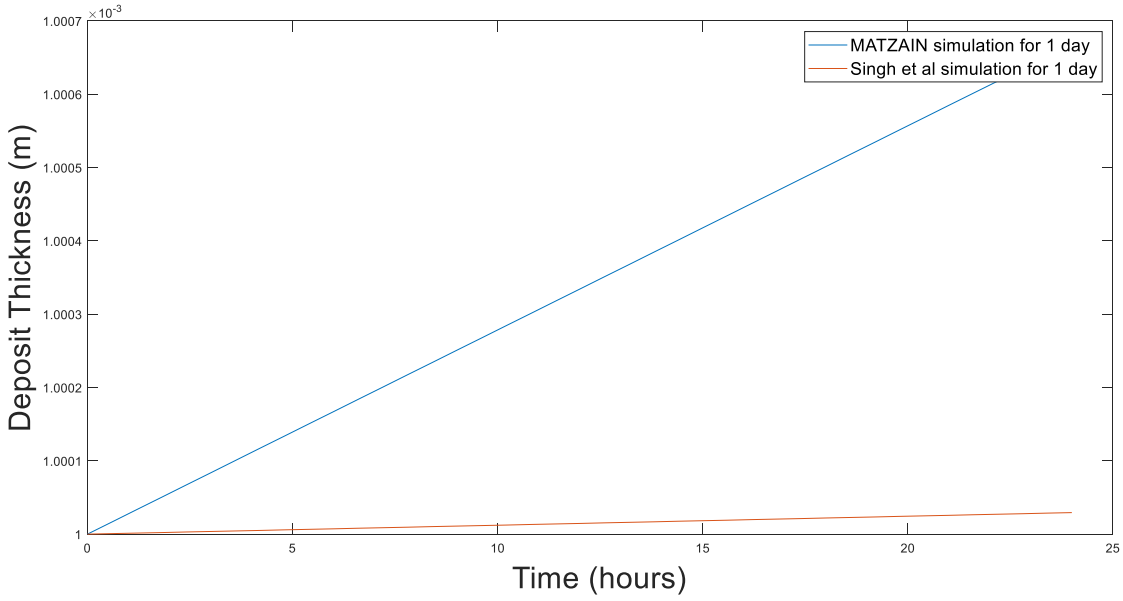

Figure 4.16: Deposit thickness profiles after 1 day obtained from the MATZAIN and Singh et al models.

Figures 4.17 through 4.20 show the wax deposit thickness profiles at the inlet of the pipeline after 2 days, 7 days, 20 days and 30 days of crude oil transportation using the MATZAIN (Matzain, 2001) and Singh et al (Singh P. e., 2001) models. The values of the wax deposit thickness at the pipeline inlet at these times are listed in Table 4.17.

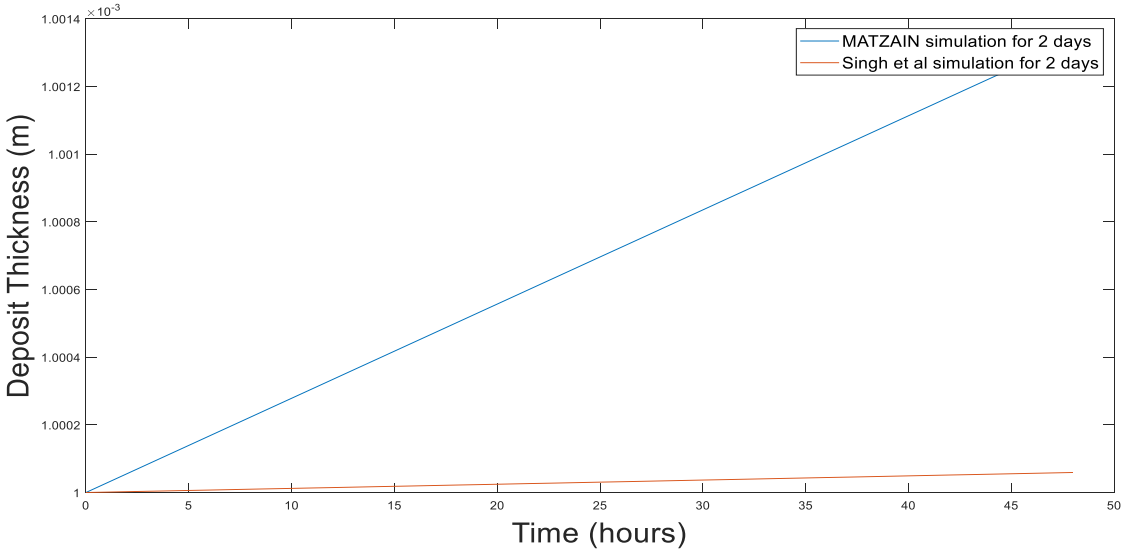

Figure 4.17: Deposit thickness profiles after 2 days from the MATZAIN and Singh et al models.

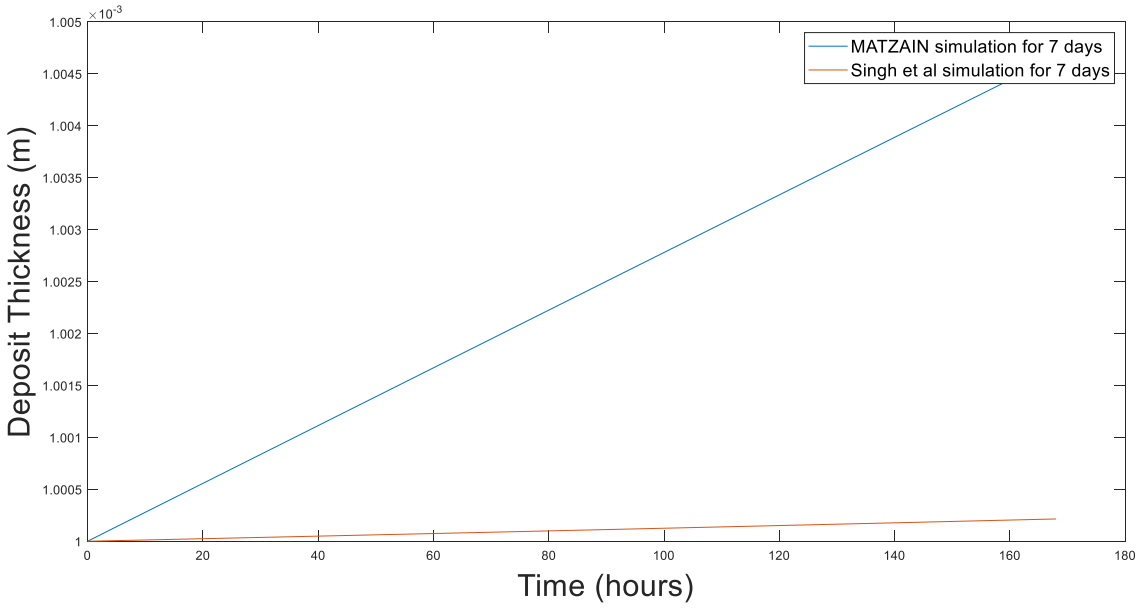

Figure 4.18: Deposit thickness profiles after 7 days obtained by the MATZAIN and Singh et al models.

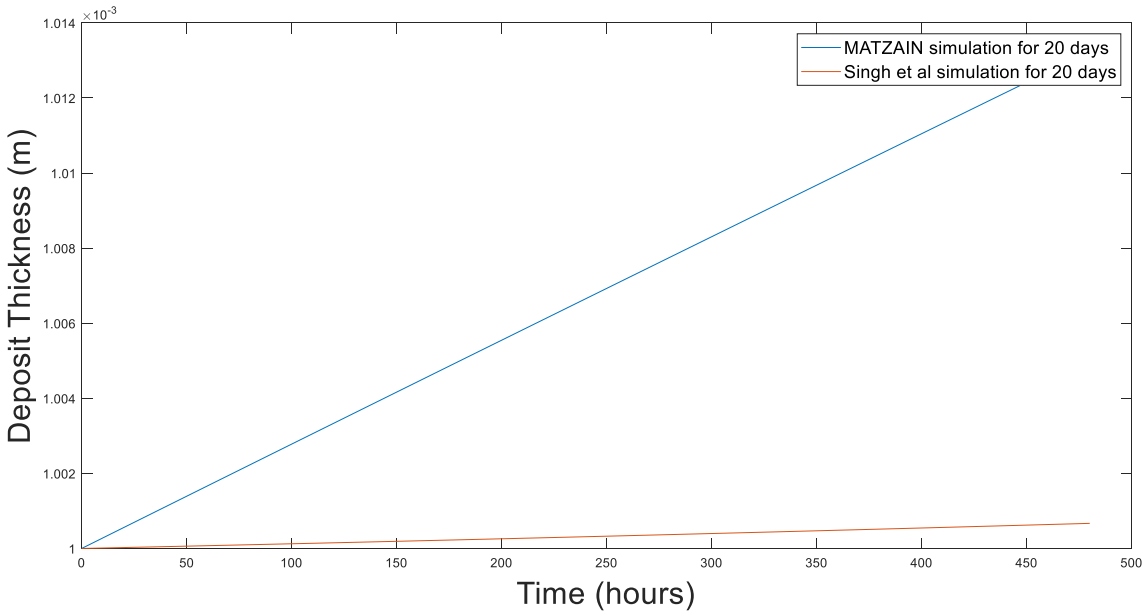

Figure 4.19: Deposit thickness profiles after 20 days obtained by the MATZAIN and Singh et al models.

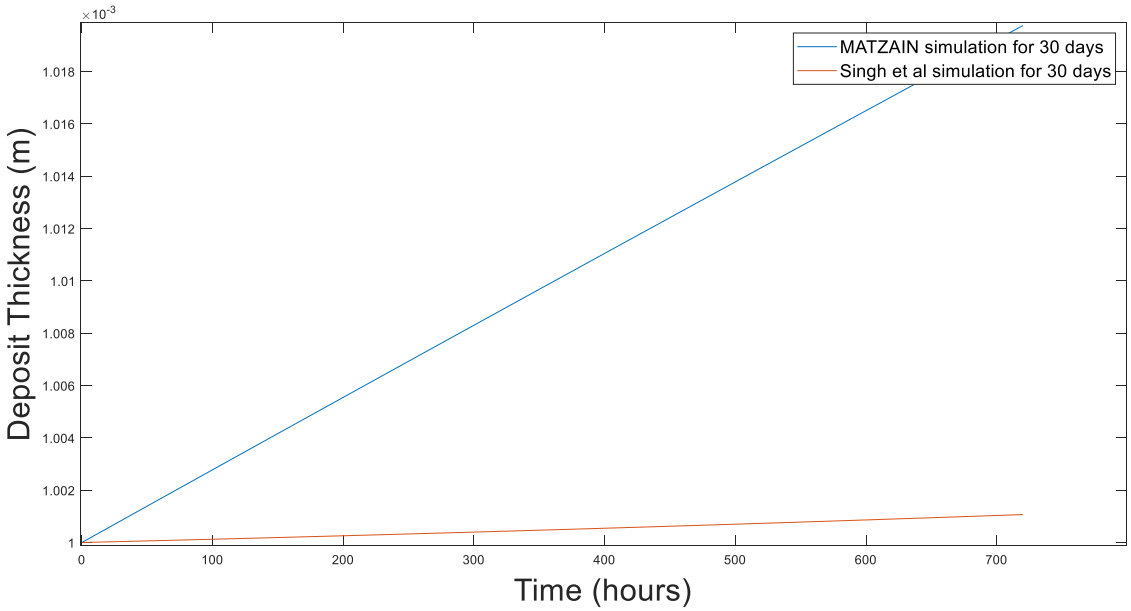

Figure 4.20: Deposit thickness profiles after 30 days obtained by the MATZAIN and Singh et al models.

Table 4.17 is a comparison of the wax deposit thickness simulated using the models proposed by MATZAIN (2001), Singh et al model, and the numerical model proposed by Stubsjoen (Marte, 2013). The wax deposit thickness is listed as a function of time for 1, 2, 7, 20, and 30 days. For the first day, the MATZAIN simulated the most deposit thickness, i.e., 1.0007mm compared to Singh et al and the numerical model which predicted 0.9998mm and 0.7786mm, respectively. The MATZAIN also simulated the most wax deposit thickness of 1.0014mm for the second day. When compared to the results predicted by the Singh et al model (1.0mm) and the numerical model which predicted a thickness of 0.7998mm.

At the end of one week, about 0.8705mm of wax had been deposited at the inlet of the pipe as obtained by the numerical model. The numerical model produced the least deposit thickness as compared to the MATZAIN model (i.e., 1.0047mm) and the Singh et al model which simulated wax deposit thickness of .0001mm at the inlet of the pipe. After twenty days, the numerical model indicated that 0.9527mm of wax had been deposited at the inlet of the pipe. It is observed that the numerical model also produced the least deposit thickness at the inlet of the pipe after 20 days of crude transportation compared to the results from the MATZAIN model (1.0135mm) and the Singh et al model (1.0005mm). Similar trends of results were obtained after thirty days with the wax deposit thickness of 1.0197mm obtained from the MATZAIN model, 1.0009mm from the Singh et al, and 0.9989mm from the numerical model.

Table 4.17: Wax deposition thickness at the Case Study Pipeline Inlet as a function of time

	Wax Deposit Thickness (mm)		
Time (days)	MATZAIN	Singh et al	Numerical model
1	1.001	0.998	0.779

2	1.002	1.000	0.800
7	1.005	1.000	0.871
20	1.014	1.001	0.953
30	1.020	1.001	1.000

4.3.1 Pertinent Remarks on The Case Study

Sample A which was gotten from the DEEIVE field in the Niger Delta contained a wax content of 14%. Using the Stubsjoen (2013) numerical model, the maximum deposit thickness was found at 51 meters from the inlet, where the WAT was reached in the near-wall region. The WAT reached corresponds with the predicted wax appearance temperature using the (Hosseinipour et al, 2019) models. The wax deposit thickness was found to increase with time. The growth rate and aging of the wax deposit are the result of the convective flux of wax molecules from the bulk fluid to the oil/deposit interface; this observation agrees with the work by Lee (Lee, 2011).

It is noted that the wax deposit profiles obtained using the MATZAIN, Singh et al, and numerical models in this current work are comparable to the results reported by various authors (e.g., see the works of (Obaseki, 2020); Stubsjoen (Marte, 2013)).

Chapter Five

Conclusion and Recommendations

The conclusions reached in this study are presented in this Chapter. It also includes a set of suggested recommendations for further studies to improve the results obtained from this research.

5.0 Summary and Conclusion

In this study, four recent models, i.e., two composition-based models (HOS-1 and HOS-2) proposed by Hosseinipour et al (2019), GOR model (Eyitayo et al., 2020) and the T_f correlation (Akinyede, 2019), were used to estimate the wax appearance temperatures (WAT) of three oil samples from the Niger Delta, North Sea, and a gas condensate field. A method of distributing heavy components was used to characterize the Niger Delta crude mixture and estimate the critical properties and acentric factor which are important in determining solid precipitation. The Whitson and Pedersen's lumping schemes were used to regroup/lump hydrocarbon components into pseudo-component groups for the T_f correlation and Hosseinipour et al (2019) composition-based WAT models. A sensitivity analysis was performed to determine how sensitive the estimated wax appearance temperature is to the lumped pseudo components used in the Hosseinipour et al (2019) composition-based (HOS-1 and HOS-2) models for calculating the WAT. The WAT for Sample A was input into the Wax deposition models coded as MATLAB computer programs to simulate the wax depositional profiles and deposit thickness in a Niger Delta pipeline case study. The results of this study underscored the importance of estimating the wax appearance temperature for the management of flow-assurance challenges in the oil and gas industry.

The following conclusions can be derived from the results of this study:

1. The accuracy of WAT models studied in this work varied with absolute deviations of 0.4 to 7.9% between the experimental and calculated values, depending on the composition of the sample, WAT correlation and the methodology used to lump the hydrocarbon components.
2. For Sample A the Hosseinipour et al composition-based HOS-1 model was the least accurate with an absolute deviation of 7.9%, and the Tf correlation was most accurate with an absolute deviation of 1.7%. The accuracy is measured by the absolute deviation between the experimental and calculated values of WAT for Sample A.
3. Comparison of the experimental vs. theoretical values before and after pseudoization of the hydrocarbon components of the samples indicated that the lumping schemes improved the accuracy of the theoretical correlations used in estimating WAT.
4. The accuracy of the hydrocarbon component lumping scheme proposed by Pedersen was not high compared to the lumping scheme proposed by Whitson because of the approximation used in the Pedersen method to calculate the total weight percent for each group of pseudo components.
5. The Tf correlation produced the most accurate results in estimating the wax appearance temperatures for all samples used in this study before and after pseudoization of the hydrocarbon components.
6. Sensitivity analysis indicated that the WAT was least sensitive to lumping of the X2 pseudo component group used in the Hosseinipour et al composition-based (HOS-1 and HOS-2) models for the three crude oil samples examined in this work.

7. The wax deposit thickness from the Niger Delta case study was found to increase with time using the Matzain, Singh et al mechanistic models and the Marte Stubsjoen numerical model.
8. The application of the Marte Stubsjoen numerical model to the Niger Delta case study indicated that the maximum wax deposit thickness is found at about 51meters from the pipeline inlet.

5.1 Recommendations

From a precipitation standpoint, wax is one of the most vulnerable hydrocarbon contents of crude oil and gas condensate. As a result, wax appearance temperature (WAT) is an important consideration for flow-assurance in the oil and gas industry. This study uses theoretical methods and correlations to estimate the wax appearance temperature. The WAT was then used in a case study to simulate the wax deposition thickness as a function of time using two pre-existing models by Matzain and Singh et al.

A possible continuation of the current work is to evaluate the use of RRR model (Rygg, O. R. (1998) and the University of Michigan model (Lee, H. S., 2011) to predict wax deposition for all three samples in a future study.

Also, there is need for further work to extend the MATLAB codes of the Matzain and Singh et al. models to simulate deposit thickness as a function of distance.

Nomenclature

α	Brownian particle diameter
A	Area
C	Concentration
ΔC_p	Heat capacity
ΔC_i	Wax concentration difference between the bulk fluid and wax saturation in the oil
$\frac{dC_i}{dr}$	Concentration gradient of component i
$\frac{dC_w}{dr}$	Concentration gradient of the wax in the bulk fluid
$\frac{dC}{dT}$	Solubility coefficient
$\frac{dT}{dr}$	Temperature gradient at the wall (radial distance) of the pipe
d	Diameter
D_b	Brownian diffusion coefficient
D_{ow}	Diffusion coefficient
D_s	Shear dispersion coefficient
f	Friction factor h heat transfer coefficient
F	Weight fraction of sold wax in gel
f_i^o	Fugacity of component i
f_i^o	Standard state fugacity coefficient of component i
g	Acceleration due to gravity
G	Mass transfer rate
$\Delta H_i^{\ f}$	Molar heat of fusion of component i
ΔH_i^{tr}	Molar heat of transition of component i

ΔH_i^{vap}	Molar heat of vaporisation of component i
l_{wax}	Wax thickness with time
J^{sr}	Negative mass transfer due to shear force
k	Shear deposition rate constant
K_i	Equilibrium ratio
k_{dep}	Thermal conductivity of wax-gel deposition
k_o	Thermal conductivity of oil phase
k_w	Thermal conductivity of wax deposition
M_b	Mass of deposited wax due to Brownian diffusion
mfr	Mass fraction
M_w	Molecular weight
M_{wi}	Molecular weight of component i
$N_{Re,f}$	Dimensionless Reynolds number
N_w	Number of wax components
P	Pressure
$P_{c,i}$	Critical pressure
r	Inner radius of pipe wall
R	Gas constant
S_f	Wetted perimeter
T	Temperature
T_i^f	Melting temperature of component i
U	Overall Heat Transfer Coefficient
V_a	Molar volume

X1	Total content of hydrocarbon components (wt. %) of the first pseudo-component group
X2	Total content of hydrocarbon components (wt. %) of the second pseudo-component group
X3	Total content of hydrocarbon components (wt. %) of the third pseudo-component group
X4	Total content of hydrocarbon components (wt. %) of the fourth pseudo-component group
x_i or z_i	Mole fraction of component i
Z	Compressibility factor

.

Subscripts

b	Brownian diffusion
dep	Deposition
i	Component i
i	Component of the bulk fluid in either of wax, liquid or vapour phase
L	Liquid; oil
m	Mixture components of the bulk fluid in the oil phase and the wax phase
o	Component of the bulk fluid in the oil phase
w	Component of the bulk fluid in the wax phase

Superscripts

f	fusion
id	ideal
o	oil
sr	shear force
sh	shear force
tr	transition
v	vapour
vap	vapour
w	wax

Symbols

α	Thickness correction factor
λ	Interaction energy
K_p	Power-law consistency index
θ	Angle of pipe inclination
φ_i	Volume fraction of component i
φ_w	Volume fraction of wax out of solution
φ	Wax porosity
ϕ_i	Fugacity coefficient of component i
ϕ_i^o	Fugacity coefficient of pure component i
δ_i	Solubility parameter of component i
δ_w	Thickness of the wax layer

ρ	Density
Re	Reynolds number
τ	Shear stress
μ	Viscosity
ω	Mass fraction of wax in the wax-gel layer
γ	Shear rate at the pipe wall
γ_i	Activity coefficient of component i

Abbreviations

ASTM	American Society of Testing and Materials
EOS	Equation of state
HOS-1	Hosseinipour et al (2019) composition-based wax appearance temperature correlation No 1.
HOS-2	Hosseinipour et al (2019) composition-based wax appearance temperature correlation No 2
NTNU	Norwegian University of Science and Technology
PR	Peng-Robinson
PVT	Pressure Volume Temperature
PVTsim	PVT simulation program by Calsep
PT	Pressure Temperature
RRR	Rygg, Rydahl and Rønningsen
SRK	Soave-Redlich-Kwong
STO	Stock tank oil
TWS	Walls surface temperature
WAT	Wax appearance temperature equivalent to WAP
Waxy fluid	Mixtures of petroleum fluid with a tendency to precipitate wax under cooling
WDT	Wax dissolution temperature

References

(n.d.). Retrieved from https://nigerianscholars.com/tutorials/organic-chemistry/aromatic-hydrocarbons/

Abass, A. O. (2021). Review of wax deposition in subsea oil pipeline systems and mitigation technologies in the petroleum industry. *Chemical Engineering Journal Advances*. Retrieved from https://doi.org/10.1016/j.ceja.2021.100104

Adesina, F., Anthony, A., Churchill, A., & Olawale, D. (2010). Modeling of wax deposition during oil production using a two-phase flash calculation. *Pet. Coal 52,* 193–202.

Aiyejina, A. e. (2011). Wax formation in oil pipelines: A critical review. *International Journal of Multiphase Flow, 37*(7), 671-694.

Ajayi, O. E. (2013). *Modelling of controlled wax deposition and loosening in oil and gas production systems.* Norwegian University of Science and Technology.

Akinyede, O. G. (2018a). Bivariate statistical analysis of wax solid-liquid equilibrium parameter. *Petroleum Science and Technology*, *36*(9-10), 625-631. Retrieved from https://doi.org/10.1080/10916466.2018.1440298

Akinyede, O. M. (2019). *Development of a Thermodynamic Model For Wax Precipitation in Produced Crude Oil -- Case Study of Hydrocarbon Fluid From Niger-Delta, Nigeria.* African University of Science and Technology,Abuja, Nigeria.

Alessandro et al, T. B. (2019). *Experimental and Numerical Study of Multiphase Flow Phenomena and Models in Oil & Gas Industry.* doi:10.1016/j.petlm.2019.04.004

Alghanduri et al, L. M.-L. (2010). Characterization of Libyan Waxy Crude Oils. *Energy & Fuels, 24*, 3101-3107.

Alian, S., Singh, K., Mohammed, A., Ismail, M., & Anwar, M. (2013, October 22). Organic Deposition: From Detection and Laboratory Analysis to Treatment and Removal. *Research Gare*. doi:10.2118/165912-MS

Ana, S. (2016). *Numerical simulation of wax deposition in pipelines and wells.* Thesis, Department of Petroleum Engineering.

Anand, G. A. (2017). Recent Trends in Fluid Mechanics Wax Deposition Modeling and Comparison with Field Data for Some Indian Oil Fields. *STM Journals, 4*(1). Retrieved from https://www.researchgate.net/publication/316922662_Recent_Trends_in_Fluid_Mechani

cs_Wax_Deposition_Modeling_and_Comparison_with_Field_Data_for_Some_Indian_Oil_Fields

ASTM D2500-17a, Standard Test Method for Cloud Point of Petroleum Products and Liquid Fuels. (n.d.). Retrieved from https://ayalytical.com/methods/astm-d2500/

Awad, M. a. (2008). Effective property models for homogeneous two-phase flow. *Experimental Thermal and Fluid Science 33*, 106–113.

Azevedo, L. a. (2003). A Critical Review of the Modeling of Wax Deposition Mechanisms. *Petroleum Science and Technology*, *21*(3-4), 393-408.

Baha, M. E. (2018). Comparable study for wax content and pour point in different types of crude oils. *American Journal of Research Communication, 6*(7), 29-54. Retrieved from www.usa-journals.com

Baker, R. O. (2015). Introduction to Reservoir Fluid. In *Practical Reservoir Engineering and Characterization* (pp. 1-32). Gulf Professional Publishing.

BelgharzaI, M. H. (2014, July). Kinematic viscosity of linseed oil, almond oil and diesel fuel. *Advances in Environmental Biology, 8*(12), 147-151.

Bendiksen, K. e. (1991). The Dynamic Two-Fluid Model OLGA: Theory and Application. *SPE Production Engineering, 6*(2), 171-180.

Bern, P. W. (1981). Wax deposition in crude oil pipelines. *EUR206.* Proc European Offshore Petroleum Conference and Exhibition, London,.

Beryl, E., Moorwood, T., Szczepanski, R., & Zhang, X. (2007, November 8). Simulating Wax Deposition in Pipelines for Flow Assurance†. *Energy Fuels*, *22*(2), 729-741. Retrieved from https://doi.org/10.1021/ef700434h

Brevik, J. (2013). *Wax control in production systems.* Statoil.

Burger, E. P. (1981, June). Studies of wax deposition in the Trans.

C.R. Wilke, P. C. (1955, June). Correlation of diffusion coefficients in dilute solutions. *AIChE Journal, 1*(2), 264-270. Retrieved from https://doi.org/10.1002/aic.690010222

Calculation of wax appearance temperature directly from hydrocarbon compositions of crude oil. (n.d.). *International Journal of Advanced and Applied Sciences*.

Calsep. (2016). *PVTSim version 20.0.* Retrieved from "C:\Program Files (x86)\PVTsim 20\PVTsim.exe"

Cavet, R. (1964). 27th Midyear Meeting API Division of Refining San Francisco California May 16th.

Chung, T. (1992, October). Thermodynamic Modeling for Organic Solid Precipitation. *SPE 24851*.

Chung, T. (1992). Thermodynamic Modeling for Organic Solid Precipitation. *SPE 24851,*. 67th Annual Technical Conference and Exhibition -Washington DC.

Coutinho et al, J. A.-L. (2005). The limitations of the cloud point measurement techniques and the influence of the oil composition on its detection. *Journal of Petroleum Science and Technology*(23(9-10)), 1113-1128. doi:10.1081/LFT-200035541

Dittus and Boetler, L. M. (1930). Heat transfer in automobile radiators of the tubular type. *The University of California Publications on Engineering*, 443-461.

Echendu, C. J. (2011). *Deepwater Petroleum Exploration And Production in the Gulf of Guinea: Comparative Analysis of Petroleum Fiscal Systems Performance.* Abuja, Nigeria: AUST.

Ekweribe, C. K. (2008). *Quiescent Gelation of Waxy Crudes and Restart of Shut-In Subsea Pipelines.* University Of Oklahoma.

Ellison, B. G. (2000). The Physical Chemistry of Wax, Hydrates and Asphaltene. *OTC 11963 paper prepared for presentation at the 2000 Offshore Technology Conference.* Houston, Texas.

Elsharkawy et al, A. M.-S. (2000). Wax Deposition from Middle East Crudeshttps://doi.org/10.1016/S0016-2361(99)00235-5. *Fuel 79*, pp. 1047-1055.https://doi.org/10.1016/S0016-2361(99)00235-5.

Eyitayo, S., Lawal, K., Guobadia, K., Ovuru, M., Okoh, M., Yadua, A., & Matemilola, S. (2020). *A Comparative Evaluation of Selected Correlations for Estimating Wax-Appearance Temperature of Crude Oils.* doi:10.2118/203618-MS

Farayola, K., Adeboye, Y., Adekomaya, O., & Olatunde, A. (2010). Thermodynamics Prediction of Wax Precipitation Using the Patel-Teja Equation of State. *Nigeria Annual International Conference and Exhibition.* doi:10.2118/136966-ms

Fernando, M. (2020). *Wax deposition analysis for oil and gas multiphase flow in pipelines.* Denmark: Aalborg University Esbjerg.

Forgács, E., & Cserháti, T. (2003). Gas Chromatography. In M. Lees (Ed.), *Food Authenticity and Traceability* (pp. 197-217). In Woodhead Publishing Series in Food Science, Technology and Nutrition,Woodhead Publishing. doi:10.1533/9781855737181.1.197.

Girma, T. C.-J. (2018). Flow start-up and transportation of waxy crude oil in pipelines-A review. *Journal of Newtonian Fluid Mechanics, 251*, 69-87. doi:10.1016/j.jnnfm.2017.11.008.

Glover, P. (2005). Chapter 2: Reservoir Fluids. In *Formation Evaluatiion MSc Course Notes.* Retrieved from http://homepages.see.leeds.ac.uk/~earpwjg/PG_EN/CD%20Contents/Formation%20Evaluation%20English/Chapter%202.PDF

Gluyas & Underhill, J. (2003, Nove). *Retrieved from http://mem.lyellcollection.org/content/20/1/327 Accessed 20 November 2018.* The Staffa Field, Block 3/8b, UK North Sea: Geological Society, London, Memoirs.

GROUP, S. (2012). Wax- Methods and assumptins. *OLGA 7.1 user Manual*.

Hamidreza, M. H. (2013). Impact of Lumping Techniques for Fluid Characterization in Gas Condensate Reservoir. *Australian Journal of Basic and Applied Sciences, 7*(1), 320-333.

Hayduk, M. a. (1982, April). Correlations for prediction of molecular diffusivities in liquids. *The Canadian Journal of Chemical Engineering, 60*(2), 295-299. Retrieved from https://doi.org/10.1002/cjce.5450600213

Hoffmann, R. a. (2010). , Single-Phase Wax Deposition Experiments. *Energy & Fuels, 24*(2), 1069-1080.

Hosseinipour et al, A. J.-J. (2019). Calculations of wax appearance temperature directly from hydrocarbon compositions of crude oil. *Int. J. Advanced Applied Sciences,, 6*(1), 90-94.

https://igiwax.com/wax-basics/. (n.d.). Overview - What is wax? *The international group, INC.* Retrieved May 18, 2021, from https://igiwax.com/wax-basics/

https://www.ihrdc.com/els/po-demo/module01/mod_001_02.htm. (n.d.). *Crude oil and natural gas, from source to final products.* Retrieved May 18, 2021

Huang et al, Z. L. (2011). A fundamental model of wax deposition in subsea oil pipelines. *Fluid Mechanics and Transport Phenomena, 57*(11), 2955-2964. doi:10.1002/aic.12517

Huang, Y. M. (2015, 4 21). Efficacy of the wen dan decoction, a Chinese herbal formula, for metabolic syndrome. In *Alternative Therapies in Health and Medicine* (pp. 54-67). https://doi.org/10.1002/apg.

Jafari, B. T. (2015). Investigation of Wax Precipitation in Crude Oil: Experimental and Modeling. Petroleum, 1(3), 223-230.

James, G. S. (2016). *Handbook of Petroleum Refining.* Routledge handbooks. Retrieved May 18, 2019, from https://www.routledgehandbooks.com/doi/10.1201/9781315374079-5

James, O. P. (2011). Wax Appearance Temperature Detection by DSC. *Perkin Elmer*.

Jandyson, M. S. (2018). Comparing Crude Oils with Different API Gravities on a Molecular Level Using Mass Spectrometric Analysis. *Energies, MPDI.*

Josh, D. R. (2017). Modeling and Simulation of Wax Deposition in Crude Oil Pipeline. *International Journal of Engineering Research and Technology, 10*(1).

Karianne, R. (2008). *Wax Deposition Models.* NTNU, Department of Petroleum Engineering and Applied Geophysics.

Kempton, E. C., & Golczynski, T. (2006, March 1). Understanding wax problems leads to deepwater flow assurance solutions. *Research gate, 227*.

Kesler, M. &. (1976). Improve Prediction of Enthalpy Fractions. *Hydrocarbon Processing, 55*(3), 153-158.

Kök, M. L. (2007). Comparative methods in the determination of wax content and pour points of crude oils. *J Therm Anal Calorim, 90*, 827–831. Retrieved from https://doi.org/10.1007/s10973-006-8254-2

Koker, J. (2013). *Quantitative Characterization of Waxy Crude Oils from Selected Niger-Delta Oil Field.* African University of Science and Technology, Abuja,Nigeria.

Kunal et al, K. a. (2000). Measurement of Waxy Crude Properties Using Novel Laboratory Techniques. *SPE 62945.* Presentation at the 2000 SPE Annual Technical Conference and Exhibition held in Dallas, Texas.

Labes-Carrier, C. e. (2002). Wax Deposition in North Sea Gas Condensate and Oil Systems: Comparison Between Operational Experience and Model Prediction,. *SPE Annual Technical Conference and Exhibition2002.* San Antonio, Texas: Society of Petroleum Engineers.

Lee et al, H. S. (2007). Waxy oil gel breaking mechanisms: adhesive versus cohesive failure. *Energy Fuels, 22*, 480–487.

Lee, H. S. (2011). *Computational and Rheological Study of Wax Deposit and Gelation in Subsea Pipelines.* PhD thesis, the University of Michigan.

Leiroz., A. a. (2005). Studies on the Mechanisms of Wax Deposition in Pipelines. *OTC 17081 paper prepared for presentation at the 2005 Offshore, May 2-5.* Houston, Texas, USA.

Lindleloff et al, N. K. (2002, April 4). A Compositional Model Simulating Wax Deposition in Pipeline Systems. *Energy Fuels, 16*(4), 887-891. Retrieved from https://doi.org/10.1021/ef10025z

Lira-Galeana, C. F. (1996, January). Thermodynamics of Wax Precipitation in Petroleum Mixtures. *AlChE Journal, 42*(1).

Lize, M. S., Nunes, R. C., Ribeiro, Y. L., Coutinho, D. M., Azevedo, D. A., Dias, J. C., & Lucas, E. F. (2018, October). Wax Behavior in Crude Oils by Pour Point Analyses. *Journal of the Brazillian Chemical Society, 29*(10). Retrieved from http://dx.doi.org/10.21577/0103-5053.20180092

Mansoori, G. A. (2017). PHASE BEHAVIOR IN PETROLEUM FLUIDS: A DETAILED DESCRIPTIVE AND ILLUSTRATIVE ACCOUNT WITH EMPHASIS ON HEAVY ORGANICS . *Encyclopedia of life support sstems(EOLSS)*.

Marte, S. (2013). *Analytical and Numerical Modelling of Paraffin Wax in Pipelines.* Norwegian University of Science and Technology, Trondheim: MSc Thesis.

Matzain, A. M.-Q. (2001). Multiphase Flow Wax Deposition Modeling. *ASME 2001 Engineering Technology Conference on Energy.* doi:10.1115/ETCE2001-17114

Montero, F. (2020). *Wax deposition analysis for oil and gas multiphase flow in pipelines.* Denmark: Aalborg University Esbjerg.

Mysara, E. M. (2019, December). Challenges during Operation and Shutdown of Waxy Crude Pipelines. (R. M. Gounder, Ed.) doi:10.5772/intechopen.89489

Nur, F. (2016). HYDRATE/WAX/ASPHALT IN SUBSEA PIPELINE. *Ocean Engineering ITB*.

Obaseki, M. P. (2020). Dynamic modeling and prediction of wax deposition thickness in crude oil pipelines. *Journal of King Saud University- Engineering Sciences*.

Oluwatosin, E. A. (2013). *Modelling of controlled wax deposition and loosening in oil and gas production systems.* Norwegian University of Science and Technology, Energy and Process Engineering, Trondheim.

Otung, D. &. (2012). A CFD Approach for Predicting Paraffin Deposition in Oilfield Installations. *SPE 162943.* Paper presented at the Nigeria Annual International Conference and Exhibition, Abuja, Nigeria.

Oyedepo, S. O. (2012, July 23). Energy and sustainable development in Nigeria: the way forward. *Energy, Sustainability and Society*, pp. https://doi.org/10.1186/2192-0567-2-15.

Palisade. (2020). @Risk software version 8.0. Retrieved March 10, 2021, from "C:\Program Files (x86)\Palisade\RISK8\Risk.exe"

Pan, S. e. (2009). Case Studies on Simulation of Wax Deposition in Pipelines, in International Petroleum Technology Conference2009. *International Petroleum Technology Conference.* Doha, Qatar.

Pedersen et al, K. S. (1991). Wax Precipitation from North Sea Crude Oils. 4. Thermodynamic Modeling. *Energy Fuel*, *5*, 924 – 932.

Pedersen, K. S. (1993). Prediction of Cloud-Point Temperatures and Amount of Wax Precipitation. *SPE 27629.* Richardson, TX: SPE.

Petrowiki. (2018). Retrieved January 21, 2021, from https://petrowiki.spe.org/Asphaltenes_and_waxes

Rygg, O. R. (1998). "Wax deposition in offshore pipeline systems. *Proc. 1st North American Conference on Multiphase technology.* Banff, Canada.

Santos, R. B. (2014). AN OVERVIEW OF HEAVY OIL PROPERTIES AND ITS RECOVERY AND TRANSPORTATION METHODS. Campinas-SP, Brazil: Brazilian journal of chemical engineering.

Schou, P. a. (2007). *Phase Behavior of Petroleum Reservoir Fluids.*

Semir, E. (2020). *Chemical Constitution of Crude Oil.* Retrieved May 18, 2021, from https://www.e-education.psu.edu/fsc432/node/5#:~:text=Constituents%20of%20crude%20oil.&text=Hydrocarbons%20are%20generally%20divided%20into,as%20different%20from%20aromatic%20compounds.

Singh, P. (2000). Formation and aging of incipient thin film wax-oil gels. *AIChE Journal, 46*(5), 1059-1074.

Singh, P. e. (2001). Morphological evolution of thick wax deposits during aging. *AIChE Journal, 47*(1), 6-18.

Sofyan, Y. G. (2003). A systematic method to predict cloud point temperature and solid precipitation. *Petroleum Science and Technology*. Retrieved from https://doi.org/10.1081/LFT-120018529

Source:. (n.d.). Retrieved from http://nfatmala.blogspot.com/2016/02/hydratewaxasphalt-in-subsea-pipeline.html

Sousa, A. M. (2019). Preventing and removing wax deposition inside vertical wells: a review. *J Petrol Explor Prod Technol, 9*, 2091–2107. Retrieved from https://doi.org/10.1007/s13202-019-0609-x

Svendsen, J. (1993). Mathematical modeling of wax deposition in oil pipeline systems. *AIChE J, 39*(8), 1377-1388. Retrieved from http://dx.doi.org/10.1002/aic.690390815

Taheri-Shakib Hamedani, J., Shekarifard, A., & Naderi, H. (2018, March 1). The influence of electromagnetic waves on the gas condensate characterisation: Experimental evaluation. *Journal of Petroleum Science and Engineering, 166*. doi:10.1016/j.petrol.2018.03.078

Taiwo et al, E. O. (2012). *Crude Oil Transportation: Nigerian Niger Delta Waxy Crude, Crude Oil Exploration in the World,Prof Mohammed Younes (Ed.) ISBN: 978-953-51-0379-0.* Retrieved from http://www.intechopen.com/books/crude-oil-exploration-in-the-world/crude-oil-transportationnigerian-niger-delta-waxy-crude-oil.

Tao, Z. (2008). *Evaluation of Wax Deposition and Its Control During Production of Alaskan North Slope Oils.* University of Alaska Fairbanks, USA.

Theyab et al, M. D. (2017). An EXperimental and Simulation Study of Wax Deposition in Hydrocarbon Pipeline. *Global Journal of Engineering Science and Researches*, 4(7):27-40.

Uba, E. K. (2004, August). Measurement of Wax Appearance Temperature of an Offshore Live Crude Oil using Laboratory Light Transmission Method. *Research Gate*. doi:10.2118/88963-MS

Vafaie-Sefti, M., Mousavi-Dehghani, S. A., & Bahar, M. (2000, August 1). Modification of multisolid phase model for prediction of wax precipitation: A new and effective solution method. *Fluid Phase Equilibria, 173*. doi:10.1016/S0378-3812(00)00405-2

Wang, J. C. (2006). A new approach to modeling the effective thermal conductivity of heterogeneous materials. *Heat and Mass Transfer 49*, 3075–3083.

Wax Problems in Production. (n.d.). *Petrowiki*. Retrieved from https://petrowiki.spe.org/Wax_problems_in_production

Whitson, C. (1983). Characterizing Hydrocarbon Plus Fractions. *SPE Journal, 23*(4), 683-694.

www.eia.gov. (n.d.).

Zhou, X. T. (1996). Modelling of Solid Precipitation from Reservoir flow. *Journal of Canadian Petroleum Technology, 35*(10), 37-45. Retrieved from https://doi.org/10.2118/96-10-03

Appendix A

The following computer programs were used in simulating the wax depositional thickness using the MATZAIN and Singh et al models. Note, the programs are MATLAB codes for 1 day of wax deposition at the pipe inlet. This can be modified to calculate the wax thickness at other times.

A.1: MATZAIN Wax deposition for 1 day

(Adapted from Parameshwar et al, 2015)

```
function SolveWaxEquation
% This is MatZain Model Function
% Code for 1 day
Tb    = 55;
Tw    = 25;
Kl    = 0.579;
hw    = 8;
Dw    = 0.00000000614;
dTdr  = (Tb - Tw)*hw/Kl;
C1    = 15;
C2    = 0.055;
C3    = 1.4;
vl    = 100;
rho   = 855;
mu    = 0.0005;
dCwdT = 0.180;
Nsr   = @(krkd) rho*vl*krkd/mu;
Cl    = @(krkd) 100*(1 - Nsr(krkd)^0.15/8);
PI1   = @(krkd) C1/(1 - Cl(krkd)/100);
PI2   = @(krkd) 1 + C2*Nsr(krkd)^C3;
d_krkd_dt = @(t, krkd) PI1(krkd)/(1 + PI2(krkd))*Dw*(dCwdT*dTdr);
tt_final = [24*1,24*2,24*7,24*20,24*30]
for ttt = 1:1 %2:2, 3:3, 4:4, 5:5
time = tt_final(ttt)*3600;
[T, Krkd] = ode45(d_krkd_dt,[0,time],0.001);
plot(T/3600, Krkd)
hold on
end
```

A.2: SINGH et al Wax deposition for 1 day

(Adapted from Bern et al, 1981)

```
% This is Singh et al Model Function
Tb     = 55;
Tw     = 25;
Kl     = 0.579;
hw     = 0.25;
Dw     = 0.00000000614;
rho    = 855;
dCdr   = 0.180*(Tb - Tw)*hw/Kl;
alpha  = 0.2;
R      = 0.1;
Phi    = @(x) 1/(1 + alpha*(x^2/(1 - x^2)));
dYdt   = @(t, Y)[Dw*dCdr*Phi(Y(1))*2*(R - Y(2))/(rho*Y(2)*(2*R - Y(2))); Dw*dCdr*(1 -
Phi(Y(1)))/(rho*Y(1))];
[T, Y] = ode45(dYdt,[0,86400],[0.1,0.001]); %2*86400, 7*86400, 20*86400, 30*86400
plot(T/3600, Y(:,2))
hold off
ylabel('Deposit Thickness (m)')
xlabel('Time (hours)')
legend('MATZAIN simulation for 1 day','Singh et al simulation for 1 day')
```

A.3: Marte Stubsjoen Numerical Model for Wax deposition

The MATLAN code for the simulating wax deposition for 1, 2, 7, 20 and 30 days using the numerical model by Marte Stubsjoen can be found in the NNTU thesis by Stubsjoen(2013).

Source: Marte, S. (2013). *Analytical and Numerical Modelling of Paraffin Wax in Pipelines.* Norwegian University of Science and Technology, Trondheim: MSc Thesis.